

Figure 2-261. Finite Element Mesh for the SC-2, End Impact, 0° Support Structure

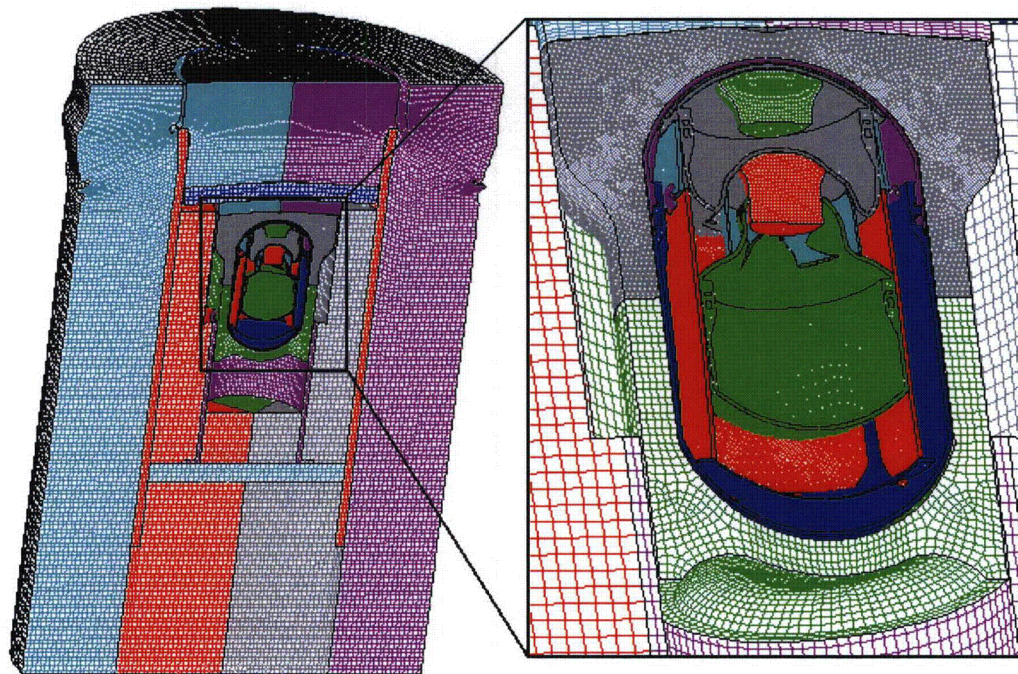


Figure 2-262. Finite Element Mesh for the SC-2, End Impact, 0° Support Structure – Final Displacement

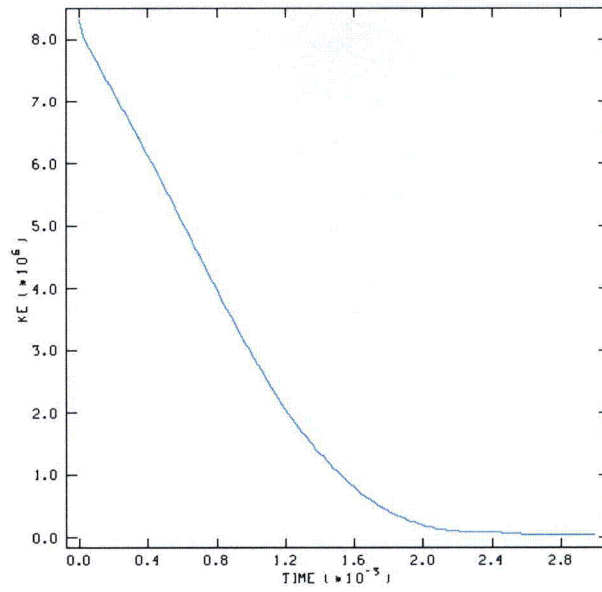


Figure 2-263. Kinetic Energy Time History for the SC-2, End Impact, 0° Support Structure

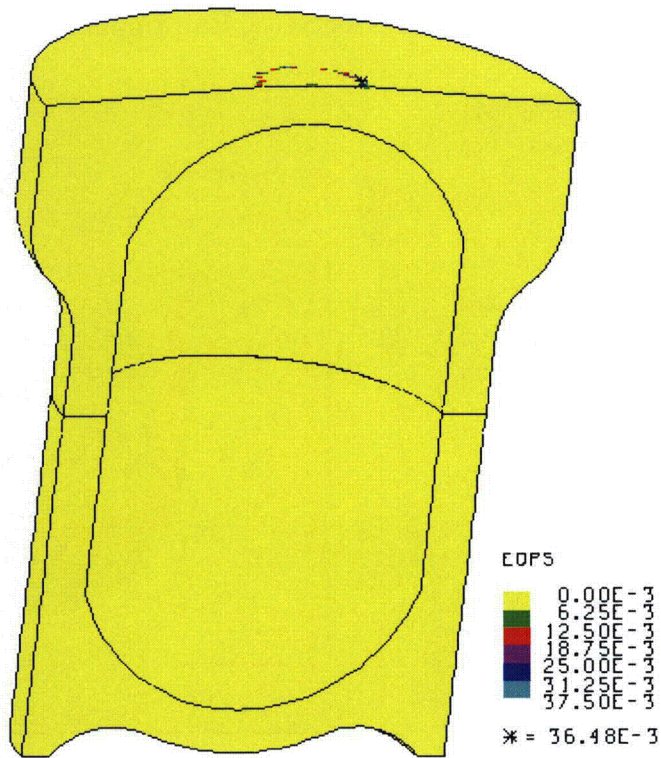


Figure 2-264. Plot of EQPS in the TB-1 for the SC-2, End Impact, 0° Support Structure

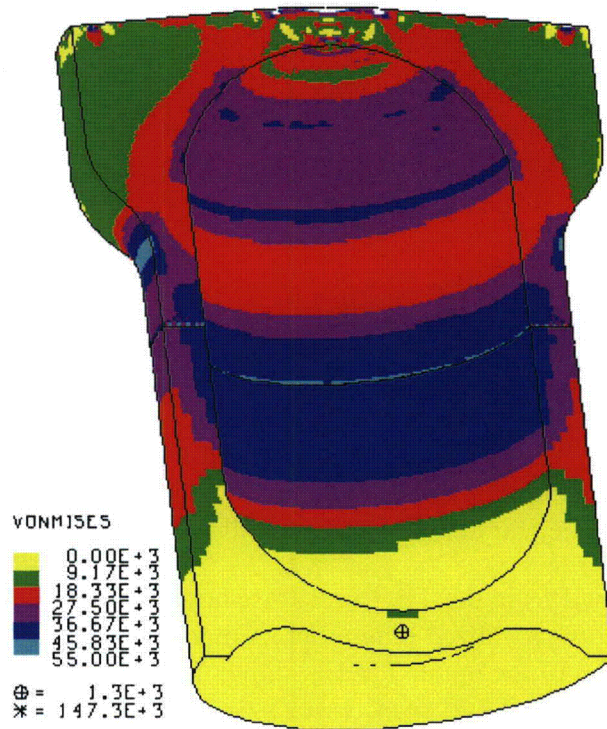


Figure 2-265. Plot of von Mises Stress in the TB-1 for the SC-2, End Impact, 0° Support Structure

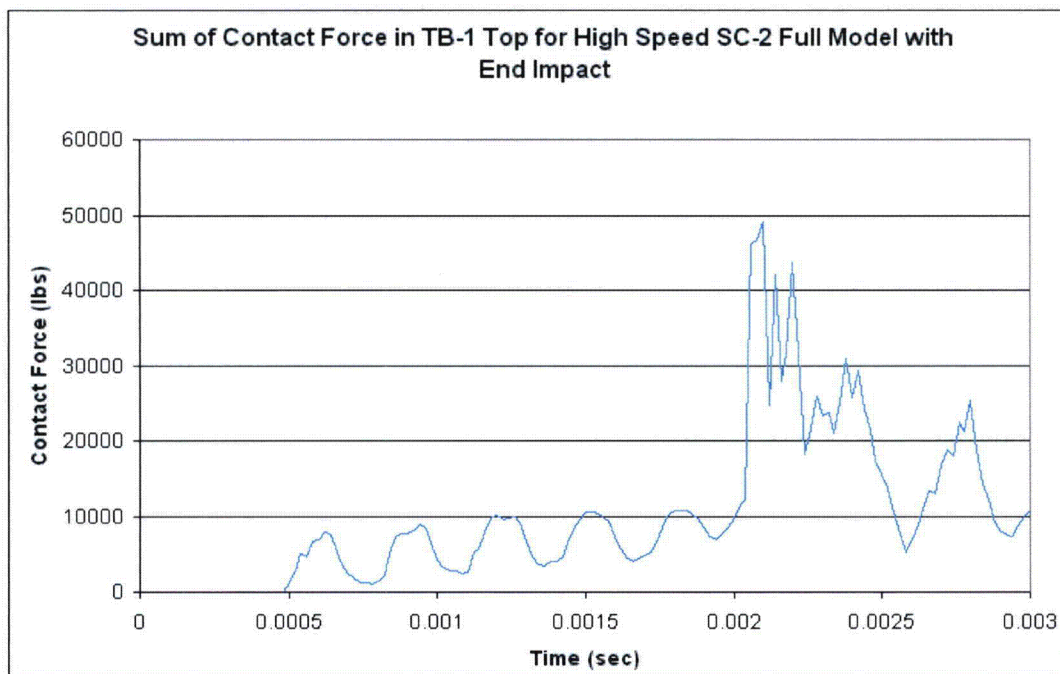


Figure 2-266. Plot of Contact Forces in the TB-1 for the SC-2, End Impact, 0° Support Structure

2.12.5.5.7 Run 17 - SC-2 Sample Container, Side Impact, Support Structure 0°

The side impact model for the larger SC-2 each with 338 g of delta Pu contents (inner cradle rotated 0 degrees) is shown in Figure 2-267. Note that each Pu cylinder is located at the far left side of each SC-2 so that its net impact velocity with the right side of the T-Ampoule is maximized. The post-impact deformation is shown in Figure 2-268 and its kinetic energy history in Figure 2-269. The Pu contents penetrate each of the SC-2 side walls and directly impact the T-Ampoule.

Average stress-triaxiality versus EQPS is shown in Figure 2-270 for the 55 elements extending beyond the tested Bao-Wierzbicki strain locus. All of these elements are outside the B-W locus, for a variety of stress triaxialities, although most of the 580,000 T-Ampoule elements are inside the B-W locus. The Tearing Parameter values for these same 55 elements are shown in Figure 2-271 and all are below the critical Tearing Parameter value of 1.012 for Ti-6Al-4V. These elements are highlighted in red in Figures 2-272 and 2-273, but note that these elements are still below the initiation of a ductile tear and thus, T-Ampoule integrity is maintained.

Equivalent Plastic Strain (EQPS) in the TB-1 vessel is shown in Figures 2-274 and 2-275 to be less than 39% but only in some localized outer contact regions with the redwood overpack. The EQPS due to internal denting of the upper TB-1 is shown in Figure 2-275 to be less than 0.07%, which is essentially elastic. The von Mises stresses (see Figure 2-276) peak at 225 ksi, is above the elevated-temperature minimum yield strength for the TB-1 of 141 ksi but more importantly, through-thickness TB-1 stress values are in the less-than-135 ksi range, which is below yield.

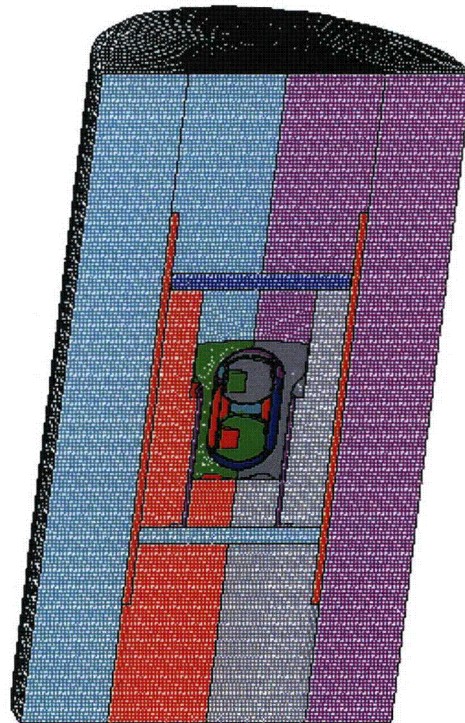


Figure 2-267. Finite Element Mesh for the SC-2, Side Impact, 0° Support Structure

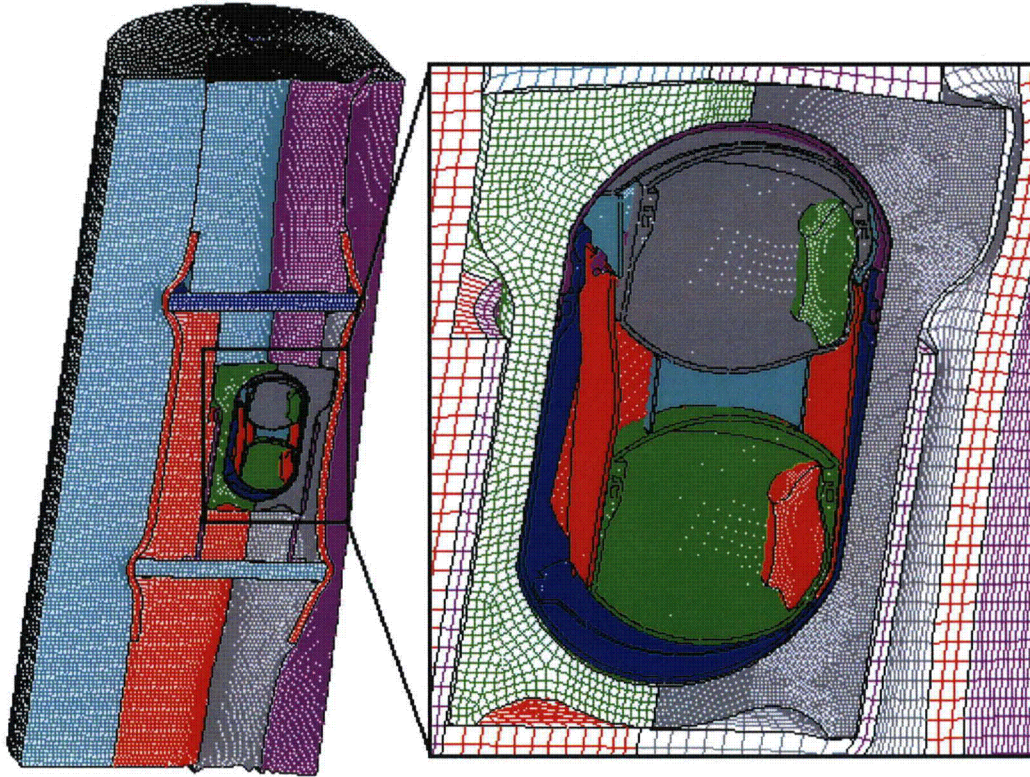


Figure 2-268. Finite Element Mesh for the SC-2, Side Impact, 0° Support Structure – Final Displacement

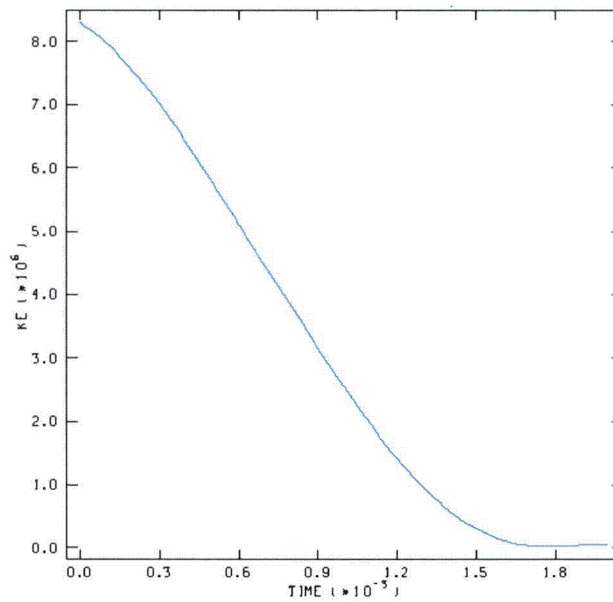


Figure 2-269. Kinetic Energy Time History for the SC-2, Side Impact, 0° Support Structure

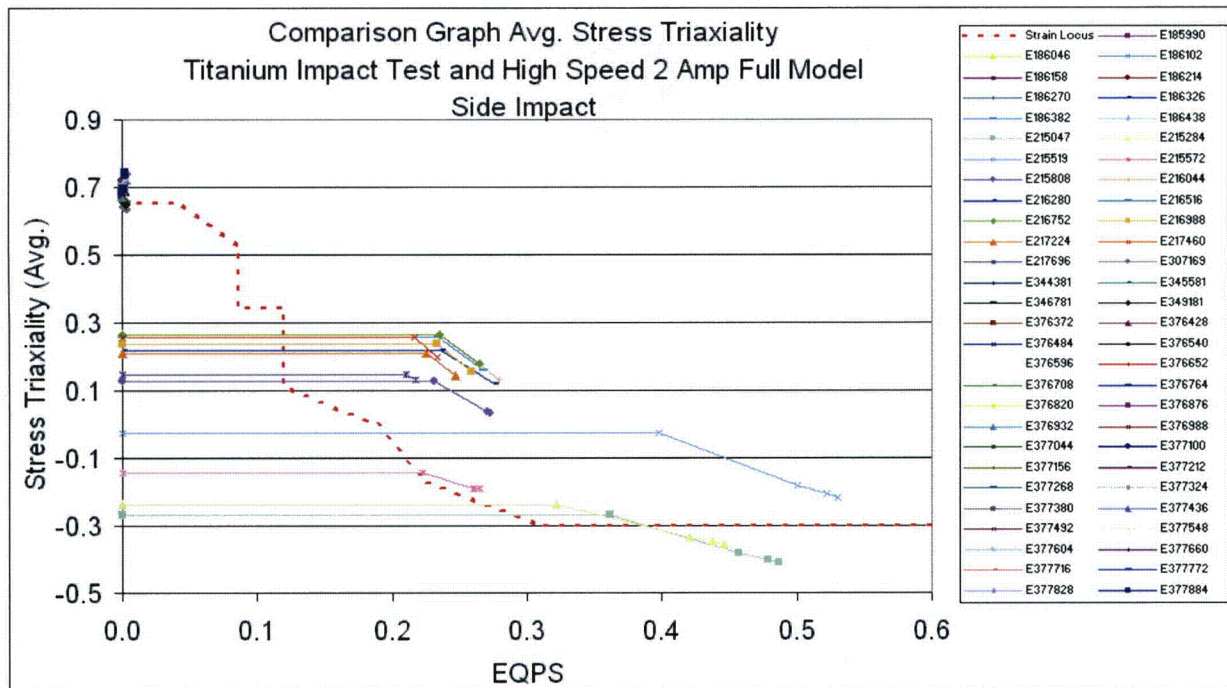


Figure 2-270. Graph of Average Stress Triaxiality versus EQPS of Elements Exceeding the Experimental Strain Locus for the SC-2, Side Impact, 0° Support Structure

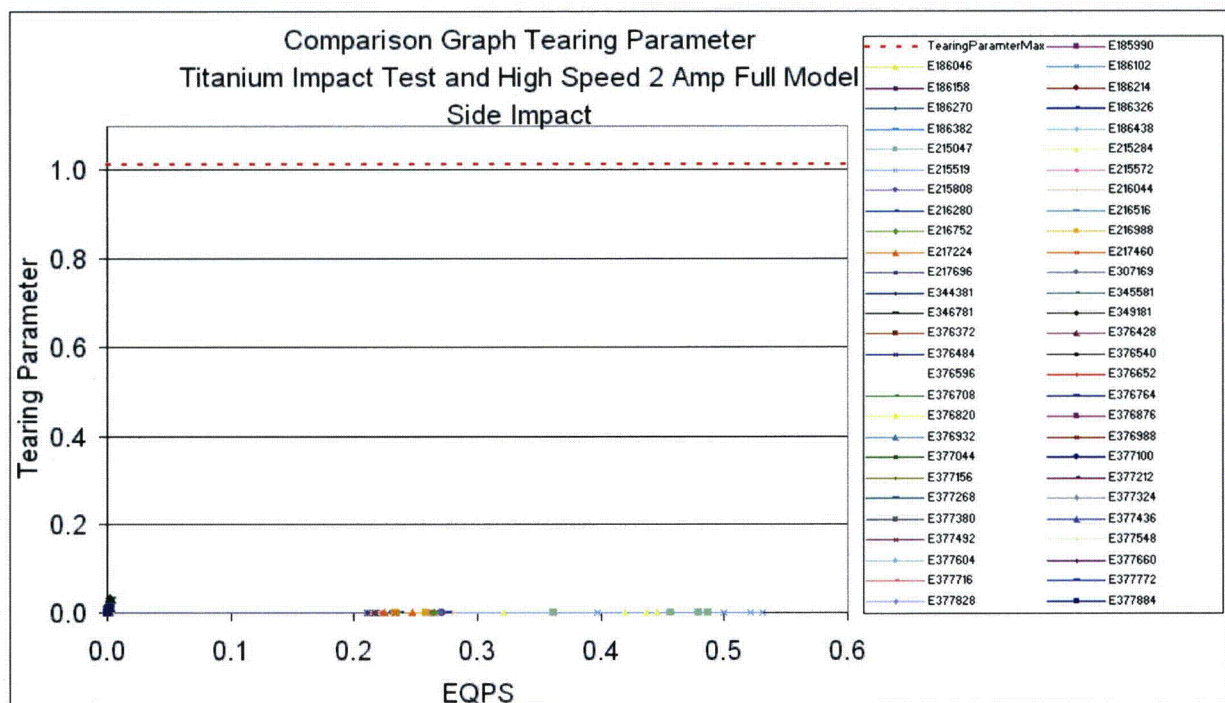


Figure 2-271. Graph of Tearing Parameter versus EQPS of Elements Exceeding the Experimental Strain Locus for the SC-2, Side Impact, 0° Support Structure

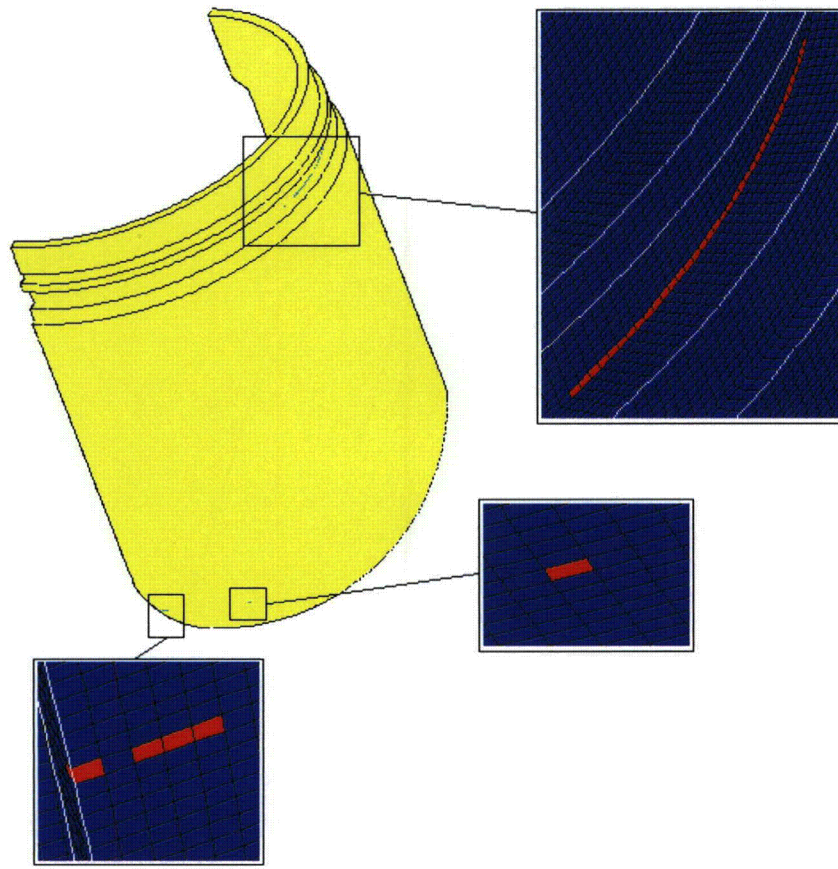


Figure 2-272. Plot of Elements Exceeding the Experimental Strain Locus for the SC-2, Side Impact, 0° Support Structure

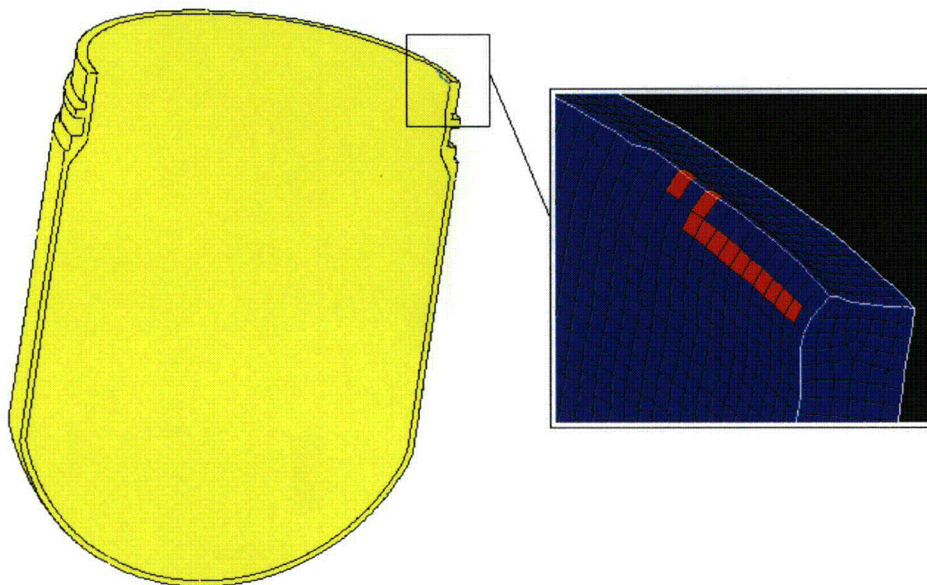


Figure 2-273. Plot of Elements Exceeding the Experimental Strain Locus for the SC-2, Side Impact, 0° Support Structure

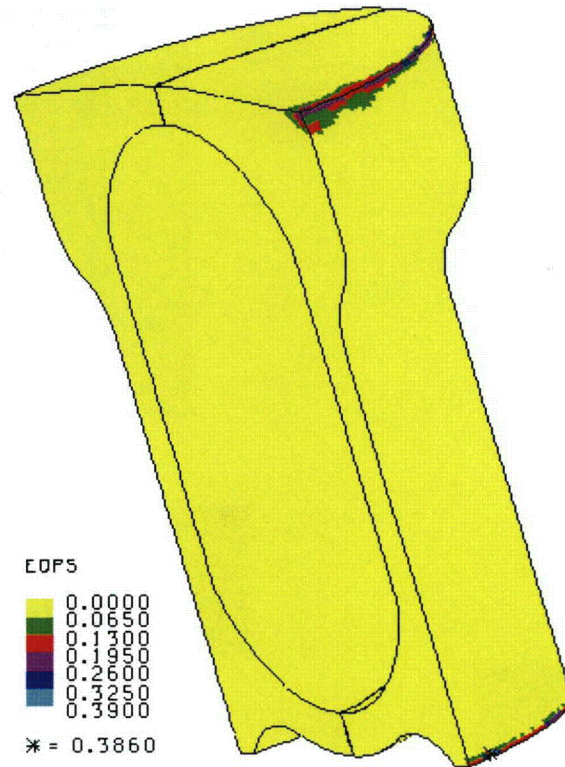


Figure 2-274. Plot of EQPS in the TB-1 for the SC-2, Side Impact, 0° Support Structure

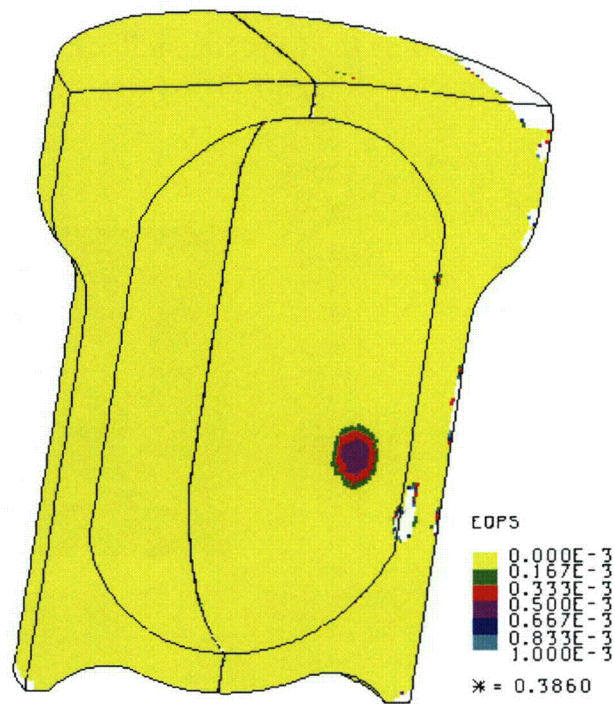
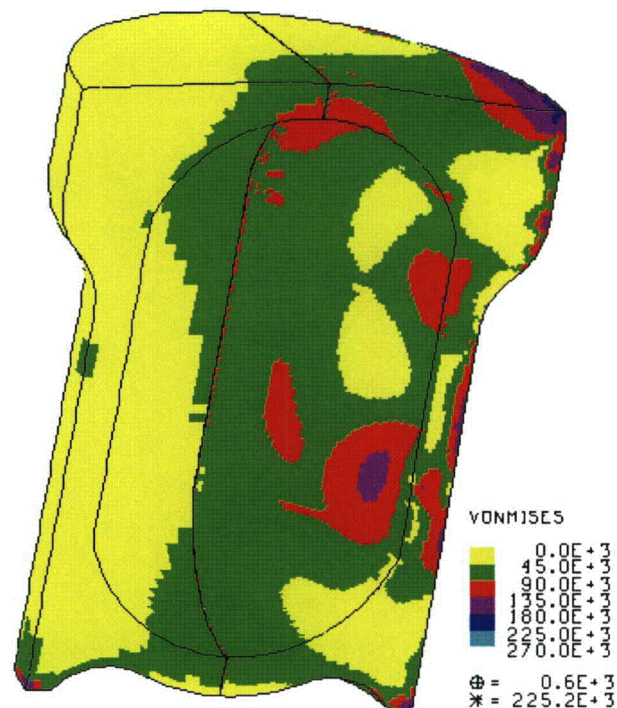


Figure 2-275. Plot of EQPS in the TB-1 for the SC-2, Side Impact, 0° Support Structure



**Figure 2-276. Plot of von Mises Stress in the TB-1 for
[the SC-2, Side Impact, 0° Support Structure**

2.12.5.5.8 Run 18 - SC-2 Sample Container, Side Impact, Support Structure 45°

The side impact model for each of the larger SC-2 sample containers with 338 g of delta Pu contents (inner cradle rotated 45 degrees for SC impingement onto sharp cradle edge) is shown in Figure 2-277. Note that each Pu cylinder is located at the far left side of each SC-2 so that its net impact velocity with the right side of the T-Ampoule is maximized. The post-impact deformation is shown in Figure 2-278 and its kinetic energy history in Figure 2-279. The Pu contents penetrate each of the SC-2 side walls and directly impact the T-Ampoule.

Average stress-triaxiality versus EQPS is shown in Figure 2-280 for the 82 elements extending beyond the tested Bao-Wierzbicki strain locus. All of these elements are outside the B-W locus, for a variety of stress triaxialities, although most of the 580,000 T-Ampoule elements are inside the B-W locus. The Tearing Parameter values for these same 82 elements are shown in Figure 2-281 and all are below the critical Tearing Parameter value of 1.012 for Ti-6Al-4V. These elements are highlighted in red in Figures 2-282 and 2-283, but note that these elements are still below the initiation of a ductile tear and thus T-Ampoule integrity is maintained.

Equivalent Plastic Strain (EQPS) in the TB-1 vessel is shown in Figures 2-284, 2-285, and 2-286 to be less than 29%, but only in some localized outer contact regions with the redwood overpack. The EQPS due to internal denting of the upper TB-1 is shown in Figure 2-286 to be less than 0.083%, which is essentially elastic. The von Mises stresses (see Figure 2-287) peak at 227 ksi, above the elevated-temperature minimum yield strength for the TB-1 of 141 ksi but more importantly, through-thickness TB-1 stress values are in the less-than-120 ksi range, which is below yield.

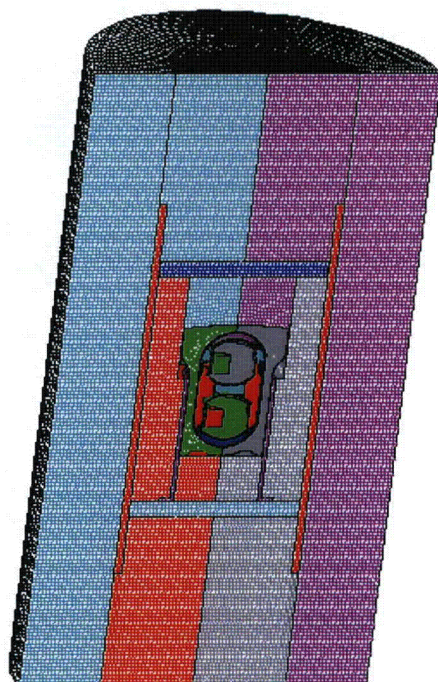


Figure 2-277. Finite Element Mesh for the SC-2, Side Impact, 45° Support Structure

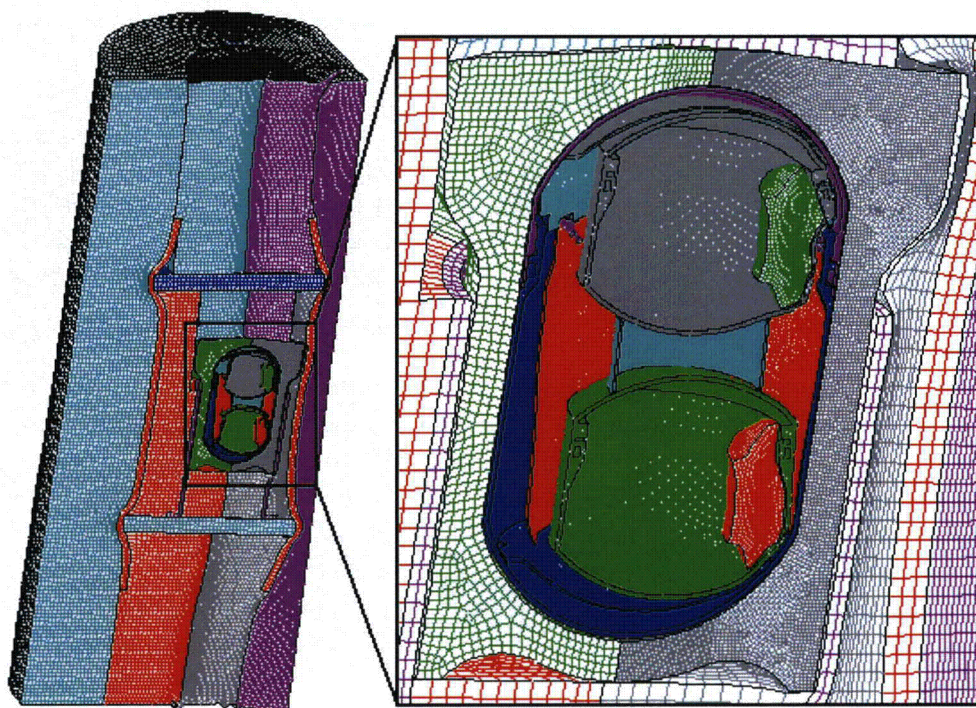


Figure 2-278. Finite Element Mesh for the SC-2, Side Impact, 45° Support Structure – Final Displacement

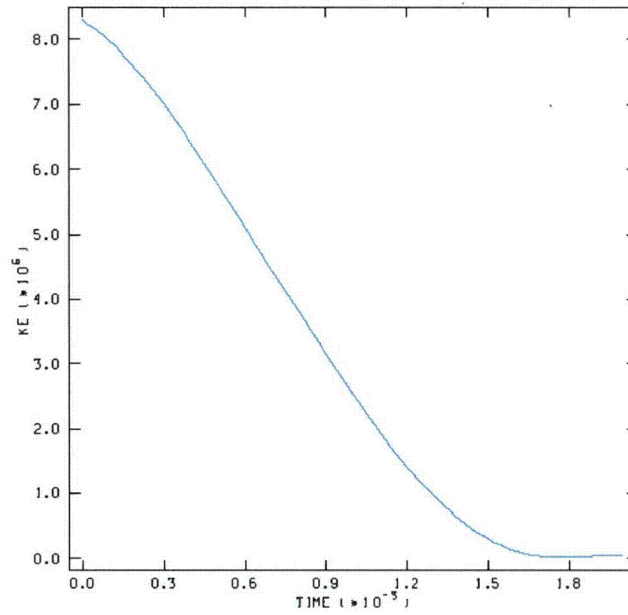


Figure 2-279. Kinetic Energy Time History for the SC-2, Side Impact, 45° Support Structure

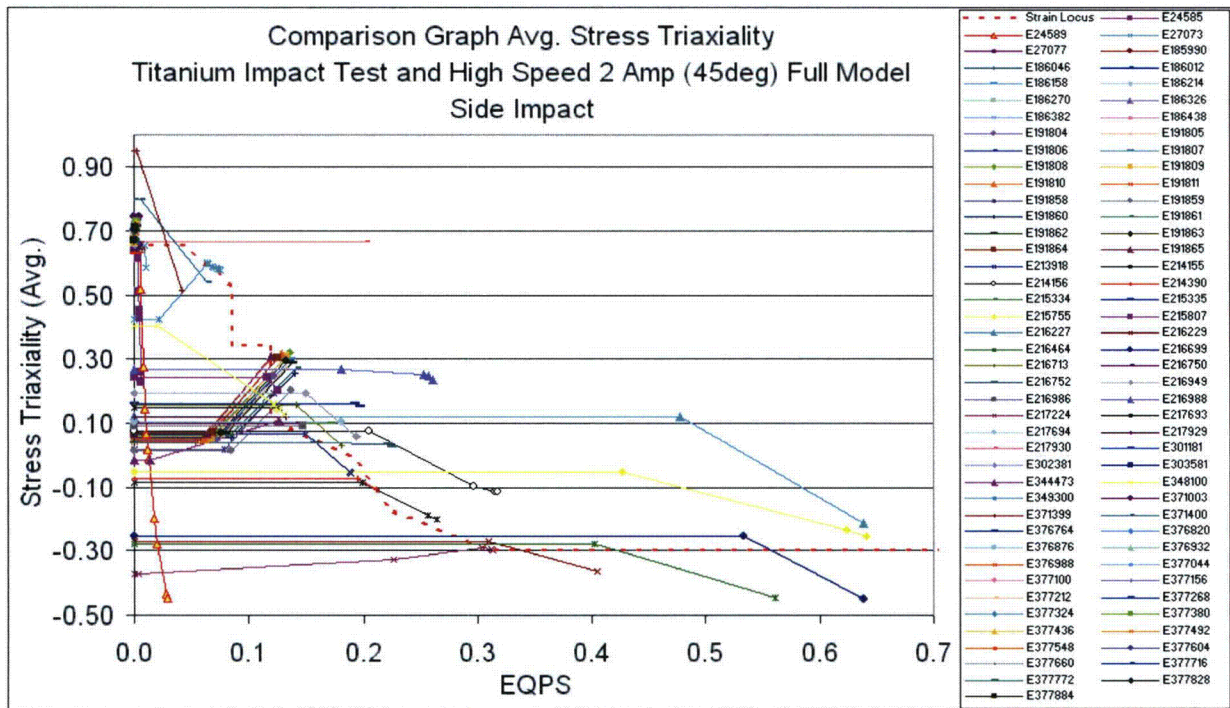


Figure 2-280. Graph of Average Stress Triaxiality versus EQPS of Elements Exceeding the Experimental Strain Locus for the SC-2, Side Impact, 45° Support Structure

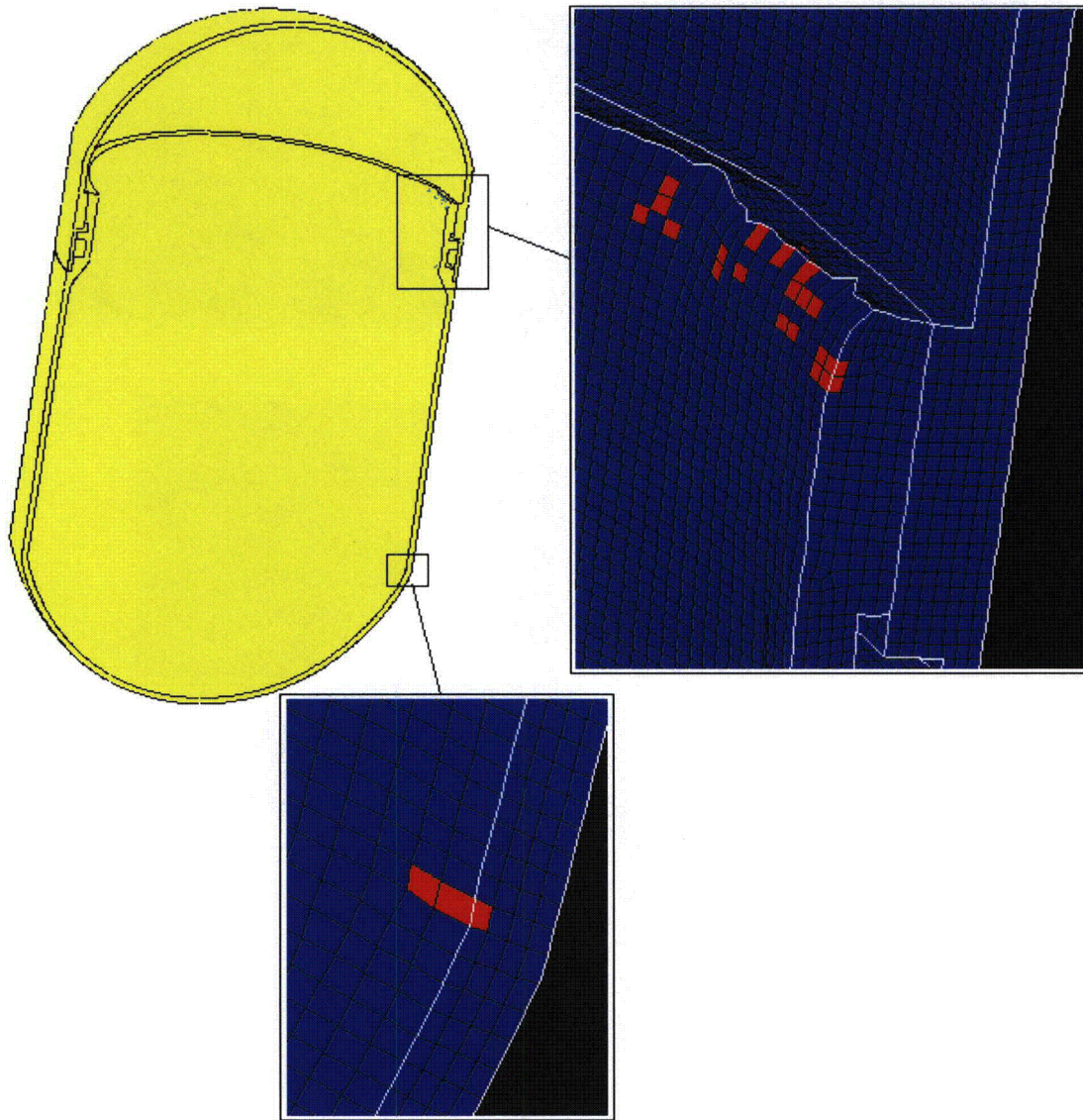


Figure 2-282. Plot of Elements Exceeding the Experimental Strain Locus for the SC-2, Side Impact, 45° Support Structure

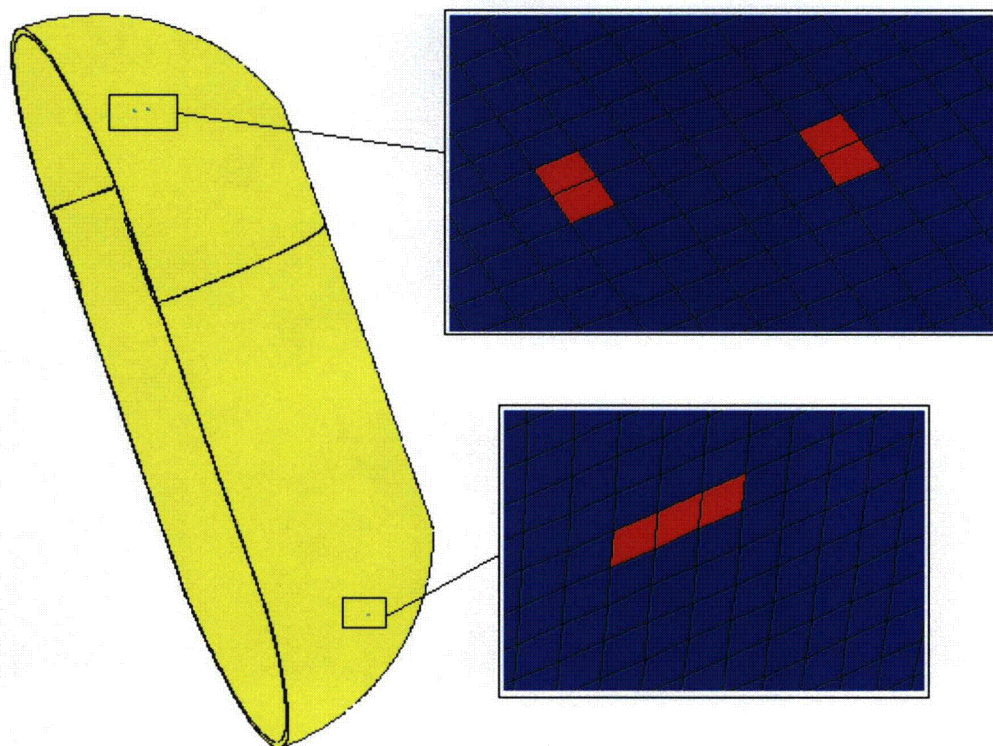


Figure 2-283. Plot of Elements Exceeding the Experimental Strain Locus for the SC-2, Side Impact, 45° Support Structure

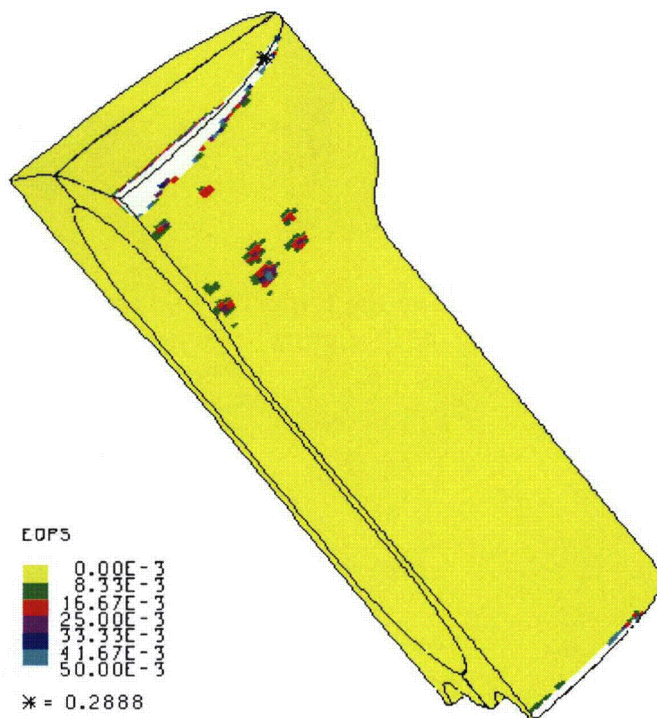


Figure 2-284. Plot of EQPS in the TB-1 for the SC-2, Side Impact, 45° Support Structure

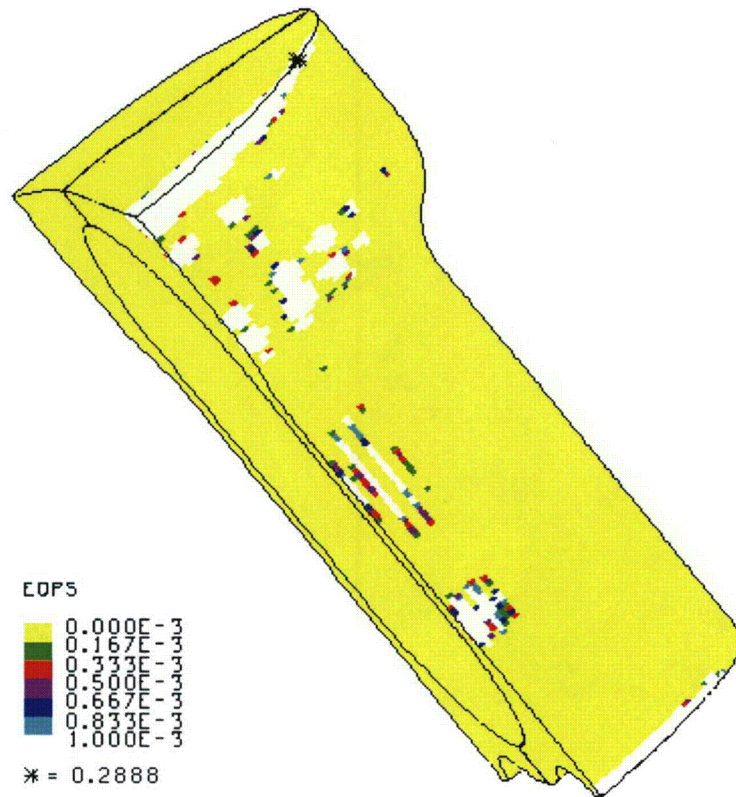


Figure 2-285. Plot of EQPS in the TB-1 for the SC-2, Side Impact, 45° Support Structure

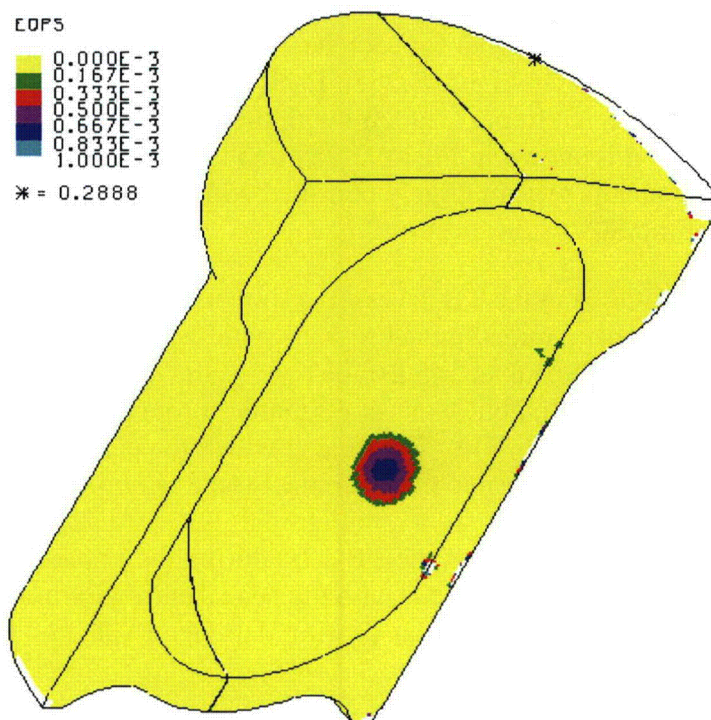


Figure 2-286. Plot of EQPS in the TB-1 for the SC-2, Side Impact, 45° Support Structure

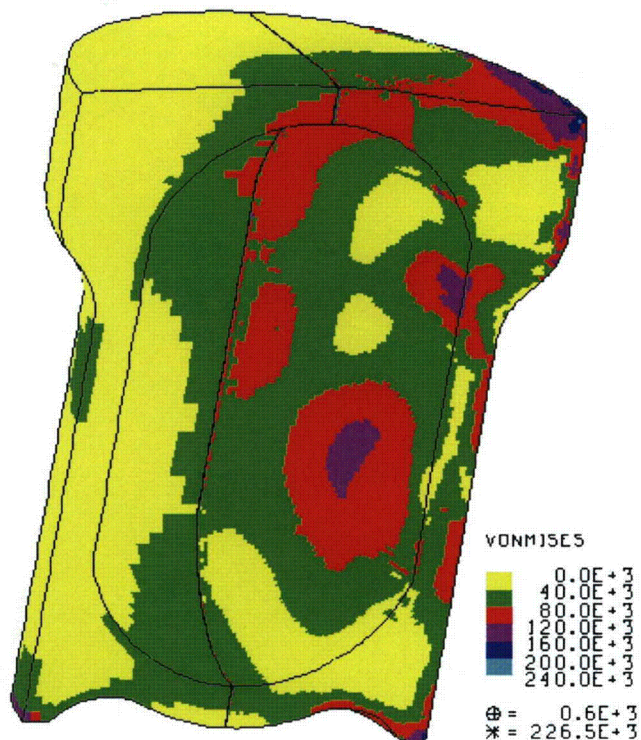


Figure 2-287. Plot of von Mises Stress in the TB-1 for the SC-2, Side Impact, 45° Support Structure

2.12.5.5.9 Run 19 - SC-2 Sample Container, CGOC Impact, Support Structure 0°

The lid end CG-over-corner impact model for each large SC-2 with delta Pu contents (inner cradle rotated 0 degrees) is shown in Figure 2-288. Each Pu cylinder is located at the rotated bottom of each SC-2 so that its net impact velocity with the top of the T-Ampoule is maximized. The post-impact deformation is shown in Figure 2-289 and its kinetic energy history in Figure 2-290. The Pu cylinder contents remain largely confined within the SC-2's, although significant localized deformation of the SC-2's has occurred.

Equivalent Plastic Strain (EQPS) in the TB-1 vessel is shown in Figure 2-291 to peak at about 18.5%, but only in some localized outer contact regions with the redwood overpack. The von Mises stresses (see Figure 2-292) peak at 145 ksi, just above the elevated-temperature minimum yield strength for the TB-1 of 141 ksi but more importantly, through-thickness TB-1 stress values are in the 47 ksi range, below yield. The time at which the peak value of the von Mises stress occurs coincides with the peak value of the contact force (summed over the lid area). A plot of this force as a function of time is shown in Figure 2-293. A maximum contact load of 34,253 lbs is applied to the inner surface of the TB-1 lid during the impact. No T-Ampoule elements exceeded the tested B-W strain locus, and the peak Tearing Parameter value (see Table 2-11, run #19) of 0.0953 was below the critical Tearing Parameter value of 1.012 for Ti-6Al-4V.

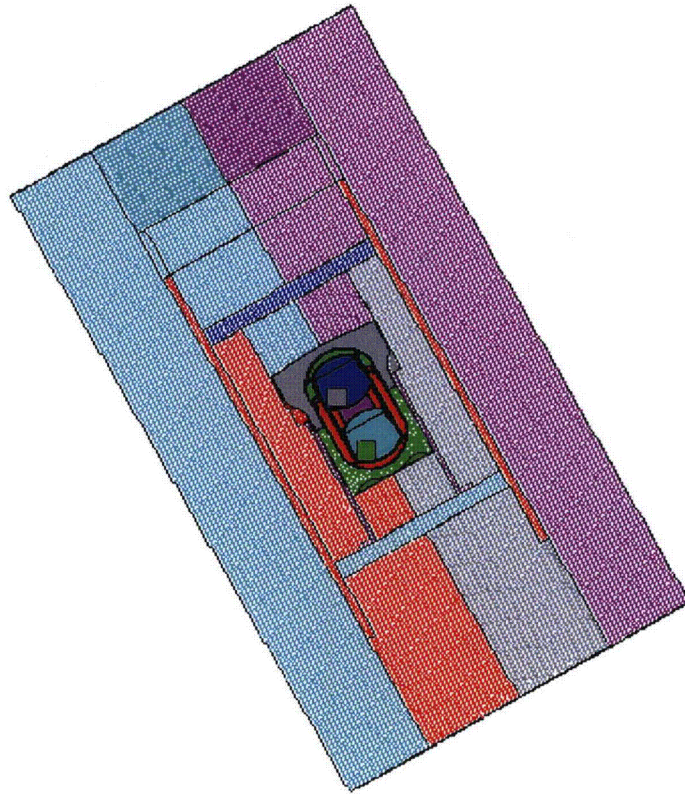


Figure 2-288. Finite Element Mesh for the SC-2, CGOC Impact, 0° Support Structure

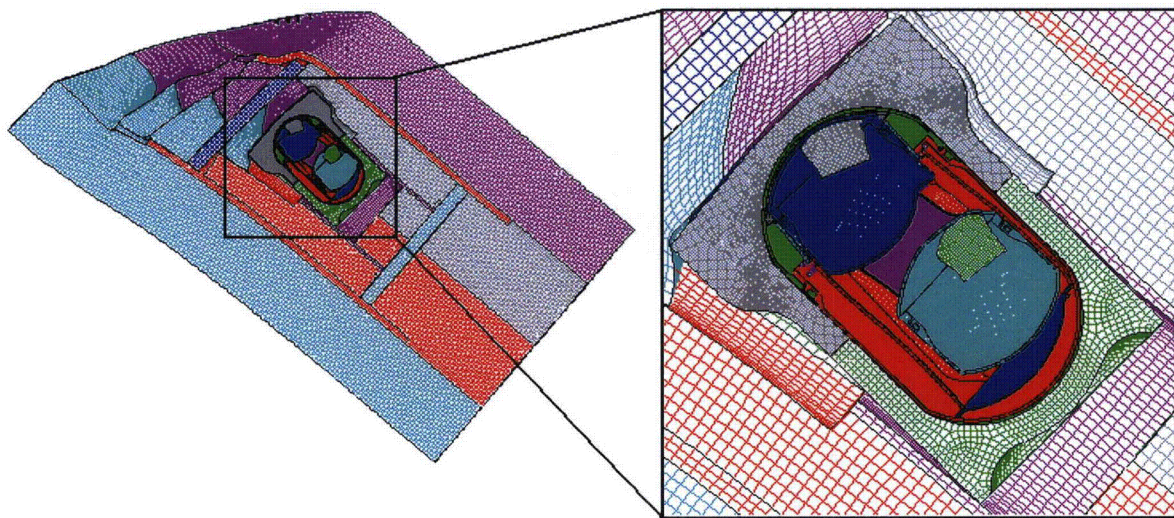


Figure 2-289. Finite Element Mesh for the SC-2, CGOC Impact, 0° Support Structure – Final Displacement

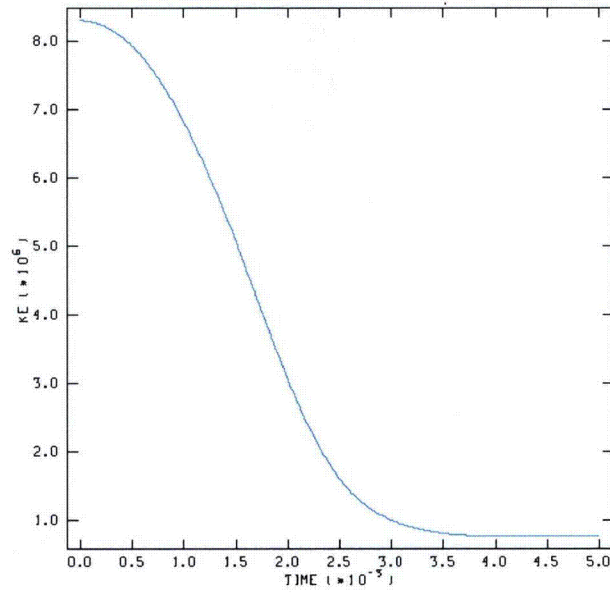


Figure 2-290. Kinetic Energy Time History for the SC-2, CGOC Impact, 0° Support Structure

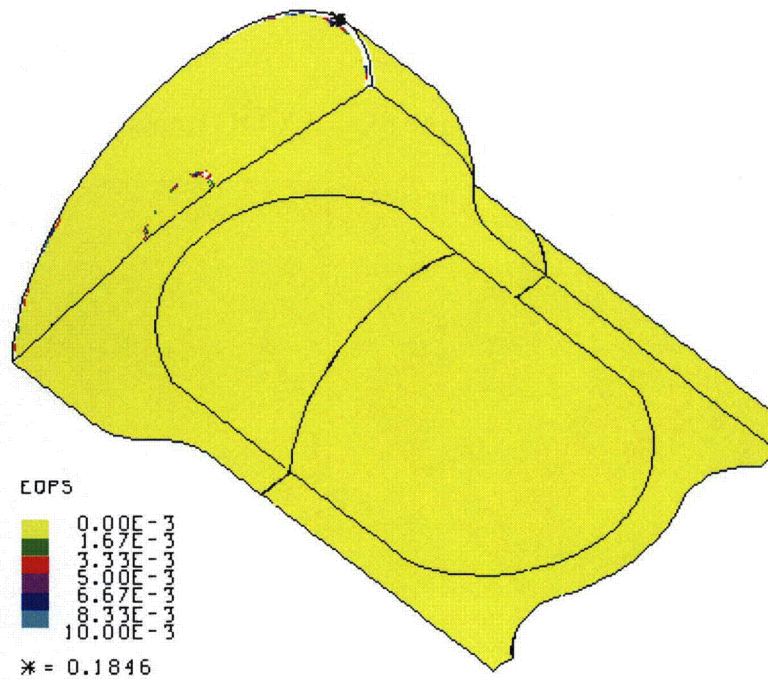


Figure 2-291. Plot of EQPS in the TB-1 for the SC-2, CGOC Impact, 0° Support Structure

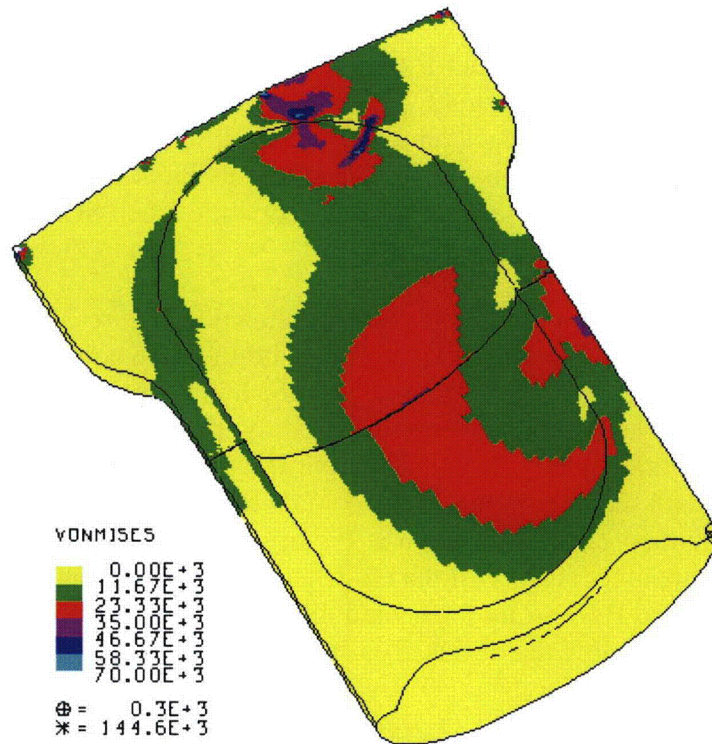


Figure 2-292. Plot of von Mises Stress in the TB-1 for the SC-2, CGOC Impact, 0° Support Structure

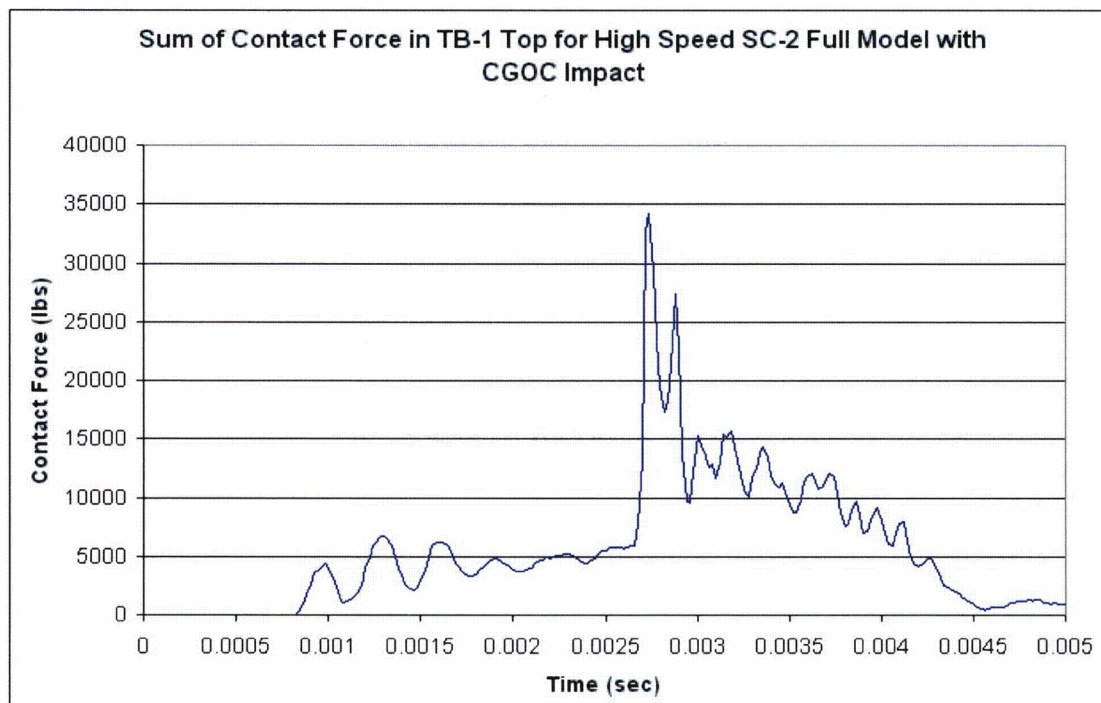


Figure 2-293. Plot of Contact Forces in the TB-1 for the SC-2, CGOC Impact, 0° Support Structure

2.12.5.5.10 Run 20 - SC-2 Sample Container, CGOC Impact, Support Structure 45°

The lid end CG-over-corner impact model for each large SC-2 with delta Pu contents (inner cradle rotated 45 degrees) is shown in Figure 2-294. Each Pu cylinder is located at the rotated bottom of each SC-2 so that its net impact velocity with the top of the T-Ampoule is maximized. The post-impact deformation is shown in Figure 2-295 and its kinetic energy history in Figure 2-296. The Pu cylinder contents remain largely confined within each SC-2, although localized deformation of the SC-2 has occurred.

Equivalent Plastic Strain (EQPS) in the TB-1 vessel is shown in Figure 2-297 to peak at about 20%, but only in some localized outer contact regions with the redwood overpack. The von Mises stresses (see Figure 2-298) peak at 143 ksi, just above the elevated-temperature minimum yield strength for the TB-1 of 141 ksi but more importantly, through-thickness TB-1 stress values are in the 37.5 ksi range, below yield. The time at which the peak value of the von Mises stress occurs coincides with the peak value of the contact force (summed over the lid area). A plot of this force as a function of time is shown in Figure 2-299. A maximum contact load of 31,307 lbs is applied to the inner surface of the TB-1 lid during the impact. No T-Ampoule elements exceeded the tested B-W strain locus, and the peak Tearing Parameter value (see Table 2-11, run #20) of 0.054 was below the critical Tearing Parameter value of 1.012 for Ti-6Al-4V.

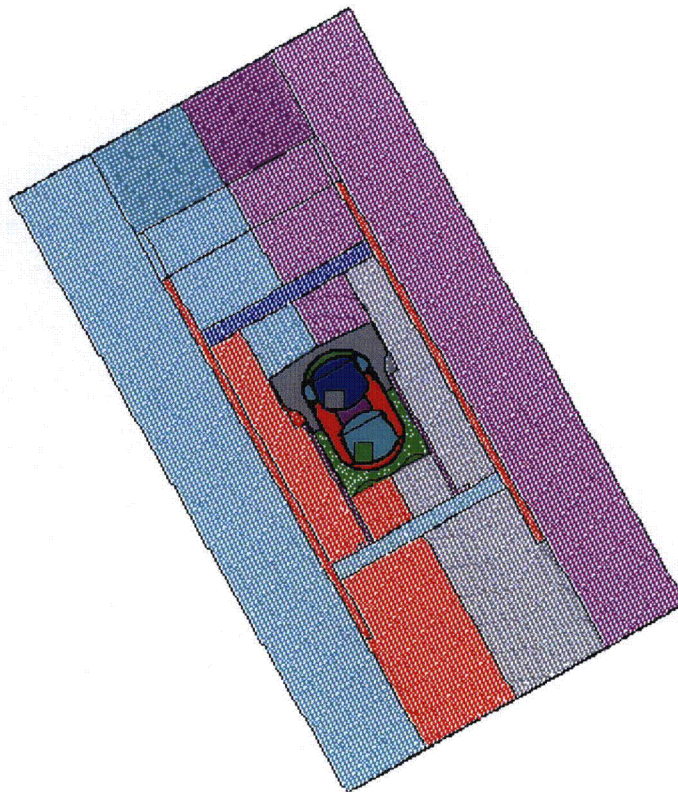


Figure 2-294. Finite Element Mesh for the SC-2, CGOC Impact, 45° Support Structure

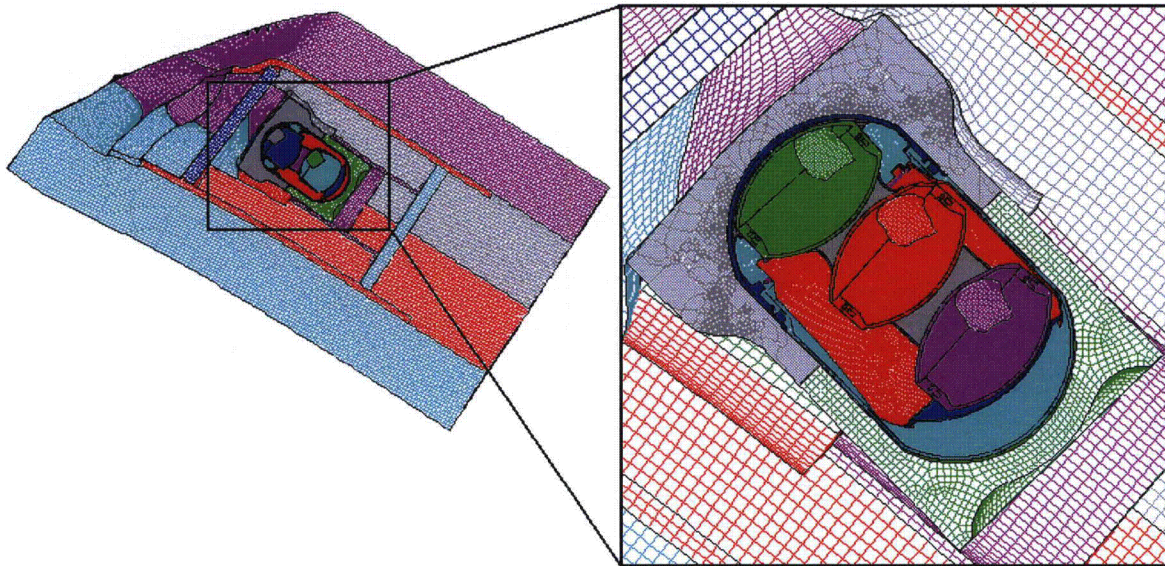


Figure 2-295. Finite Element Mesh for the SC-2, CGOC Impact, 45° Support Structure – Final Displacement

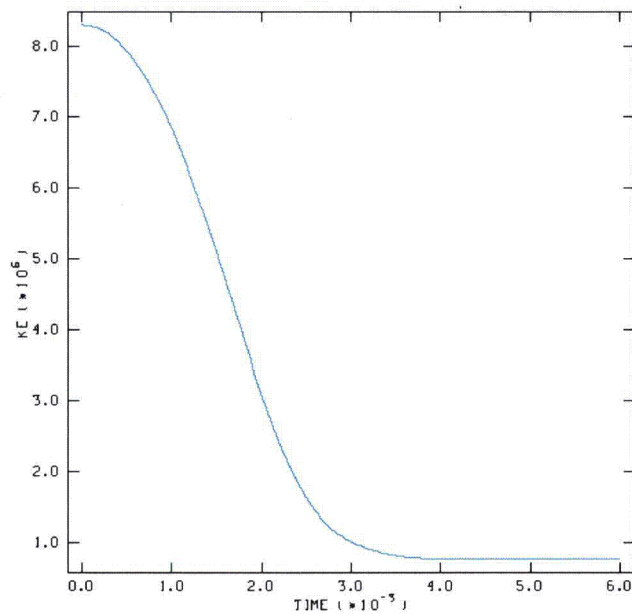


Figure 2-296. Kinetic Energy Time History for the SC-2, CGOC Impact, 45° Support Structure

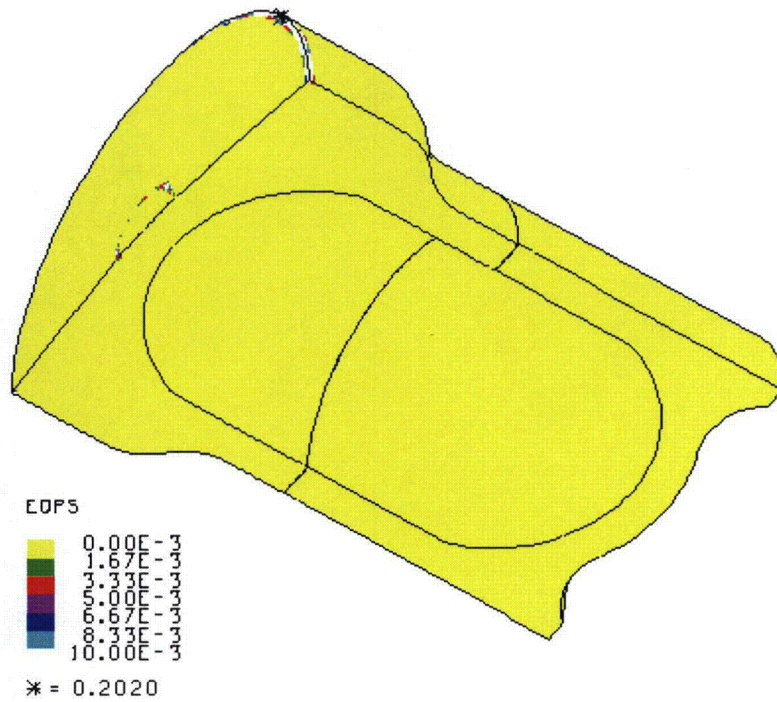


Figure 2-297. Plot of EQPS in the TB-1 for the SC-2, CGOC Impact, 45° Support Structure

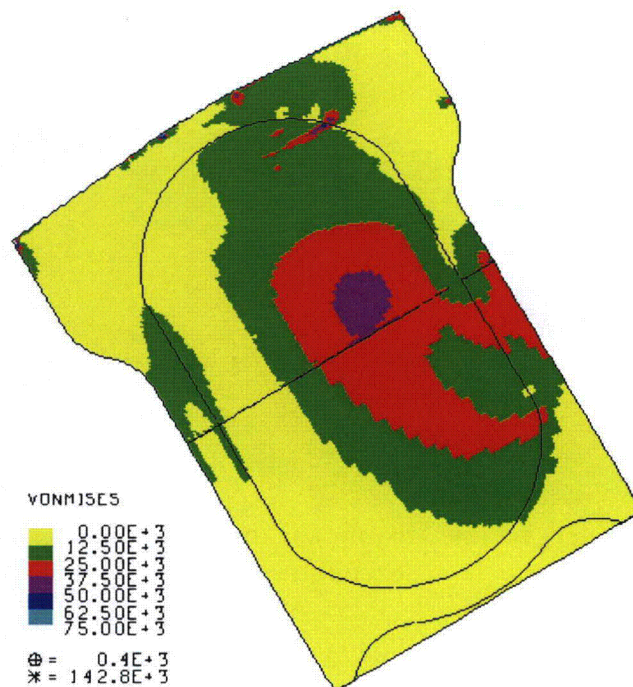


Figure 2-298. Plot of von Mises Stress in the TB-1 for the SC-2, CGOC Impact, 45° Support Structure

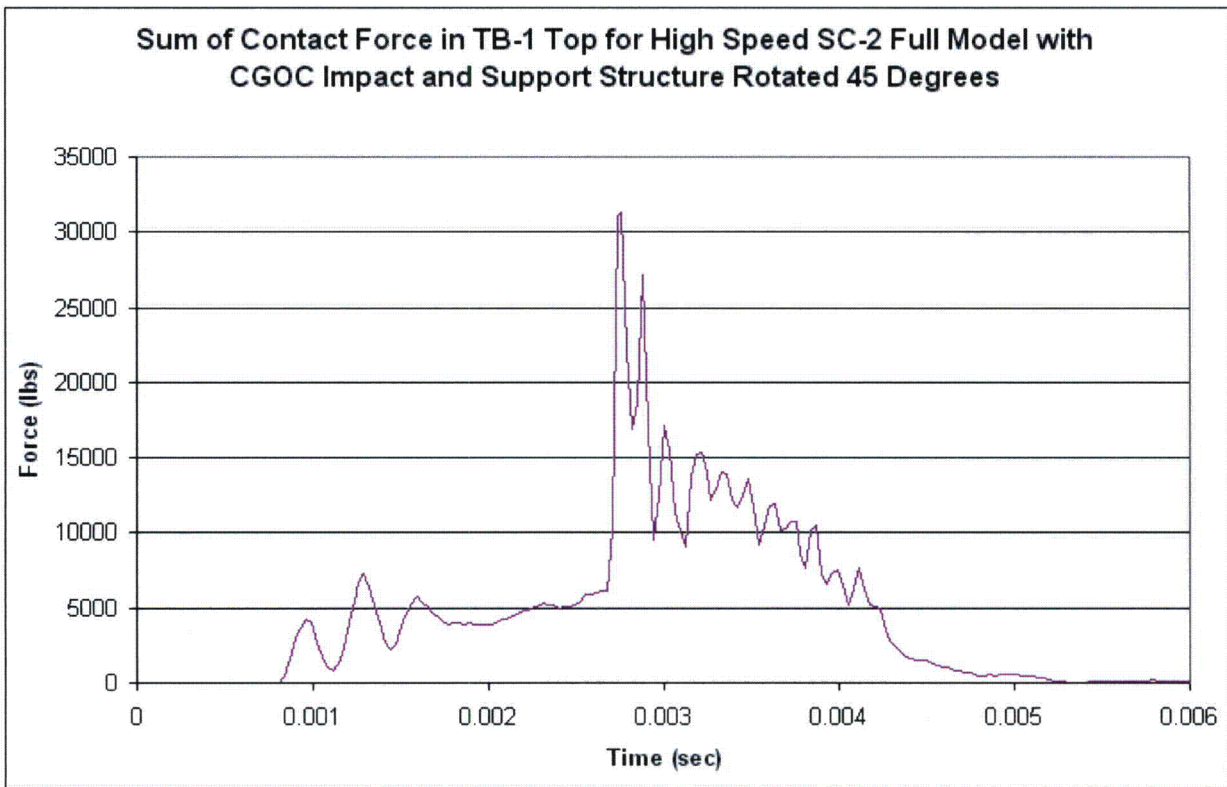


Figure 2-299. Plot of Contact Forces in the TB-1 for the SC-2, CGOC Impact, 45° Support Structure

2.12.5.5.11 Run 21 – SC-1 Sample Container, End Impact, Support Structure 0°, Be Contents

The top end impact model for each SC-1 with a smaller solid cylinder Be composite contents is shown in Figure 2-300. Note that each Be cylinder is located at the bottom of each SC-1 so that its net impact velocity with the top of the T-Ampoule is maximized. Also note that the orientation of each Be cylinder is CG-over-corner so its sharp corner is first to impact the SC-1 and the T-Ampoule. The post-impact deformation is shown in Figure 2-301 and its kinetic energy history in Figure 2-302. The top SC-1 is crushed from the subsequent impacts from the lower SC-1, and its Be contents do not quite locally penetrate its upper wall, which directly impacts the T-Ampoule. Note the relatively smaller deformation of the Be cylinders versus the previous (softer) Pu cylinders.

Equivalent Plastic Strain (EQPS) in the TB-1 vessel is shown in Figure 2-303 to be less than 3%, and only in some localized outer contact regions with the redwood overpack. A very small area of localized internal denting occurs, with plasticity less than 0.05%. The von Mises stresses (see Figure 2-304) peak at 143 ksi, just above the elevated-temperature minimum yield strength for the TB-1 of 141 ksi, but more importantly, through-thickness TB-1 stress values are in the less-than-75 ksi range, below yield. No T-Ampoule elements exceeded the tested B-W strain locus, and the peak Tearing Parameter value (see, Table 2-11 run #21) of 0.0155 was below the critical Tearing Parameter value of 1.012 for Ti-6Al-4V.

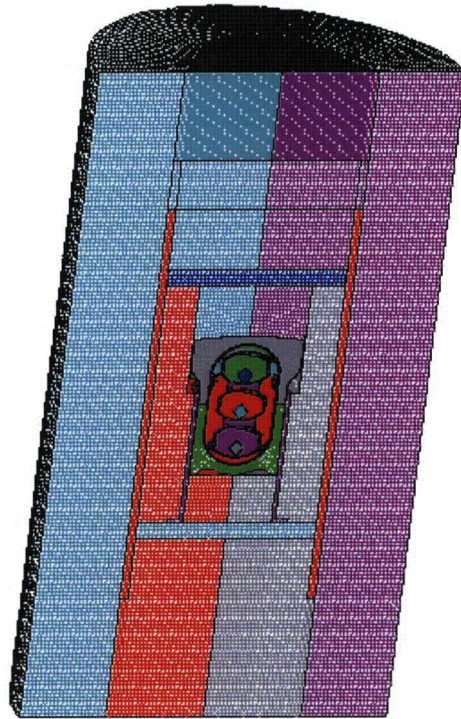


Figure 2-300. Finite Element Mesh for the SC-1, End Impact, 0° Support Structure, Be Contents

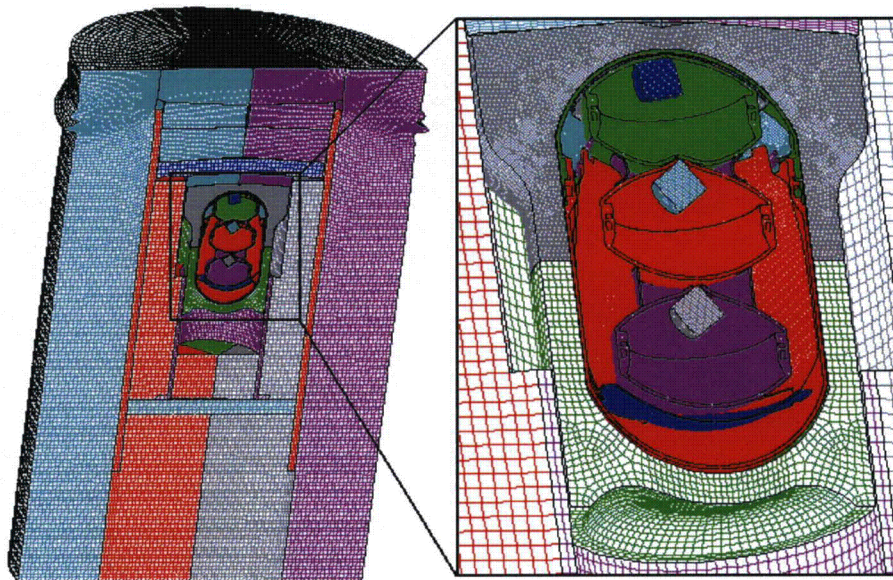


Figure 2-301. Finite Element Mesh for the SC-1, End Impact, 0° Support Structure, Be Contents – Final Displacement

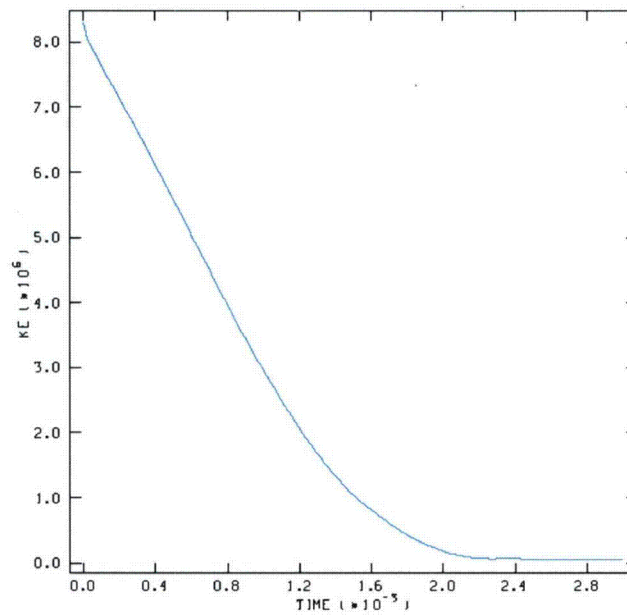


Figure 2-302. Kinetic Energy Time History for the SC-1, End Impact, 0° Support Structure, Be Contents

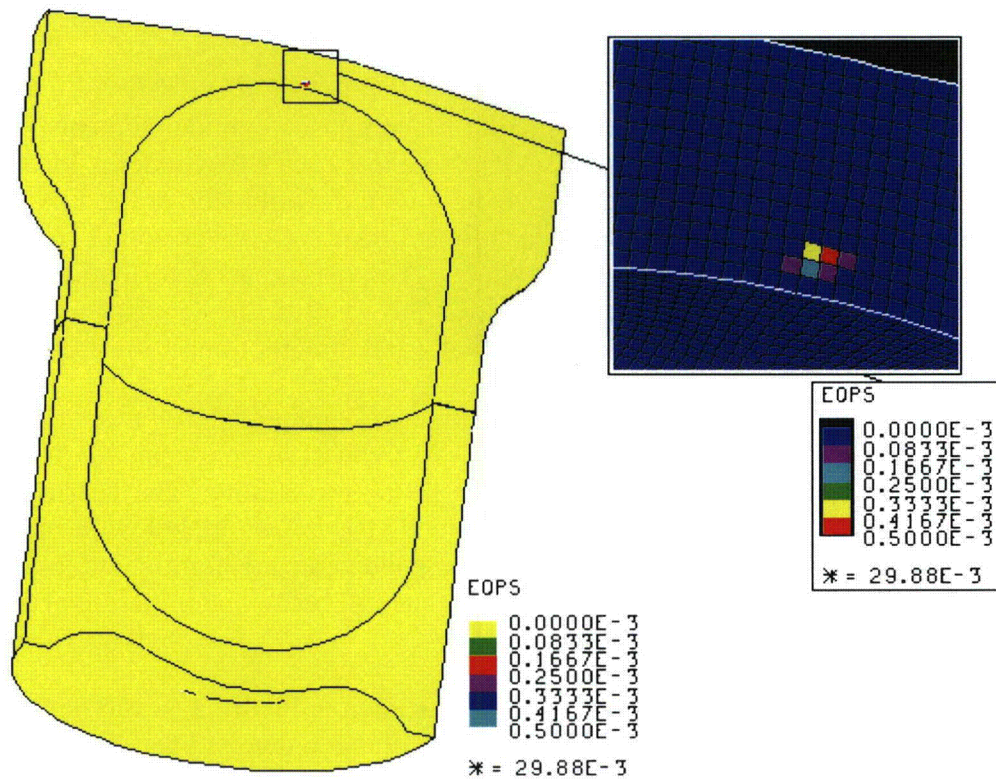


Figure 2-303. Plot of EQPS in the TB-1 for the SC-1, End Impact, 0° Support Structure, Be Contents

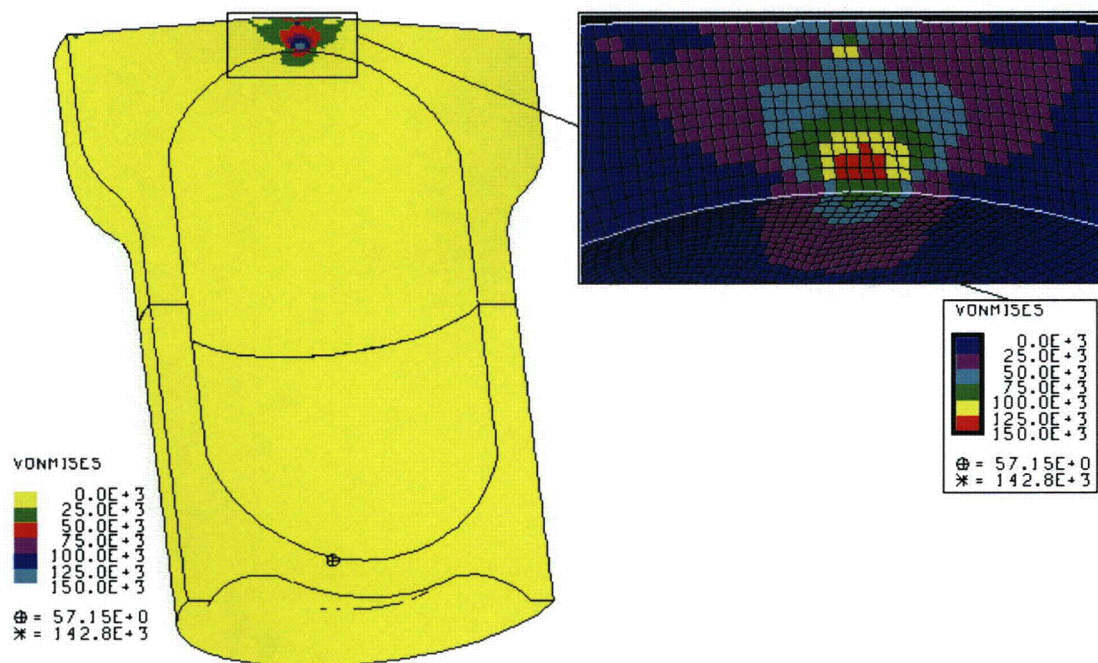


Figure 2-304. Plot of von Mises Stress in the TB-1 for the SC-1, End Impact, 0° Support Structure, Be Contents

2.12.5.5.12 Run 22 – SC-1 Sample Container, Side Impact, Support Structure 0°, Be Contents

The side impact model for each SC-1 with a smaller Be composite cylinder contents (inner cradle rotated 0 degrees) is shown in Figure 2-305. Note that each Be cylinder is located at the far left side of each SC-1 so that its net impact velocity with the right side of the T-Ampoule is maximized. Also note that the orientation of each Be cylinder is CG-over-corner so its sharp corner is first to impact the SC-1 and the T-Ampoule. The post-impact deformation is shown in Figure 2-306 and its kinetic energy history in Figure 2-307. Unlike the heavier Pu cylinders, the lighter Be contents do not penetrate the SC-1 side walls and directly impact the T-Ampoule.

Average stress-triaxiality versus EQPS is shown in Figures 2-308 and 2-309 (zoomed in view) for the 14 elements extending beyond the tested Bao-Wierzbicki strain locus. All of these elements are outside the B-W locus, in a region of high stress triaxiality. The Tearing Parameter values for these same 14 elements are shown in Figure 2-310, and all are below the critical Tearing Parameter value of 1.012 for Ti-6Al-4V. These elements are highlighted in red in Figures 2-311 and 2-312, but note that these elements are still below the initiation of a ductile tear and thus T-Ampoule integrity is maintained.

Equivalent Plastic Strain (EQPS) in the TB-1 vessel is shown in Figure 2-313 to be less than 37%, but only in some localized outer contact regions with the redwood overpack. The EQPS due to internal denting of the upper TB-1 is less than 0.07%, which is nearly elastic. The von Mises stresses (see Figure 2-314) peak at 205 ksi, above the elevated-temperature minimum yield strength for the TB-1 of 141 ksi, but more importantly, through-thickness TB-1 stress values are in the 85 ksi range, below yield.

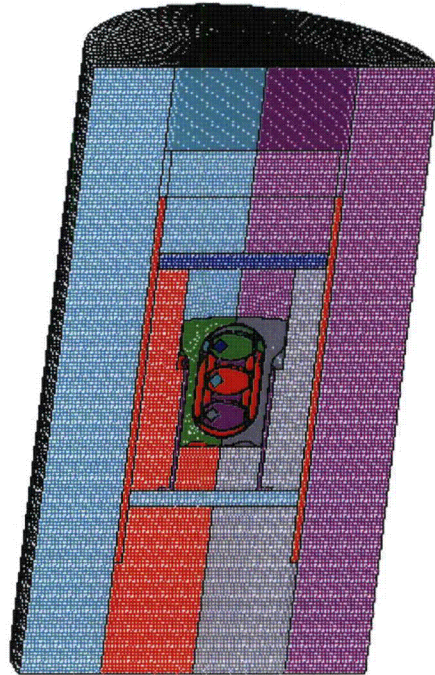


Figure 2-305. Finite Element Mesh for the SC-1, Side Impact, 0° Support Structure, Be Contents

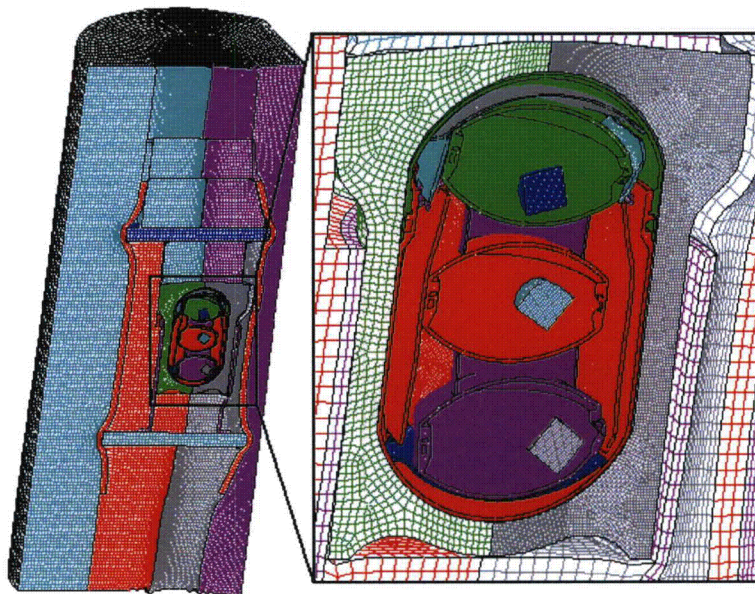


Figure 2-306. Finite Element Mesh for the SC-1, Side Impact, 0° Support Structure, Be Contents - Final Displacement

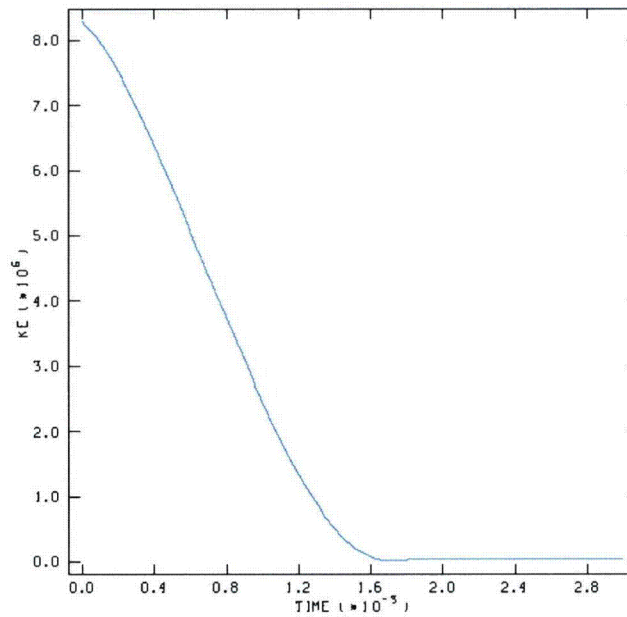


Figure 2-307. Kinetic Energy Time History for the SC-1, Side Impact, 0° Support Structure, Be Contents

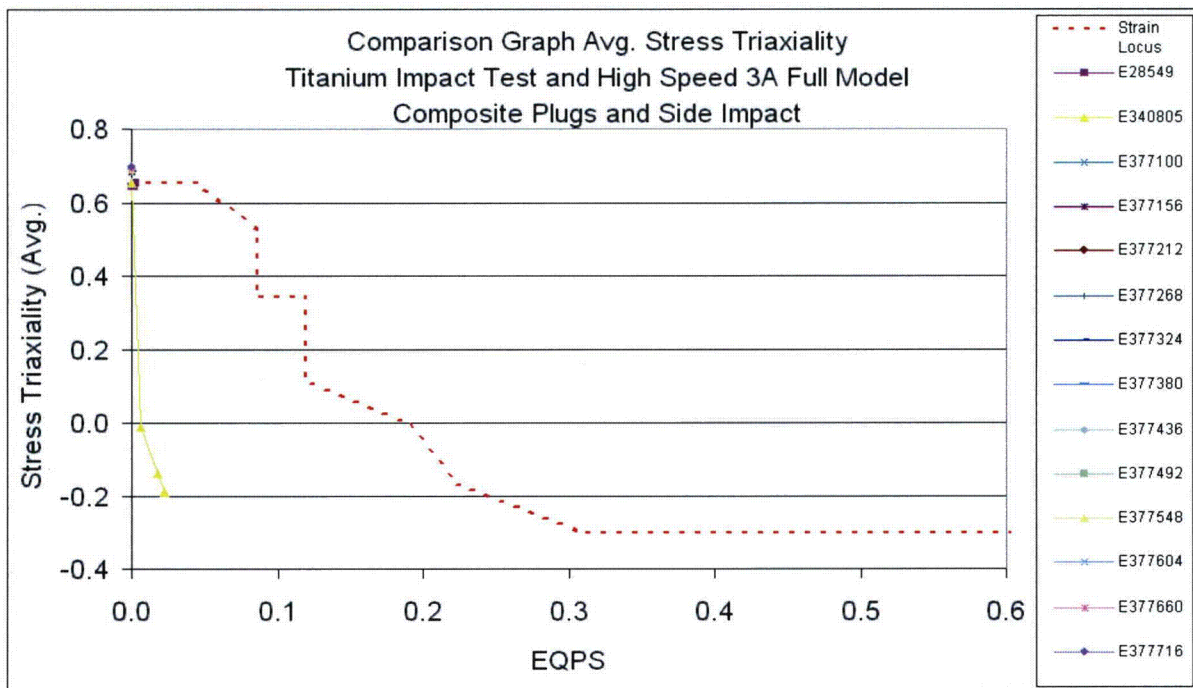


Figure 2-308. Graph of Average Stress Triaxiality versus EQPS of the Elements Exceeding the Experimental Strain Locus for the SC-1, Side Impact, 0° Support Structure, Be Contents

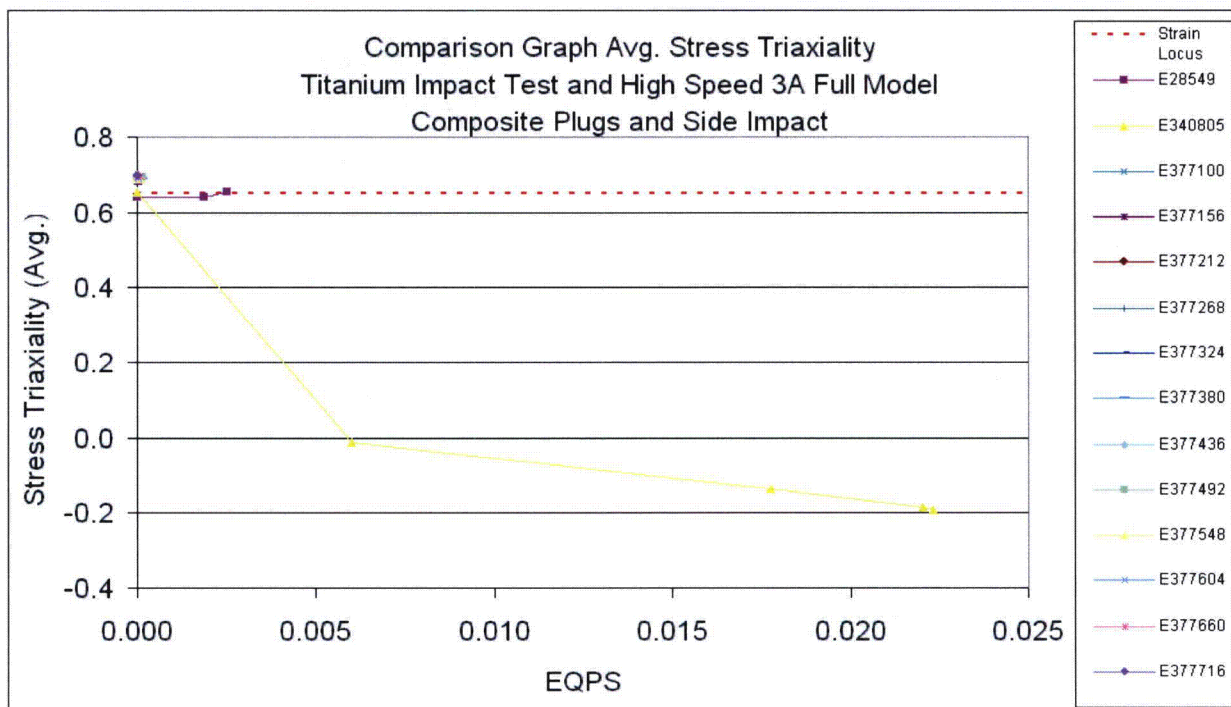


Figure 2-309. Graph of Average Stress Triaxiality versus EQPS of the Elements Exceeding the Experimental Strain Locus (Zoomed In) for the SC-1, Side Impact, 0° Support Structure, Be Contents

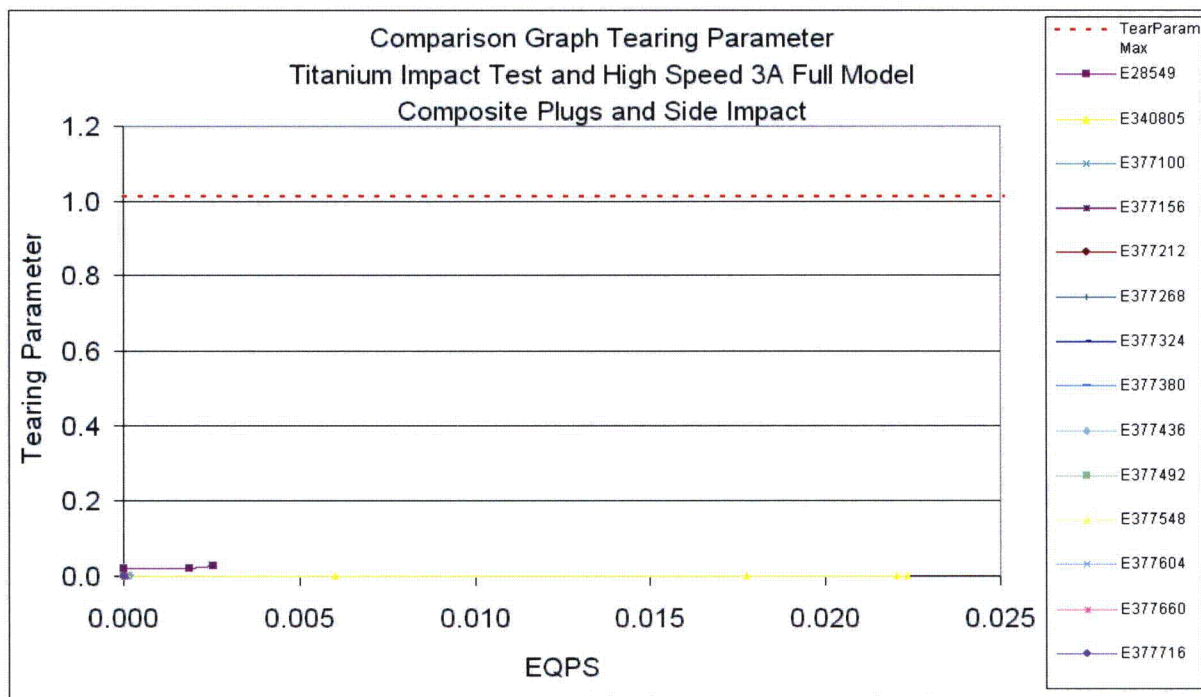


Figure 2-310. Graph of Tearing Parameter versus EQPS of the Elements Exceeding the Experimental Strain Locus for the SC-1, Side Impact, 0° Support Structure, Be Contents

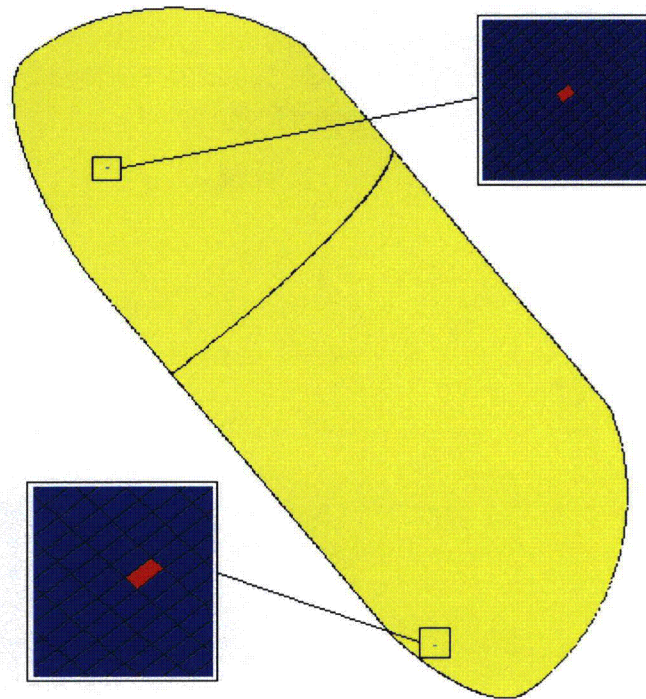


Figure 2-311. Plot of the Elements Exceeding the Experimental Strain Locus for the SC-1, Side Impact, 0° Support Structure, Be Contents

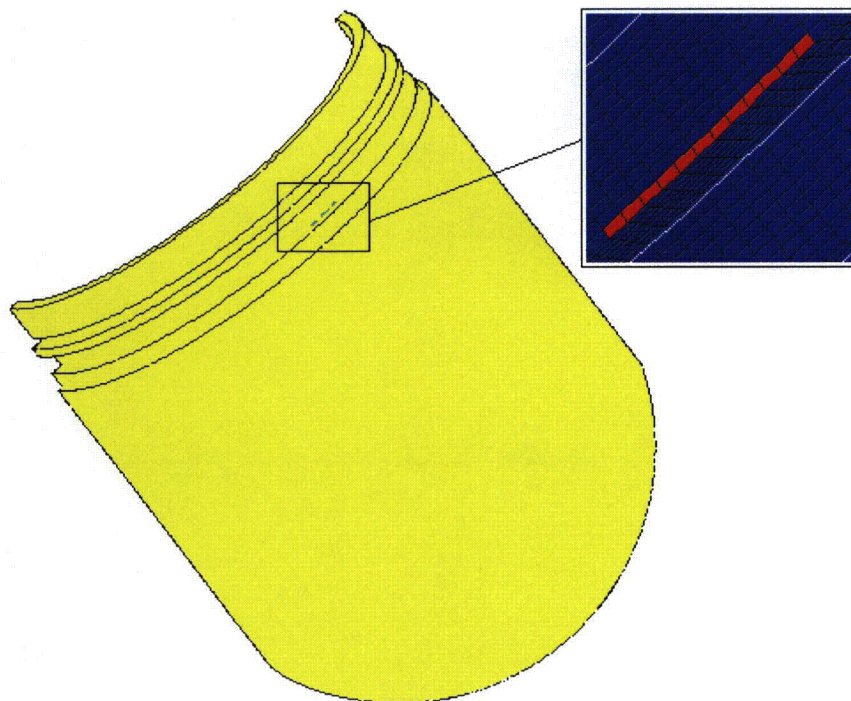


Figure 2-312. Plot of the Elements Exceeding the Experimental Strain Locus for the SC-1, Side Impact, 0° Support Structure, Be Contents

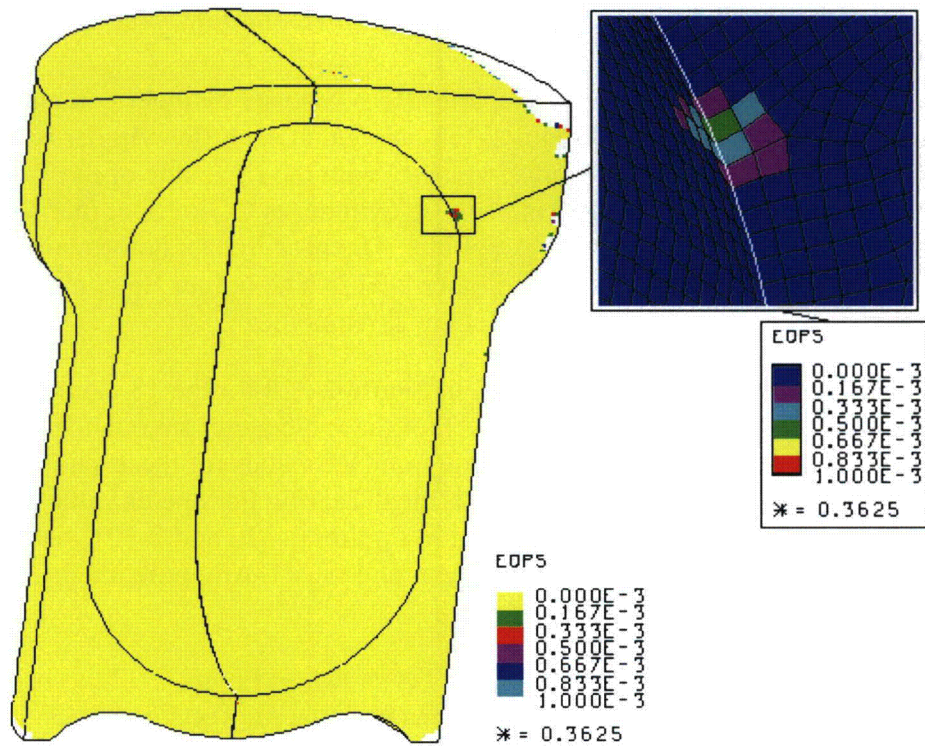


Figure 2-313. Plot of EQPS in the TB-1 for the SC-1, Side Impact, 0° Support Structure, Be Contents

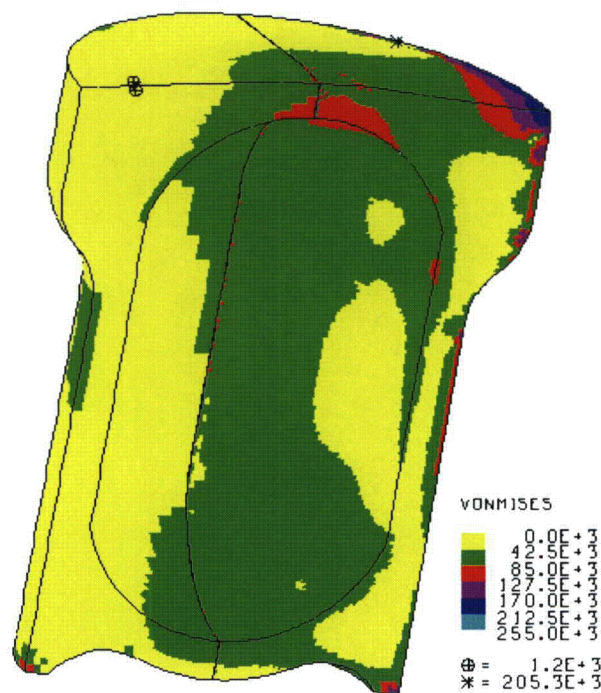


Figure 2-314. Plot of von Mises Stress in the TB-1 for the SC-1, Side Impact, 0° Support Structure, Be Contents

2.12.5.5.13 Run 23 – SC-1 Sample Container, Side Impact, Support Structure 45°, Be Contents

The side impact model for each SC-1 with a smaller Be composite cylinder contents (inner cradle rotated 45 degrees) is shown in Figure 2-315. Note that each Be cylinder is located at the far left side of each SC-1 so that its net impact velocity with the right side of the T-Ampoule is maximized. Also note that the orientation of each Be cylinder is CG-over-corner so its sharp corner is first to impact the SC-1 and the T-Ampoule. The post-impact deformation is shown in Figure 2-316 and its kinetic energy history in Figure 2-317. The lighter Be contents do not penetrate the SC-1 side walls and directly impact the T-Ampoule.

Average stress-triaxiality versus EQPS is shown in Figure 2-318 for the 13 elements extending beyond the tested Bao-Wierzbicki strain locus. All of these elements are outside the B-W locus, in a region of high stress triaxiality. The Tearing Parameter values for these same 13 elements are shown in Figure 2-319, and all are below the critical Tearing Parameter value of 1.012 for Ti-6Al-4V. These elements are highlighted in red in Figures 2-320 and 2-321, but note that these elements are still below the initiation of a ductile tear and thus T-Ampoule integrity is maintained.

Equivalent Plastic Strain (EQPS) in the TB-1 vessel is shown in Figure 2-322 to be less than 28%, but only in some localized outer contact regions with the redwood overpack. The EQPS due to internal denting of the upper TB-1 is less than 0.083%, which is nearly elastic. The von Mises stresses (see Figure 2-323) peak at 206 ksi, above the elevated-temperature minimum yield strength for the TB-1 of 141 ksi, but more importantly, through-thickness TB-1 stress values are in the 75 ksi range, below yield.

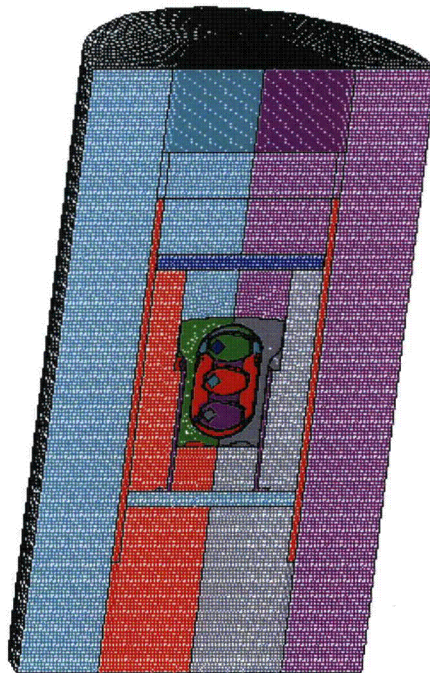


Figure 2-315. Finite Element Mesh for the SC-1, Side Impact, 45° Support Structure, Be Contents

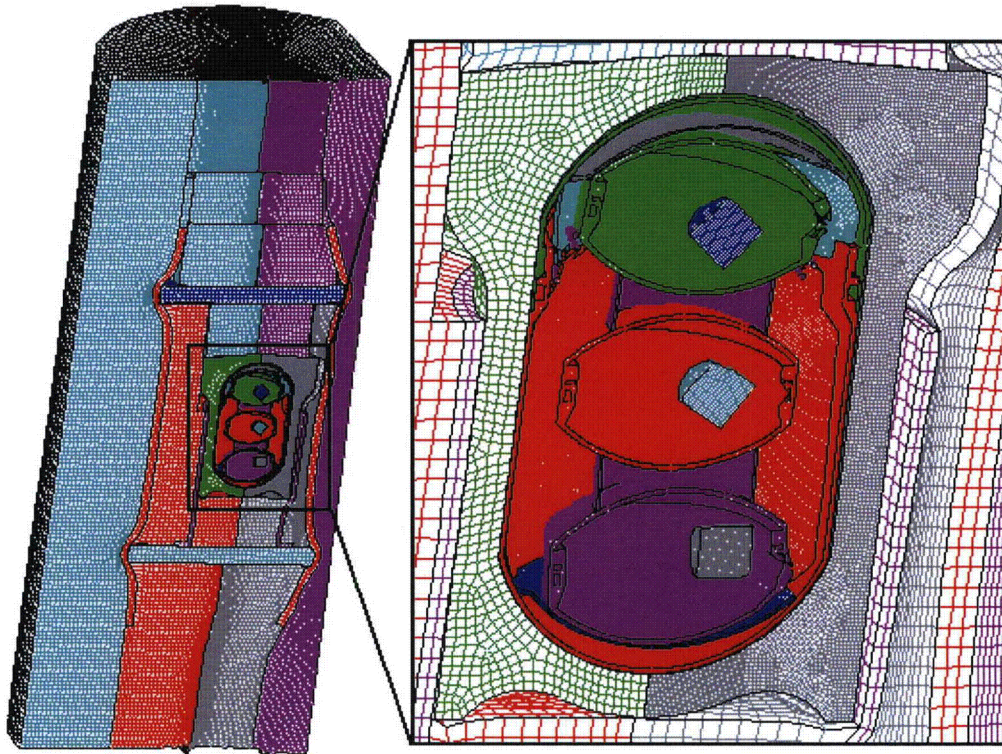


Figure 2-316. Finite Element Mesh for the SC-1, Side Impact, 45° Support Structure, Be Contents – Final Displacement

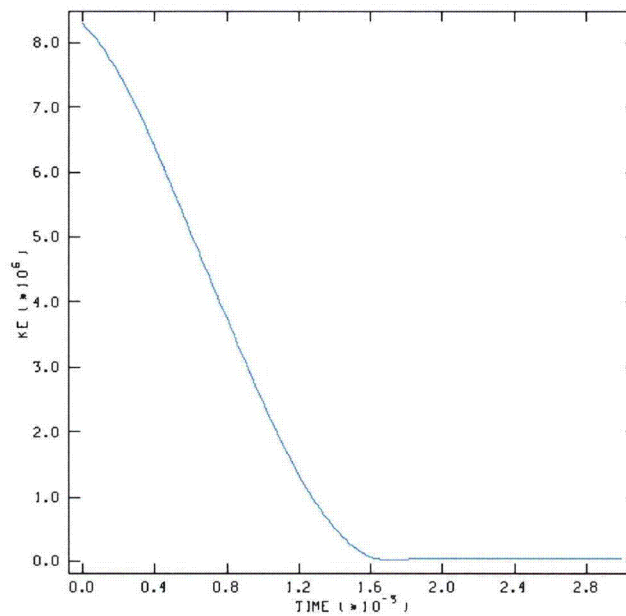


Figure 2-317. Kinetic Energy Time History for the SC-1, Side Impact, 45° Support Structure, Be Contents

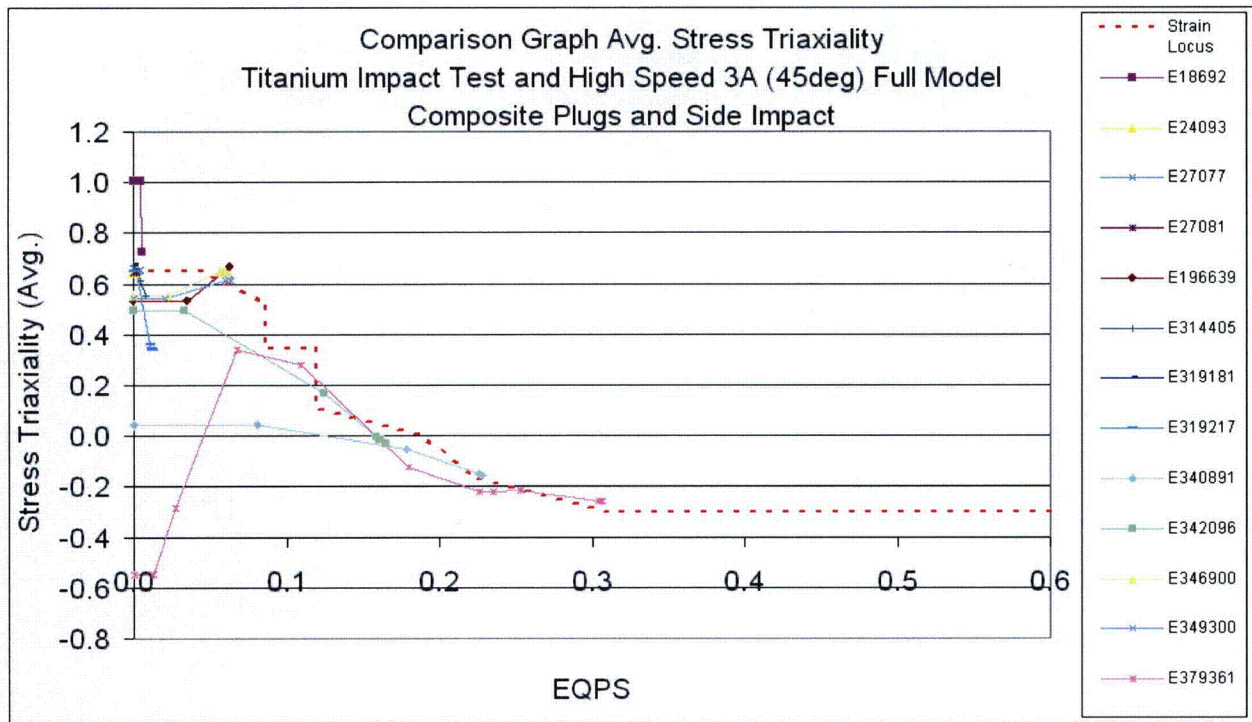


Figure 2-318. Graph of Average Stress Triaxiality versus EQPS of Elements Exceeding the Experimental Strain Locus for the SC-1, Side Impact, 45° Support Structure, Be Contents

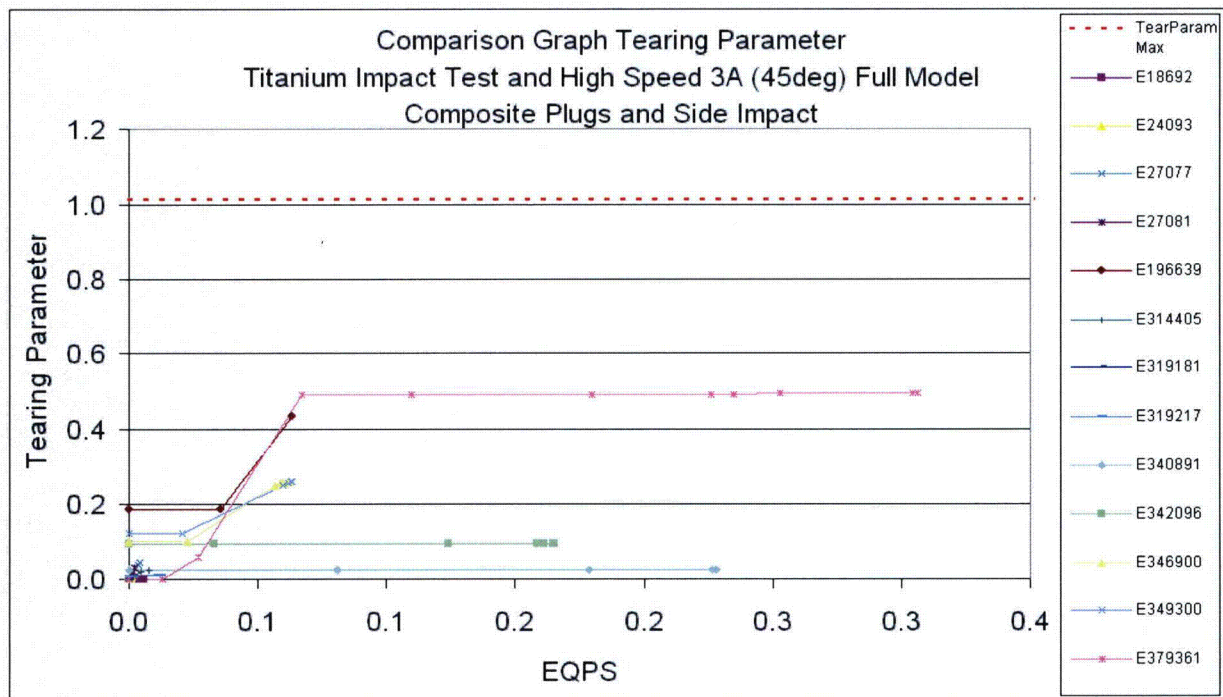


Figure 2-319. Graph of Tearing Parameter versus EQPS of Elements Exceeding the Experimental Strain Locus for the SC-1, Side Impact, 45° Support Structure, Be Contents

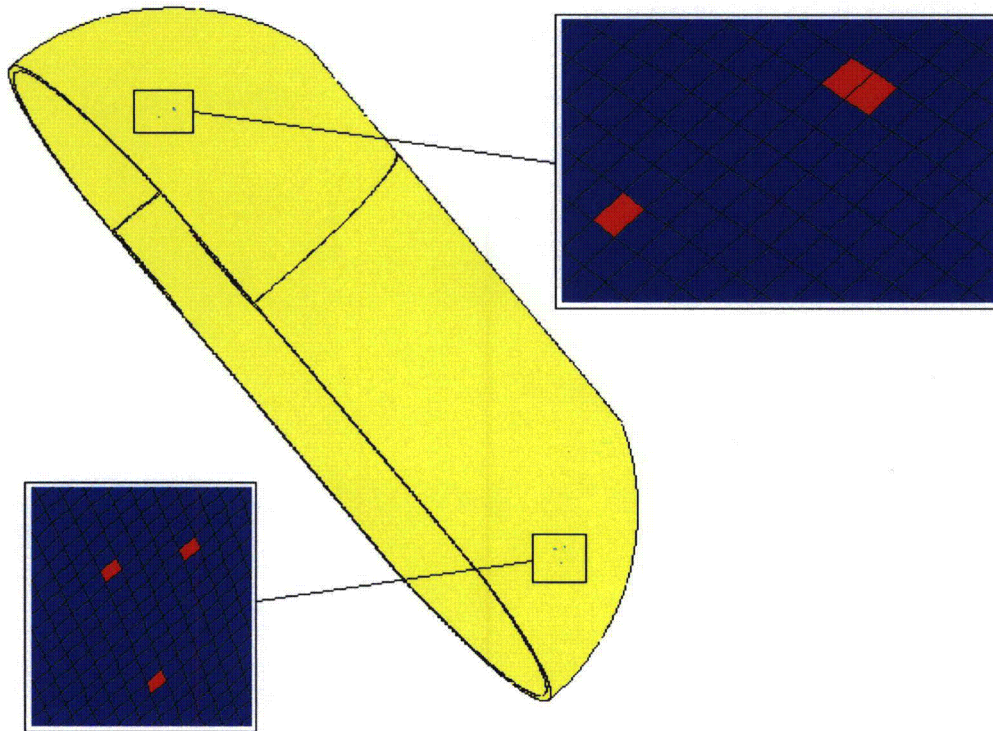


Figure 2-320. Plot of Elements Exceeding the Experimental Strain Locus for the SC-1, Side Impact, 45° Support Structure, Be Contents

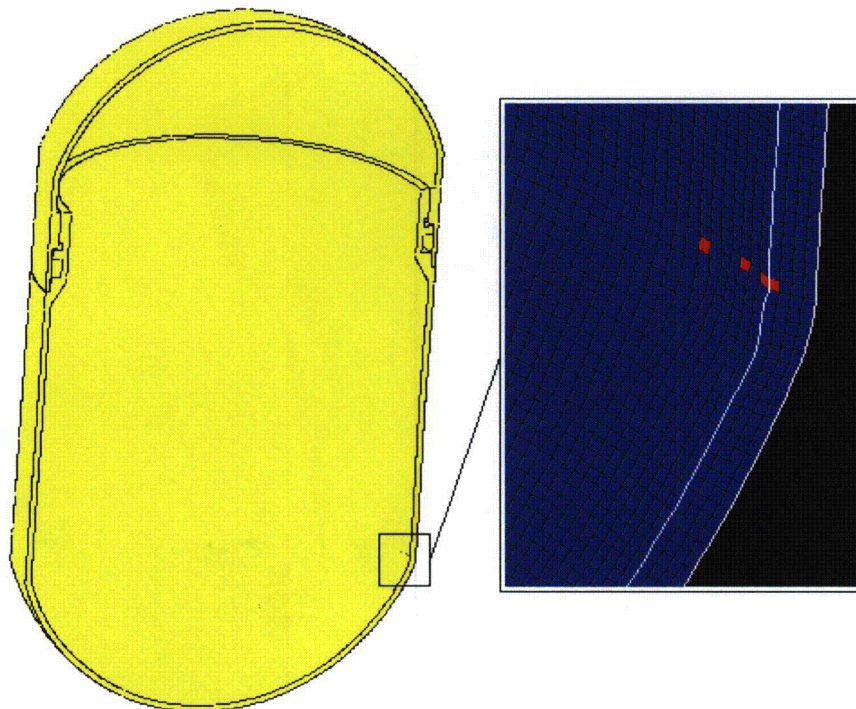


Figure 2-321. Plot of Elements Exceeding the Experimental Strain Locus for the SC-1, Side Impact, 45° Support Structure, Be Contents

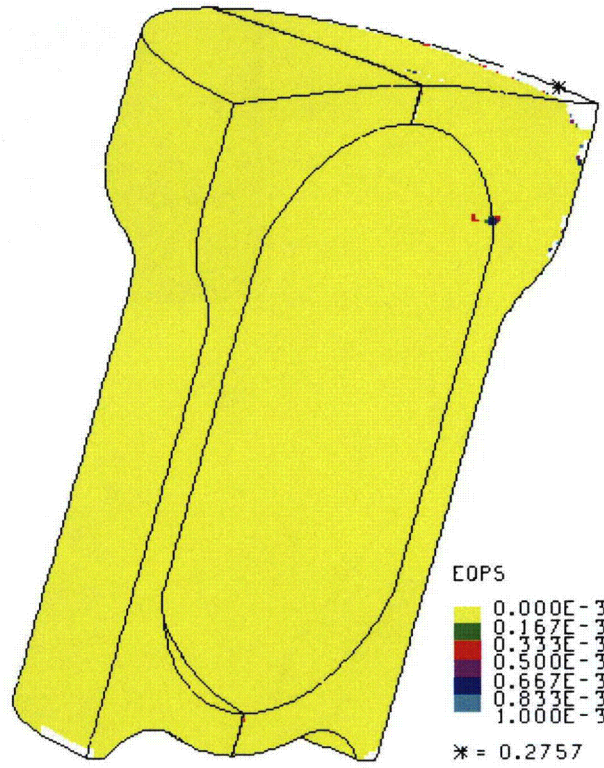


Figure 2-322. Plot of EQPS in the TB-1 for the SC-1, Side Impact, 45° Support Structure, Be Contents

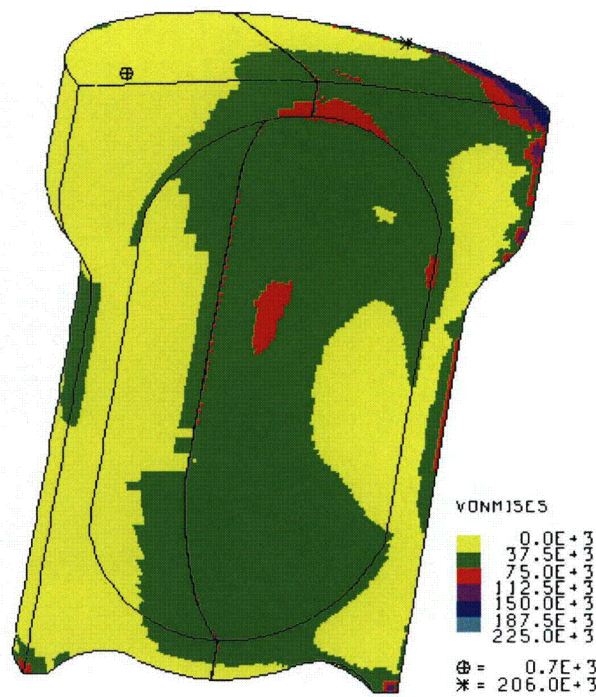


Figure 2-323. Plot of von Mises Stress in the TB-1 for the SC-1, Side Impact, 45° Support Structure, Be Contents

2.12.5.5.14 Run 24 – SC-1 Sample Container, CGOC Impact, Support Structure 0°, Be Contents

The lid end CG-over-corner impact model for each SC-1 with Be composite contents (inner cradle rotated 0 degrees) is shown in Figure 2-324. Each Be cylinder is located at the rotated bottom of each SC-1 so that its net impact velocity with the top of the T-Ampoule is maximized. The post-impact deformation is shown in Figure 2-325 and its kinetic energy history in Figure 2-326. The Be cylinder contents remain largely confined within the SC-1's, although localized deformation of the SC-1's has occurred.

Equivalent Plastic Strain (EQPS) in the TB-1 vessel is shown in Figure 2-327 to peak at about 19%, but only in some localized outer contact regions with the redwood overpack. The von Mises stresses (see Figure 2-328) peak at 181 ksi, just above the elevated-temperature minimum yield strength for the TB-1 of 141 ksi, but more importantly, through-thickness TB-1 stress values are in the 23 ksi range, below yield. No T-Ampoule elements exceeded the tested B-W strain locus, and the peak Tearing Parameter value (see Table 2-11, run #24) of 0.0597 was below the critical Tearing Parameter value of 1.012 for Ti-6Al-4V.

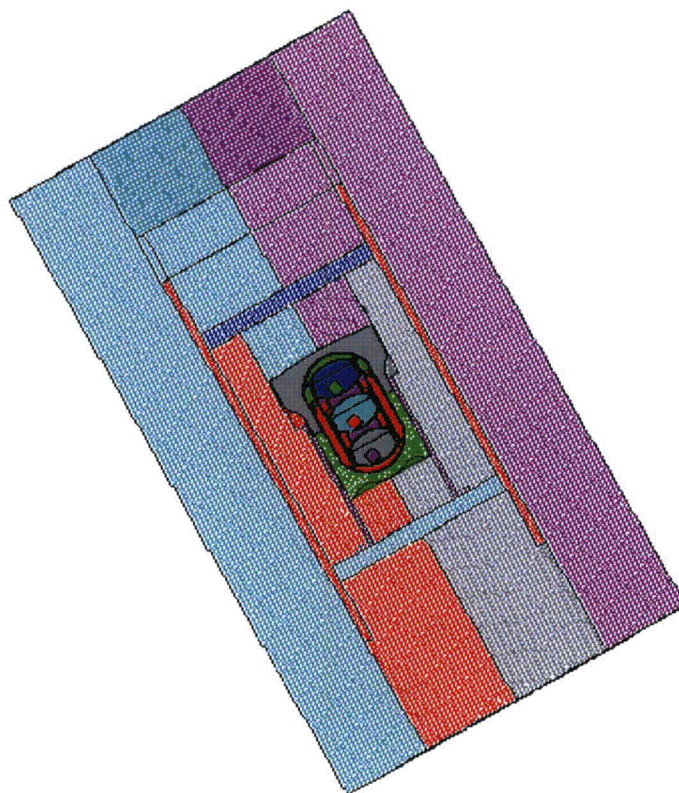


Figure 2-324. Finite Element Mesh for the SC-1, CGOC Impact, 0° Support Structure, Be Contents

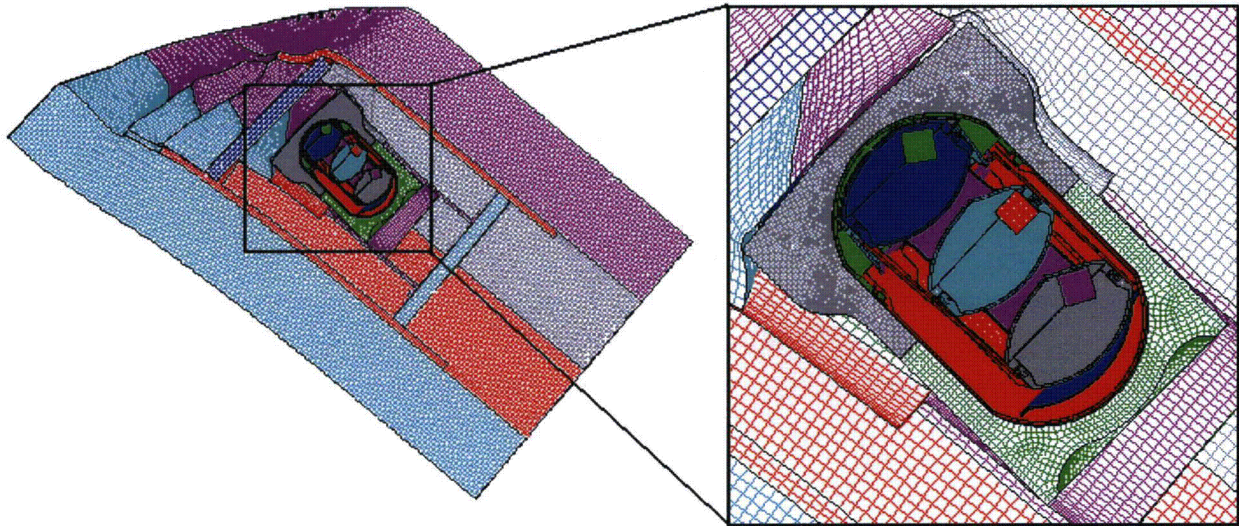


Figure 2-325. Finite Element Mesh for the SC-1, CGOC Impact, 0° Support Structure, Be Contents – Final Displacement

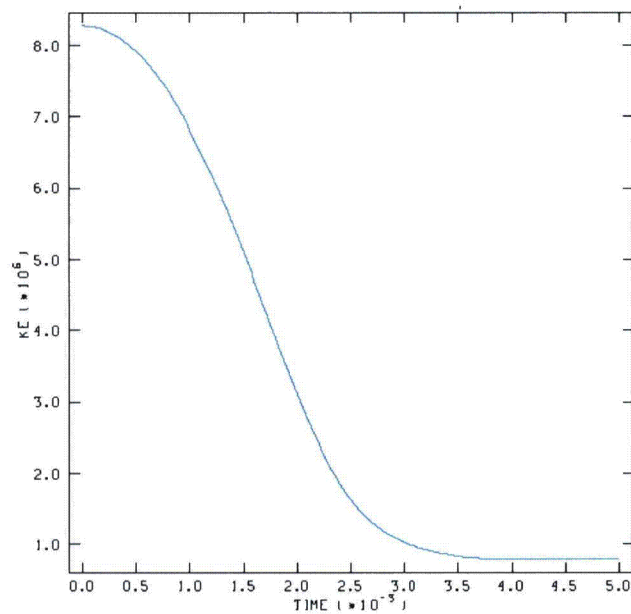


Figure 2-326. Kinetic Energy Time History for the SC-1, CGOC Impact, 0° Support Structure, Be Contents

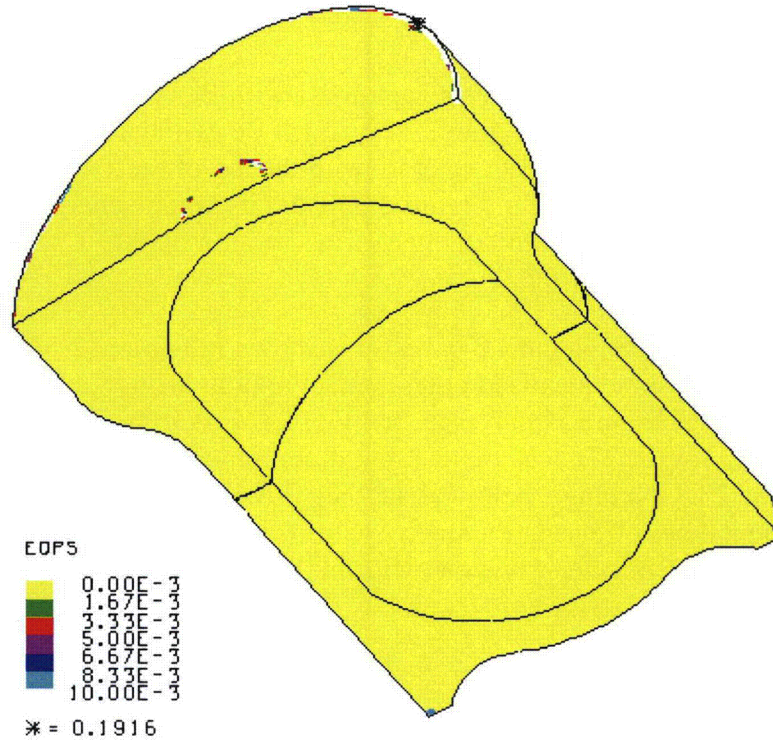


Figure 2-327. Plot of EQPS in the TB-1 for the SC-1, CGOC Impact, 0° Support Structure, Be Contents

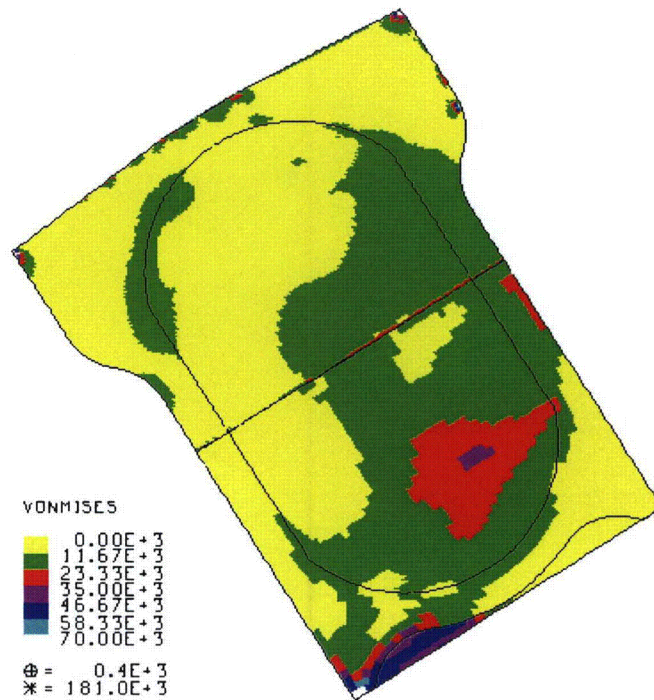


Figure 2-328. Plot of von Mises Stress in the TB-1 for the SC-1, CGOC Impact, 0° Support Structure, Be Contents

2.12.5.5.15 Run 25 – SC-1 Sample Container, CGOC Impact, Support Structure 45°, Be Contents

The lid end CG-over-corner impact model for each SC-1 with Be composite contents (inner cradle rotated 45 degrees) is shown in Figure 2-329. Each Be cylinder is located at the rotated bottom of each SC-1 so that its net impact velocity with the top of the T-Ampoule is maximized. The post-impact deformation is shown in Figure 2-330 and its kinetic energy history in Figure 2-331. The Be cylinder contents remain largely confined within the SC-1's, although localized deformation of the SC-1's has occurred.

Equivalent Plastic Strain (EQPS) in the TB-1 vessel is shown in Figures 2-332 and 2-333 to peak at about 21.3%, but only in some localized outer contact regions with the redwood overpack. The von Mises stresses (see Figure 2-334) peak at 143.3 ksi, just above the elevated-temperature minimum yield strength for the TB-1 of 141 ksi, but more importantly, through-thickness TB-1 stress values are in the 23.3 ksi range, below yield. No T-Ampoule elements exceeded the tested B-W strain locus, and the peak Tearing Parameter value (see Table 2-11, run #25) of 0.1197 was below the critical Tearing Parameter value of 1.012 for Ti-6Al-4V.

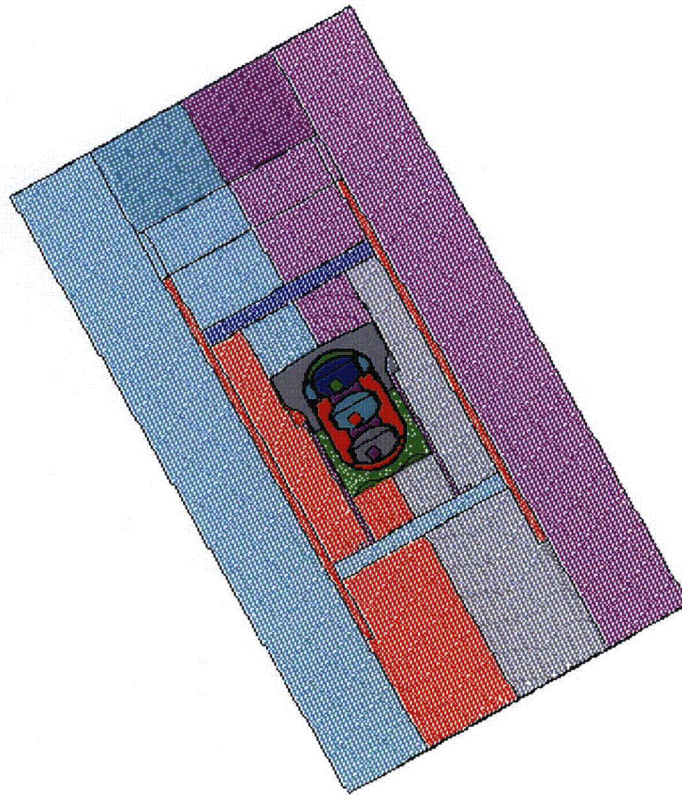


Figure 2-329. Finite Element Mesh for the SC-1, CGOC Impact, 45° Support Structure, Be Contents

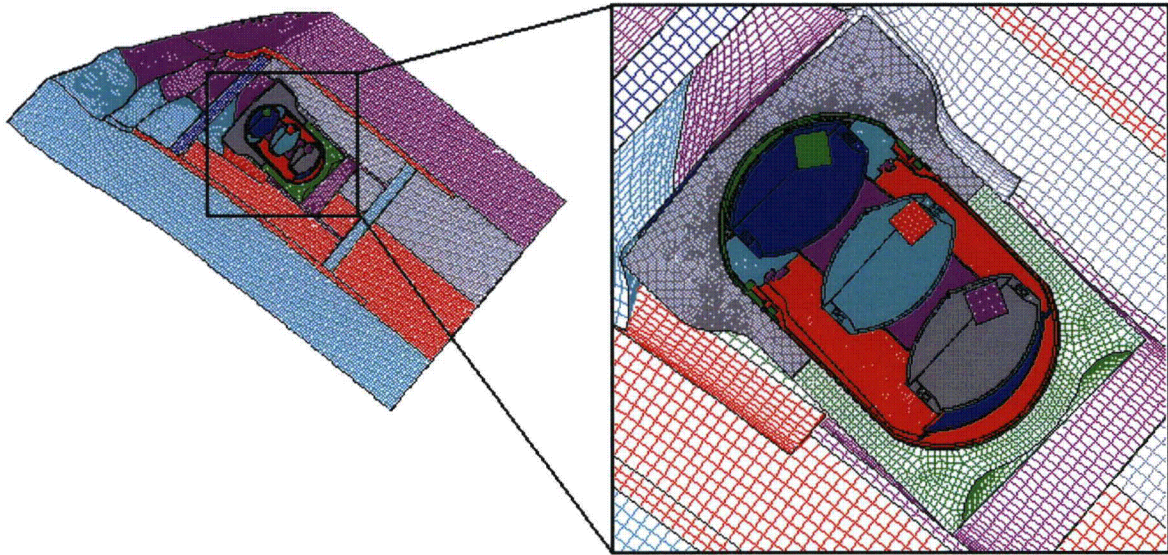


Figure 2-330. Finite Element Mesh for the SC-1, CGOC Impact, 45° Support Structure, Be Contents – Final Displacement

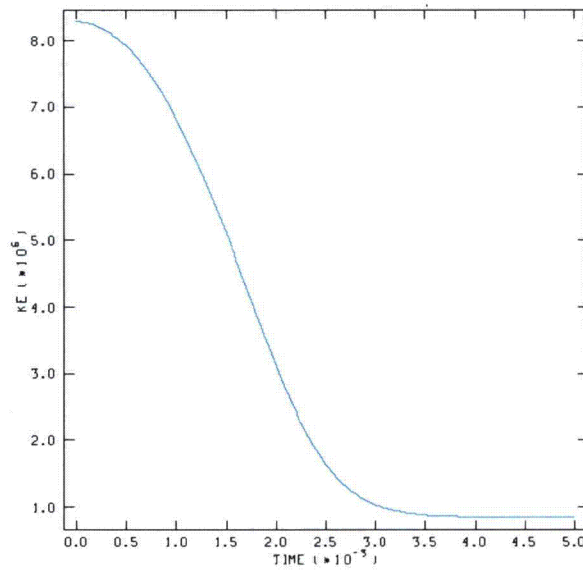


Figure 2-331. Kinetic Energy Time History for the SC-1, CGOC Impact, 45° Support Structure, Be Contents

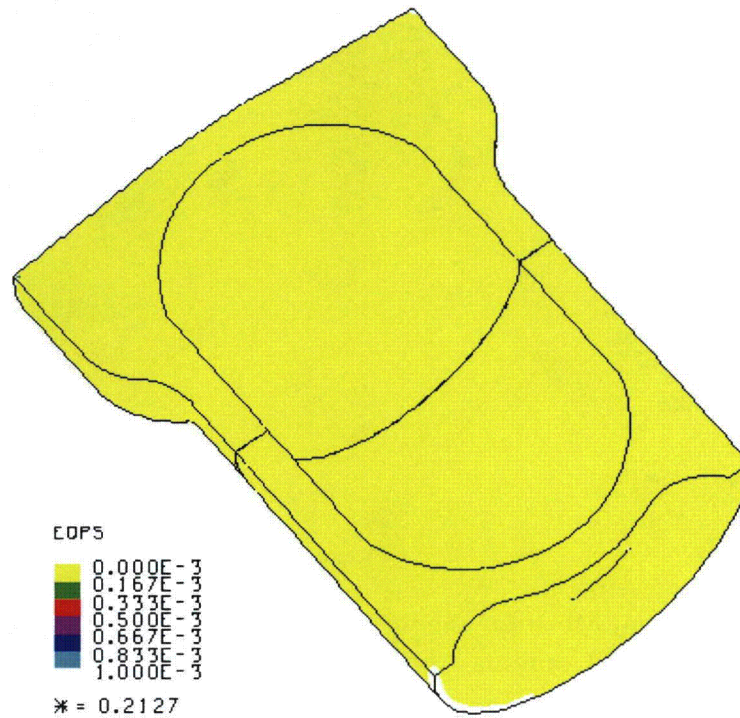


Figure 2-332. Plot of EQPS in the TB-1 for the SC-1, CGOC Impact, 45° Support Structure, Be Contents



Figure 2-333. Plot of EQPS in the TB-1 for the SC-1, CGOC Impact, 45° Support Structure, Be Contents

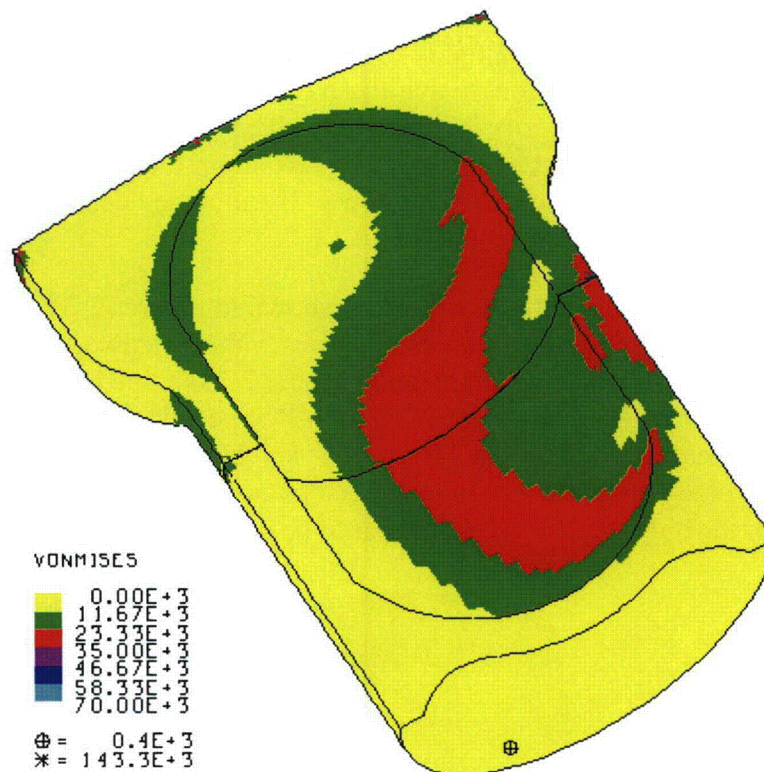


Figure 2-334. Plot of von Mises Stress in the TB-1 for the SC-1, CGOC Impact, 45° Support Structure, Be Contents

2.12.5.5.16 Run 26 – SC-2 Sample Container, Side Impact, Support Structure 45°, Friction 0.4

Two additional analyses were performed to determine the effect of variation in dynamic friction coefficient. The baseline values for all the analyses are 0.30 for dynamic friction and 0.36 for static between each SC and the T-Ampoule, as well as between the Pu cylinders and the T-Ampoule (since they penetrate the SC-2). This analysis was performed increasing the baseline dynamic friction coefficient by 33% to 0.40 (static is the same value). The side impact model for each larger SC-2 with 338 g of delta Pu contents (inner cradle rotated 45 degrees for SC impingement onto sharp cradle edge) was chosen for this parameter study since it produced some element with a relatively high Tearing Parameter value using baseline friction coefficients.

The side impact model with higher friction is shown in Figure 2-335. Note that each Pu cylinder is located at the far left side of each SC-2 so that its net impact velocity with the right side of the T-Ampoule is maximized. The post-impact deformation is shown in Figure 2-336 and its kinetic energy history in Figure 2-337. The Pu contents penetrate each of the SC-2 side walls and directly impact the T-Ampoule.

Average stress-triaxiality versus EQPS is shown in Figure 2-338 for the 73 elements extending beyond the tested Bao-Wierzbicki strain locus (similar to the 82 elements for the 0.3 friction case). All of these elements are outside the B-W locus, for a variety of stress triaxialities, although most of the 580,000 T-Ampoule elements are inside the B-W locus. The Tearing

Parameter values for these same 73 elements are shown in Figure 2-339, and all are below the critical Tearing Parameter value of 1.012 for Ti-6Al-4V. These elements are highlighted in red in Figures 2-340, 2-341, and 2-342, but note that these elements are still below the initiation of a ductile tear and thus T-Ampoule integrity is maintained. The higher friction coefficients produced only slightly fewer elements exceeding the B-W strain locus, and essentially the same peak Tearing Parameter values (~0.5), indicating lower T-Ampoule “deformation” dependence on the friction coefficient at higher friction values.

Equivalent Plastic Strain (EQPS) in the TB-1 vessel is shown in Figures 2-343 and 2-344 to be less than 29%, but only in some localized outer contact regions with the redwood overpack. The EQPS due to internal denting of the upper SC-1 is shown in Figure 2-344 to be less than 0.067%, which is essentially elastic. The von Mises stresses (see Figure 2-345) peak at 226 ksi, above the elevated-temperature minimum yield strength for the TB-1 of 141 ksi, but more importantly, through-thickness TB-1 stress values are in the less-than-120 ksi range, which is below yield. Stresses and strains in the TB-1 for the higher-friction case appear to be similar to the baseline case.

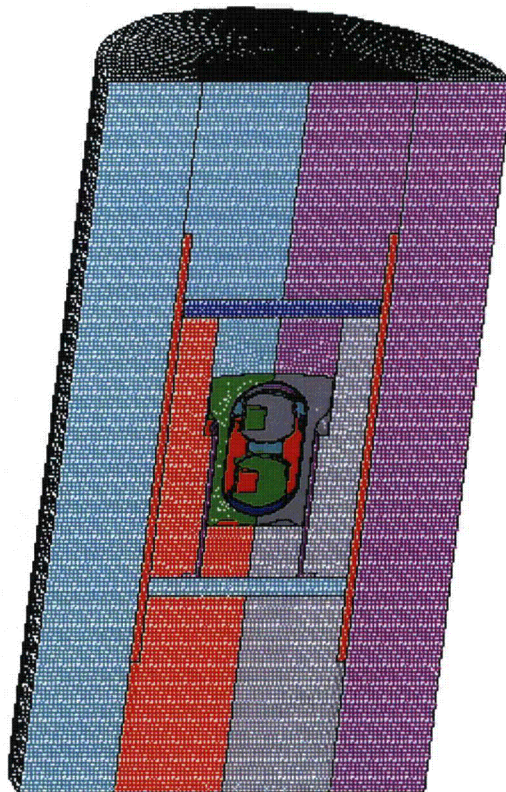


Figure 2-335. Finite Element Mesh for the SC-2, Side Impact, 45° Support Structure, Friction 0.4

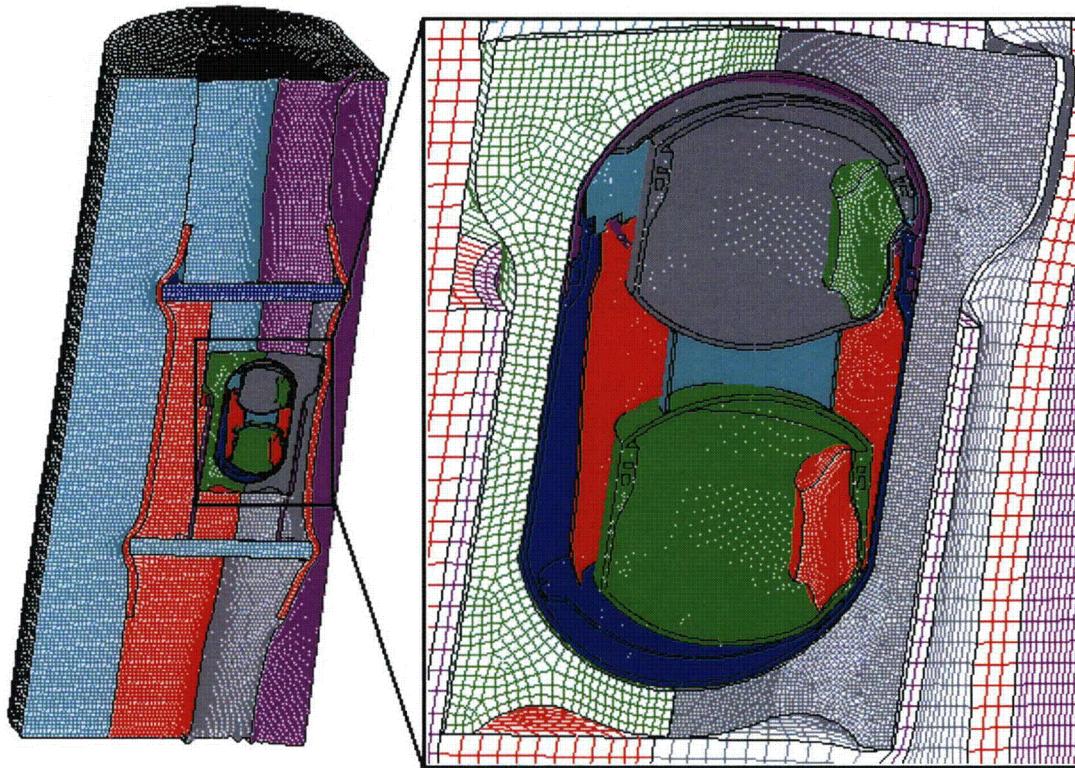


Figure 2-336. Finite Element Mesh for the SC-2, Side Impact, 45° Support Structure, Friction 0.4 – Final Displacement

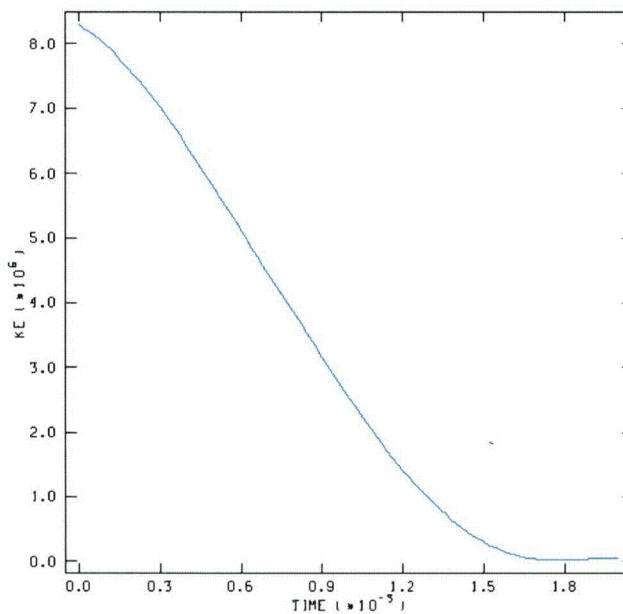


Figure 2-337. Kinetic Energy Time History for the SC-2, Side Impact, 45° Support Structure, Friction 0.4

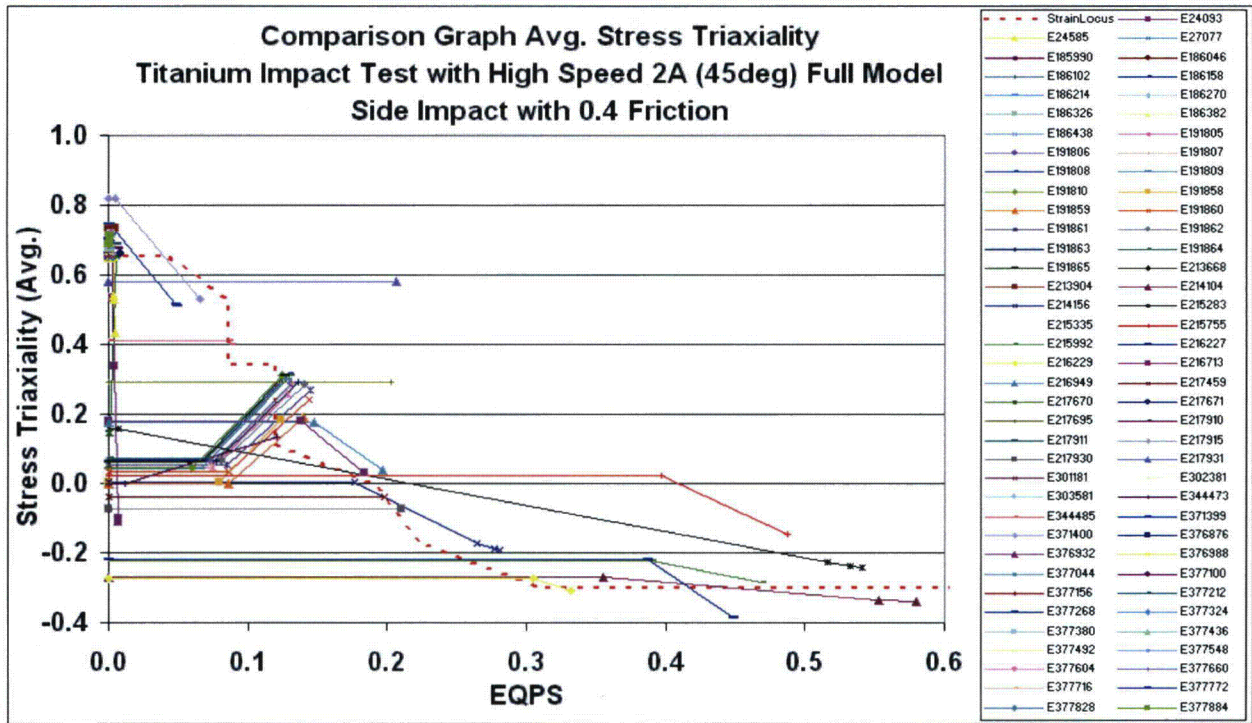


Figure 2-338. Graph of Average Stress Triaxiality versus EQPS of Elements Exceeding the Experimental Strain Locus for the SC-2, Side Impact, 45° Support Structure, Friction 0.4

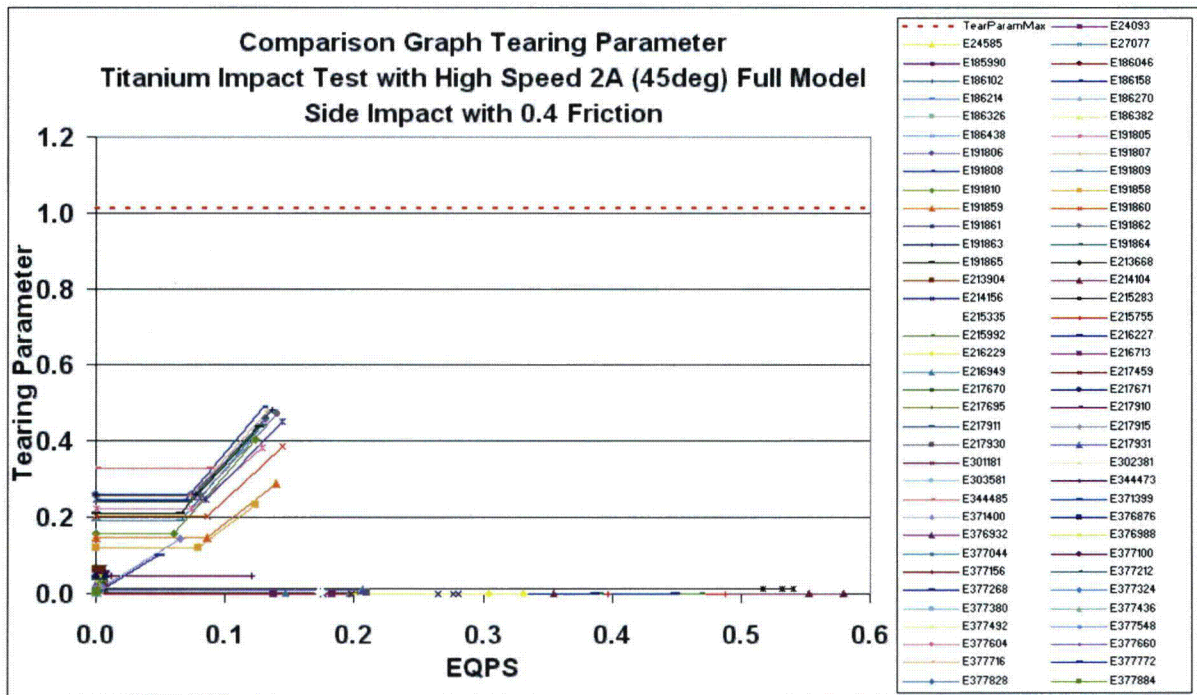


Figure 2-339. Graph of Tearing Parameter versus EQPS of Elements Exceeding the Experimental Strain Locus for the SC-2, Side Impact, 45° Support Structure, Friction 0.4

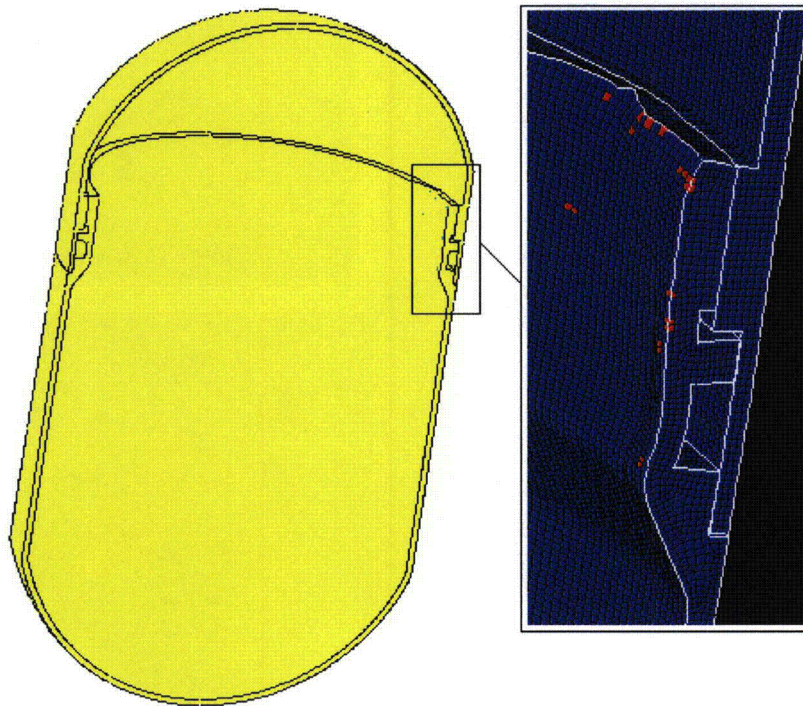


Figure 2-340. Plot of Elements Exceeding the Experimental Strain Locus for the SC-2, Side Impact, 45° Support Structure, Friction 0.4

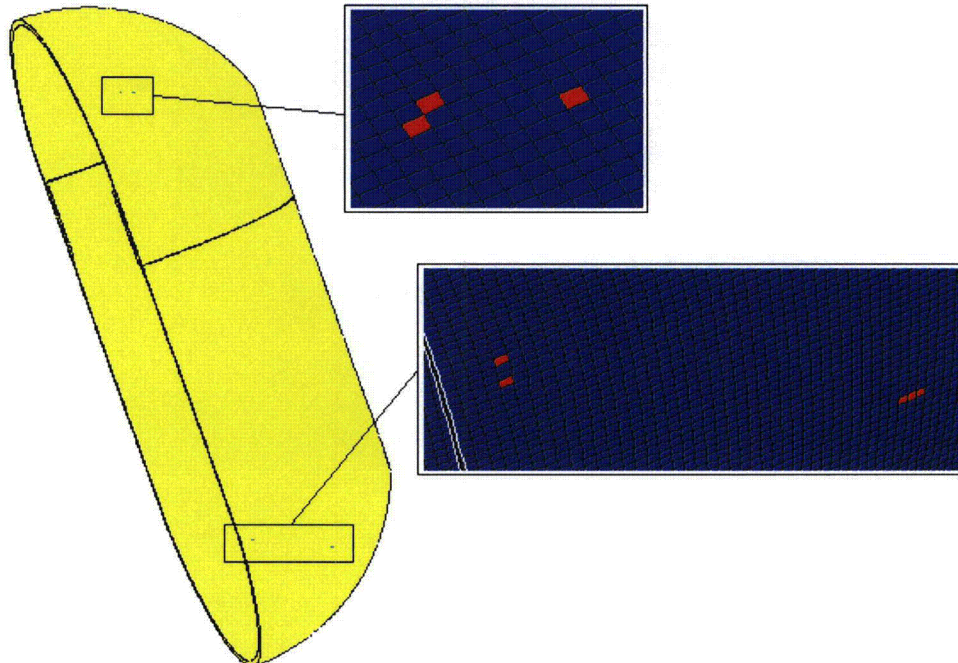


Figure 2-341. Plot of Elements Exceeding the Experimental Strain Locus for the SC-2, Side Impact, 45° Support Structure, Friction 0.4

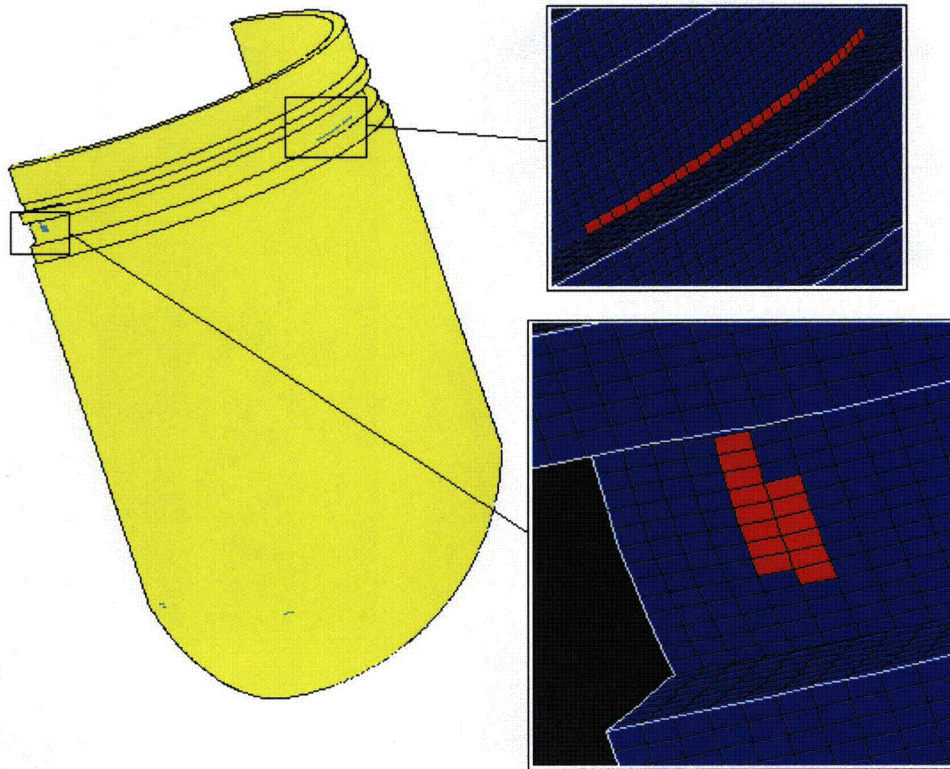


Figure 2-342. Plot of Elements Exceeding the Experimental Strain Locus for the SC-2, Side Impact, 45° Support Structure, Friction 0.4

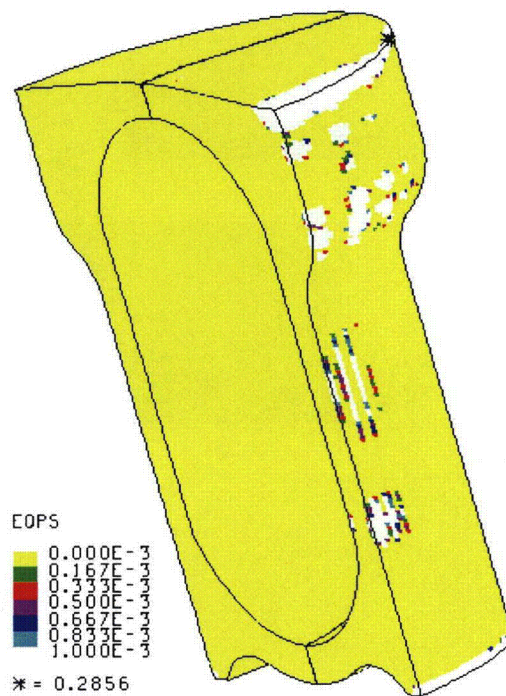


Figure 2-343. Plot of EQPS in the TB-1 for the SC-2, Side Impact, 45° Support Structure, Friction 0.4

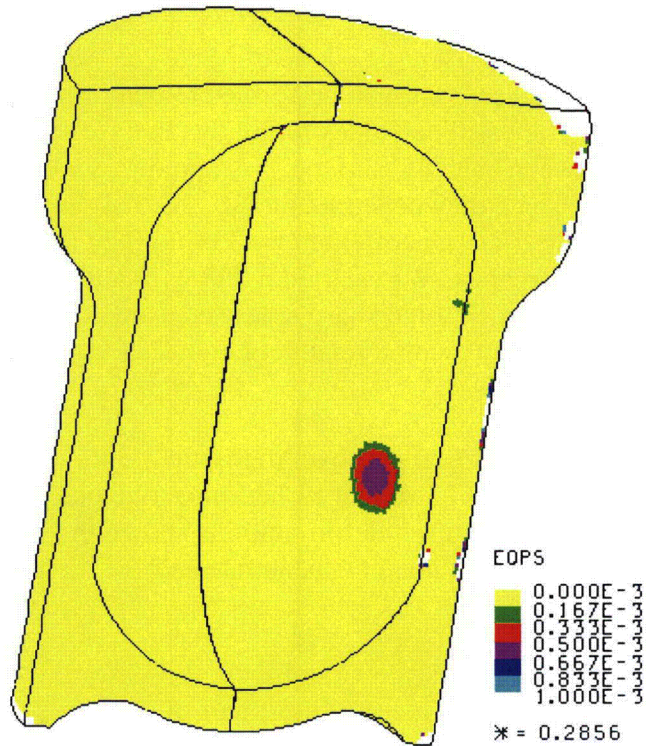


Figure 2-344. Plot of EQPS in the TB-1 for the SC-2, Side Impact, 45° Support Structure, Friction 0.4

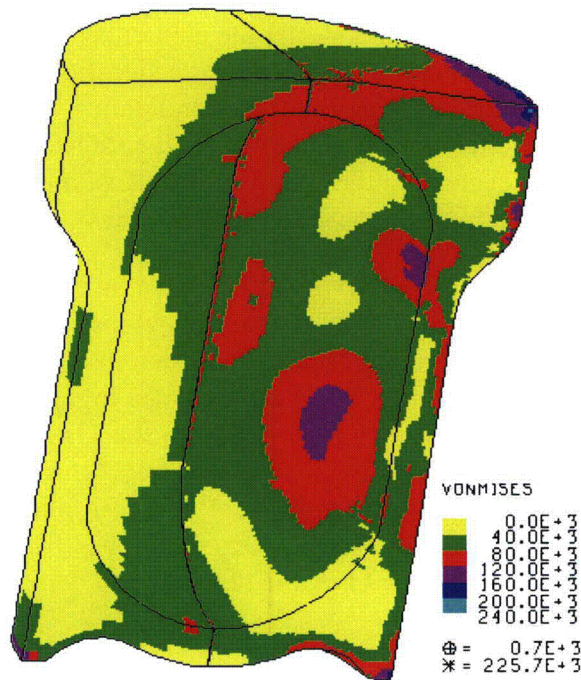


Figure 2-345. Plot of von Mises Stress in the TB-1 for the SC-2, Side Impact, 45° Support Structure, Friction 0.4

2.12.5.5.17 Run 27 – SC-2 Sample Container, Side Impact, Support Structure 45°, Friction 0.2

The second of two additional analyses was also performed to determine the effect of variation in dynamic friction coefficient. The baseline values for all the analyses are 0.30 for dynamic friction and 0.36 for static between each SC and the T-Ampoule, as well as between the Pu cylinders and the T-Ampoule (since they penetrate the SC-2). This analysis was performed decreasing the baseline dynamic friction coefficient by 33% to 0.20 (static is the same value). The side impact model for the larger SC-2's each with 338 g of delta Pu contents (inner cradle rotated 45 degrees for SC impingement onto sharp cradle edge) was chosen for this parameter study since it produced some elements with a relatively high Tearing Parameter value using baseline friction coefficients.

The side impact model with lower friction is shown in Figure 2-346. Note that each Pu cylinder is located at the far left side of each SC-2 so that its net impact velocity with the right side of the T-Ampoule is maximized. The post-impact deformation is shown in Figure 2-347 and its kinetic energy history in Figure 2-348. The Pu contents penetrate each of the SC-2 side walls and directly impact the T-Ampoule.

Average stress-triaxiality versus EQPS is shown in Figure 2-349 for the 49 elements extending beyond the tested Bao-Wierzbicki strain locus (almost half of that for the 0.3 friction case). All of these elements are outside the B-W locus, for a variety of stress triaxialities, although most of the 580,000 T-Ampoule elements are inside the B-W locus. The Tearing Parameter values for these same 49 elements are shown in Figure 2-350, and all are below the critical Tearing Parameter value of 1.012 for Ti-6Al-4V. These elements are highlighted in red in Figures 2-351 and 2-352, but note that these elements are still below the initiation of a ductile tear and thus T-Ampoule integrity is maintained. Fewer T-Ampoule elements extended beyond the B-W locus with lower friction, and the Tearing Parameter values were significantly lower (~0.1 vs. ~0.5, peak), so reducing friction generally decreases the traction loading and deformation in the T-Ampoule. Although the zero-friction case was not included here because it is not realistic, there were zero T-Ampoule elements exceeding the tested strain locus, indicating a high T-Ampoule "deformation" dependence on the friction coefficient at lower friction values.

Equivalent Plastic Strain (EQPS) in the TB-1 vessel is shown in Figures 2-353 and 2-354 to be less than 20.2%, but only in some localized outer contact regions with the redwood overpack. The EQPS due to internal denting of the upper SC-1 is shown in Figure 2-354 to be less than 0.0833%, which is nearly elastic. The von Mises stresses (see Figure 2-355) peak at 225 ksi, above the elevated-temperature minimum yield strength for the TB-1 of 141 ksi, but more importantly, through-thickness TB-1 stress values are in the less-than-120 ksi range, which is below yield. Stresses and strains in the TB-1 appear relatively similar to the baseline and higher-friction analyses. From this lower-friction analysis and the higher-friction analysis, there does not appear to be a strong TB-1 stress or T-Ampoule deformation dependency on friction, at least in the nominal plus/minus 33% range.

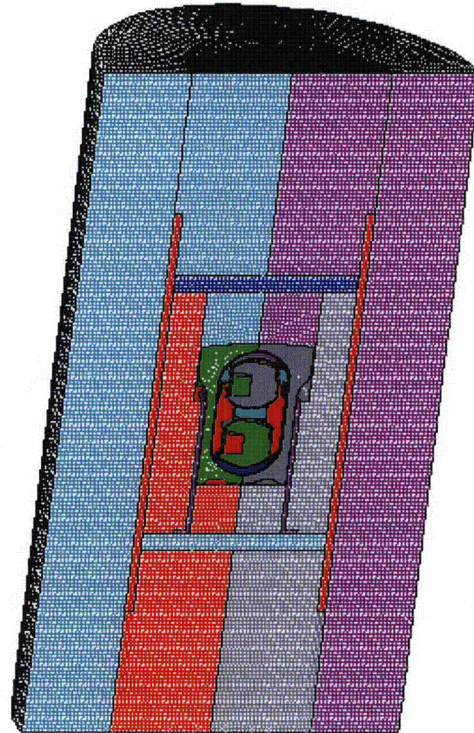


Figure 2-346. Finite Element Mesh for the SC-2, Side Impact, 45° Support Structure, Friction 0.2

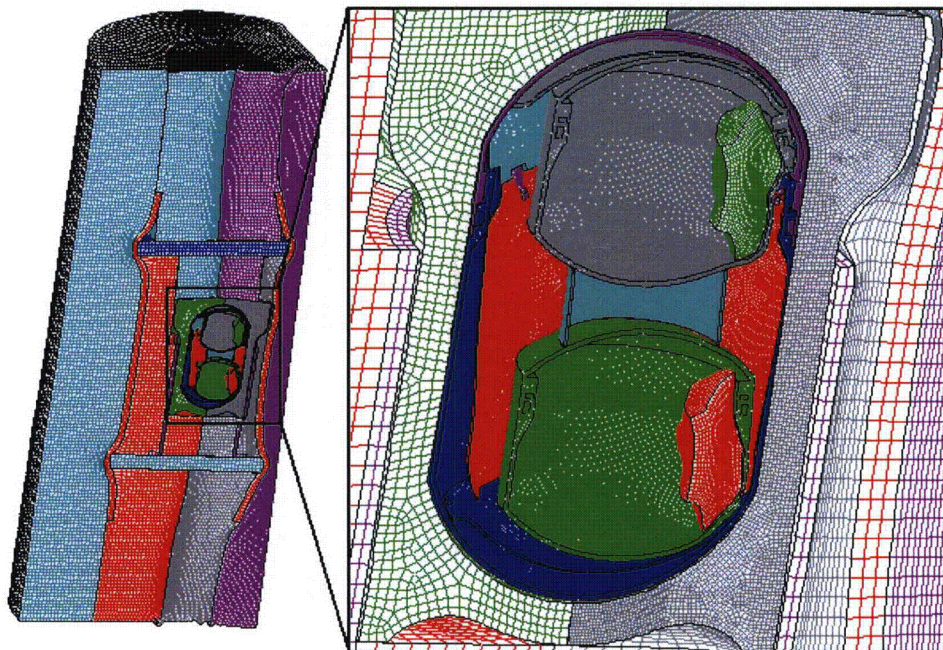


Figure 2-347. Finite Element Mesh for the SC-2, Side Impact, 45° Support Structure, Friction 0.2 – Final Displacement

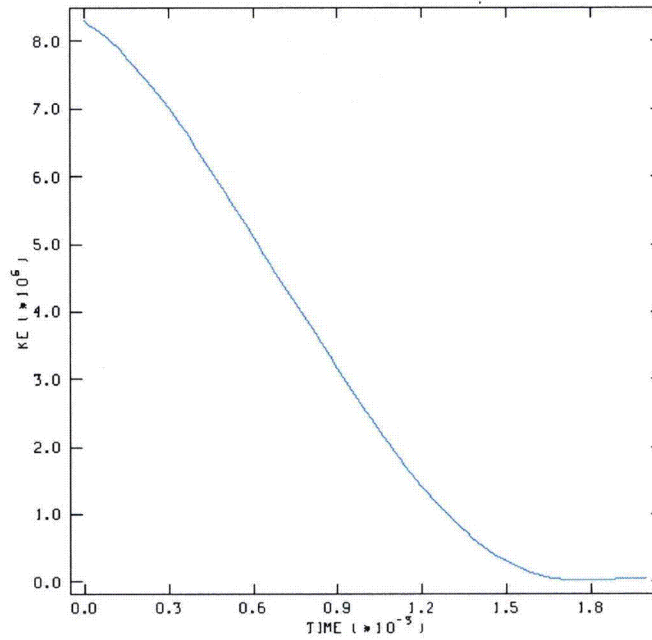


Figure 2-348. Kinetic Energy Time History for the SC-2, Side Impact, 45° Support Structure, Friction 0.2

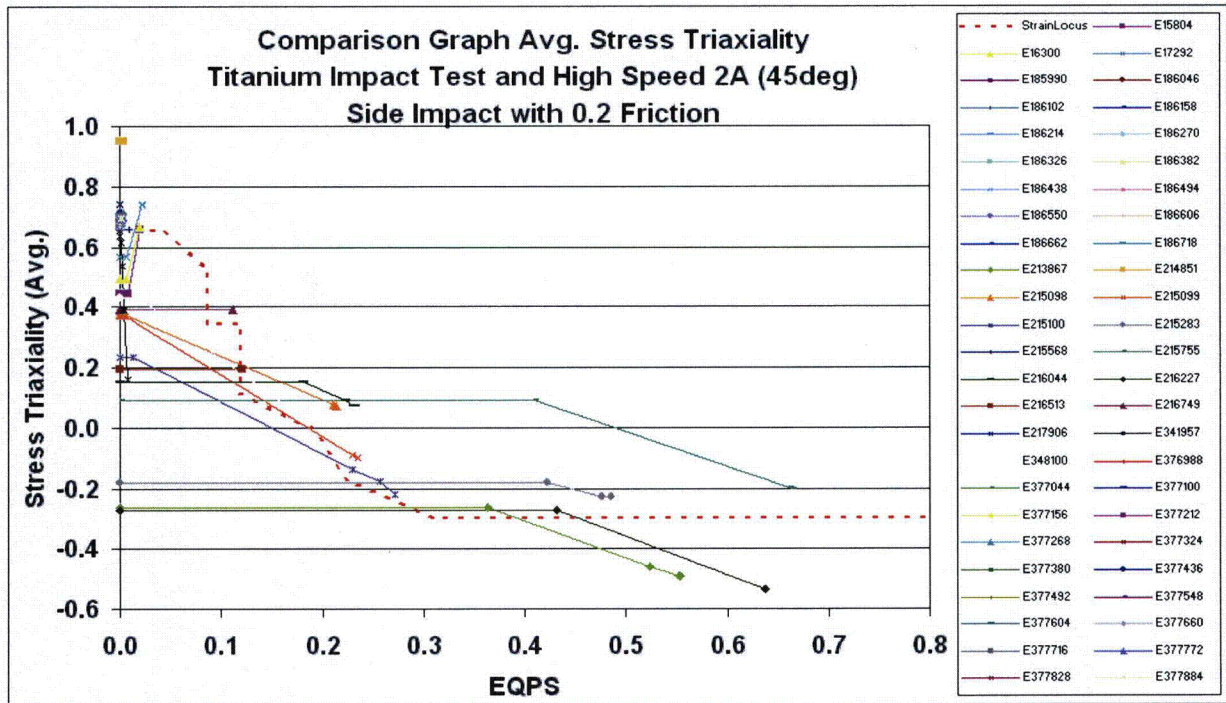


Figure 2-349. Graph of Average Stress Triaxiality versus EQPS of Elements Exceeding the Experimental Strain Locus for the SC-2, Side Impact, 45° Support Structure, Friction 0.2

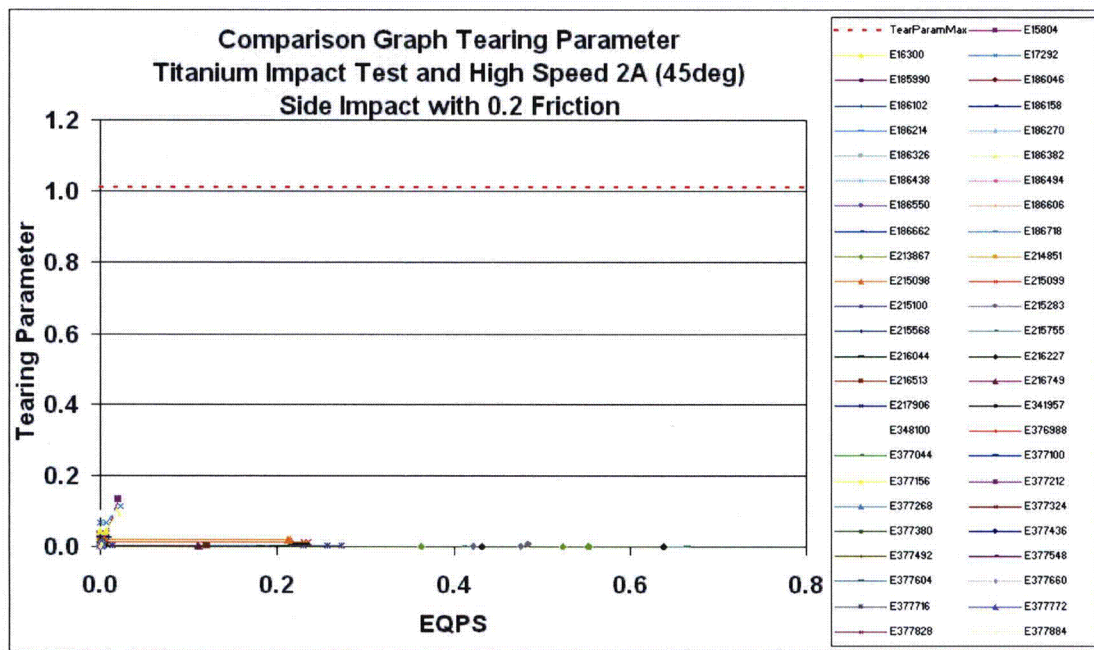


Figure 2-350. Graph of Tearing Parameter versus EQPS of Elements Exceeding the Experimental Strain Locus for the SC-2, Side Impact, 45° Support Structure, Friction 0.2

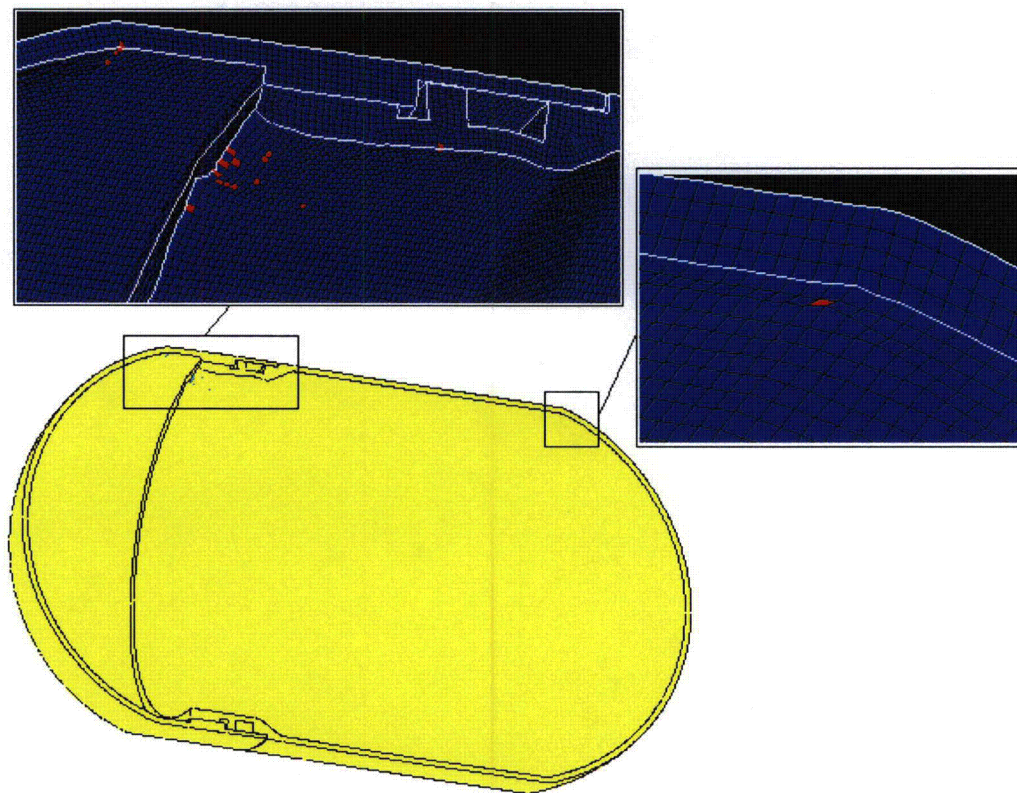


Figure 2-351. Plot of Elements Exceeding the Experimental Strain Locus for the SC-2, Side Impact, 45° Support Structure, Friction 0.2

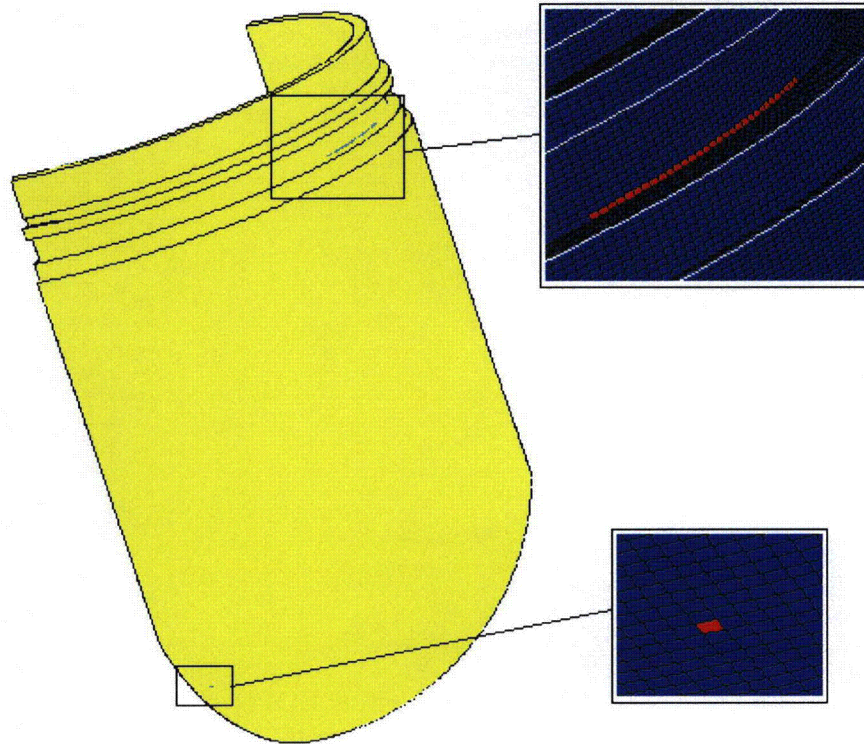


Figure 2-352. Plot of Elements Exceeding the Experimental Strain Locus for the SC-2, Side Impact, 45° Support Structure, Friction 0.2

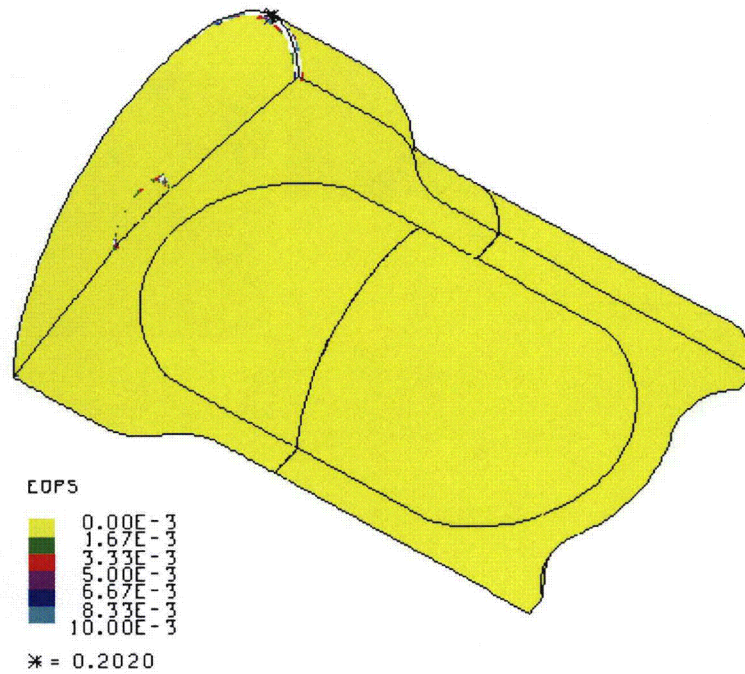


Figure 2-353. Plot of EQPS in the TB-1 for the SC-2, Side Impact, 45° Support Structure, Friction 0.2

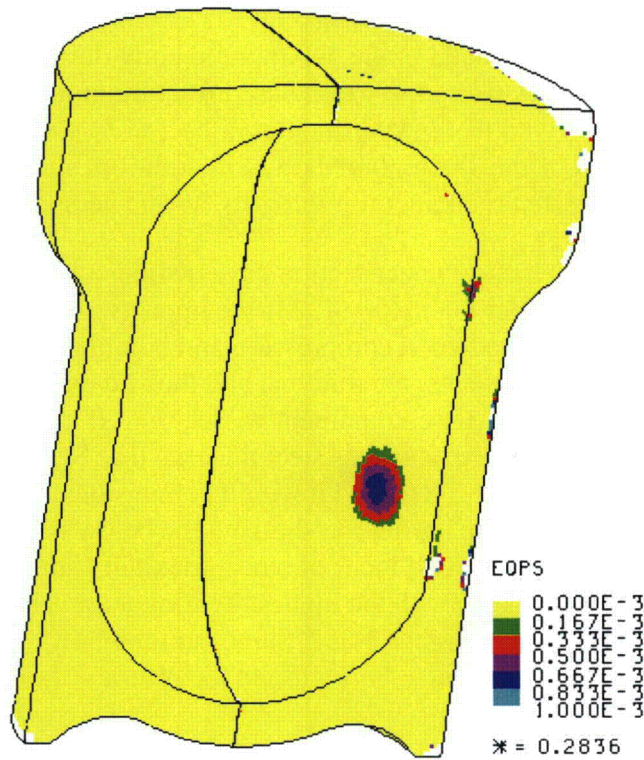


Figure 2-354. Plot of EQPS in the TB-1 for the SC-2, Side Impact, 45° Support Structure, Friction 0.2

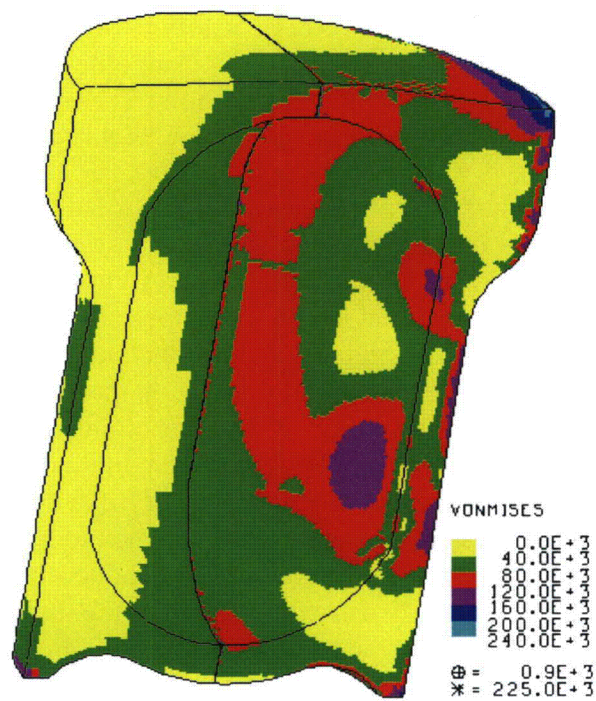


Figure 2-355. Plot of von Mises Stress in the TB-1 for the SC-2, Side Impact, 45° Support Structure, Friction 0.2

2.12.5.5.18 Summary and Conclusion (for High Velocity Impact Analyses)

Although plastic deformation is produced in the T-Ampoule body during the high-speed aircraft accident condition (10 CFR 71.74), using the strain based fracture model developed by Bao and Wierzbicki⁵ along with data derived from experimental impact tests, these strains were found not to pose a threat to the integrity of the T-Ampoule body. In addition, stresses in the TB-1 remain virtually elastic and do not threaten the structural integrity of this vessel.

Analyses presented in the high velocity impact section have demonstrated that the PAT-1 package maintains its structural integrity under regulatory 422 ft/sec impacts. Bolt loads, as shown in Figure 2-356 comparing the sum of redwood compression and bolt preload against the under-lid forces from impacting solid metal contents, are minimal and thus lid closure is maintained. Through-thickness stresses in the primary containment vessel, the TB-1, are shown to be below yield values for the S13800 high strength stainless steel material (see Section 2.12.4.9). Only localized minor "denting" occurs in the TB-1, and it would be invisible to the naked eye. And deformations in the T-Ampoule eutectic barrier are shown to be below levels that could initiate a ductile tear, and are largely within the tested locus of stress-triaxiality and plastic strain that precludes failure. Many of the elements with the highest Tearing Parameter values are plotted in stress-triaxiality versus EQPS space in Figure 2-357, demonstrating how close they are to the tested locus, which is not a failure boundary: it is a tested locus of non-failure.

All 27 of the high velocity impact analysis are summarized in Table 2-19, which lists the T-Ampoule contents, overall model and contents orientations, as well as the maximum Tearing Parameter value for all T-Ampoule elements in that particular run or analysis number. The lowest factor of safety against merely *initiating* a ductile tear occurs for a single element in run number 3 with a maximum Tearing Parameter value of 0.6177 (compared to a critical Tearing Parameter value of 1.012 for Ti-6Al-4V, so Factor of Safety = $1.012/0.6177 = 1.64$). This factor of safety pertains to the integrity of the eutectic barrier T-Ampoule, NOT the TB-1 containment boundary, which has been shown in previous certification tests and the current analyses to fully maintain its integrity (through-thickness stresses below yield), as well.

The numerous additional conservatisms associated with all of these impact analyses should provide additional confidence that containment (and eutectic barrier integrity) would be maintained, even under severe aircraft accident conditions. Additional conservatisms include: neglecting the tantalum foil packing material which would perform some small load spreading and energy absorbing function; neglecting the rolled lid of the outer package skin in aircraft impacts; always assuming the content location and orientation most damaging to the T-Ampoule, e.g., "strongest" plutonium metal hollow cylinder dimensions to resist buckling; most dense, compact, and sharp shape for the delta Pu and Be composite cylinders; delta Pu contents have higher density of alpha Pu; sharpest orientation for the strong Be cylinders, etc. Also, the material properties for these contents are conservatively assumed to have infinite plasticity, when in fact the alpha Pu is very brittle and the Be has rather limited ductility. The Be cylinders were conservatively assumed to have delta Pu density, thus maximizing their impact velocity (due to smaller size). These conservative assumptions maximize the loading and damage potential to the T-Ampoule (as well as TB-1), yet it retains structural integrity as a eutectic barrier.

2.12.5.5.18 Summary and Conclusion (for High Velocity Impact Analyses)

Although plastic deformation is produced in the T-Ampoule body during the high-speed aircraft accident condition (10 CFR 71.74), using the strain based fracture model developed by Bao and Wierzbicki⁵ along with data derived from experimental impact tests, these strains were found not to pose a threat to the integrity of the T-Ampoule body. In addition, stresses in the TB-1 remain virtually elastic and do not threaten the structural integrity of this vessel.

Analyses presented in the high velocity impact section have demonstrated that the PAT-1 package maintains its structural integrity under regulatory 422 ft/sec impacts. Bolt loads, as shown in Figure 2-356 comparing the sum of redwood compression and bolt preload against the under-lid forces from impacting solid metal contents, are minimal and thus lid closure is maintained. Through-thickness stresses in the primary containment vessel, the TB-1, are shown to be below yield values for the S13800 high strength stainless steel material (see Section 2.12.4.9). Only localized minor “denting” occurs in the TB-1, and it would be invisible to the naked eye. And deformations in the T-Ampoule eutectic barrier are shown to be below levels that could initiate a ductile tear, and are largely within the tested locus of stress-triaxiality and plastic strain that precludes failure. Many of the elements with the highest Tearing Parameter values are plotted in stress-triaxiality versus EQPS space in Figure 2-357, demonstrating how close they are to the tested locus, which is not a failure boundary: it is a tested locus of non-failure.

All 27 of the high velocity impact analysis are summarized in Table 2-19, which lists the T-Ampoule contents, overall model and contents orientations, as well as the maximum Tearing Parameter value for all T-Ampoule elements in that particular run or analysis number. The lowest factor of safety against merely *initiating* a ductile tear occurs for a single element in run number 3 with a maximum Tearing Parameter value of 0.6177 (compared to a critical Tearing Parameter value of 1.012 for Ti-6Al-4V, so Factor of Safety = $1.012/0.6177 = 1.64$). This factor of safety pertains to the integrity of the eutectic barrier T-Ampoule, NOT the TB-1 containment boundary, which has been shown in previous certification tests and the current analyses to fully maintain its integrity (through-thickness stresses below yield), as well.

The numerous additional conservatisms associated with all of these impact analyses should provide additional confidence that containment (and eutectic barrier integrity) would be maintained, even under severe aircraft accident conditions. Additional conservatisms include: neglecting the tantalum foil packing material which would perform some small load spreading and energy absorbing function; neglecting the rolled lid of the outer package skin in aircraft impacts; always assuming the content location and orientation most damaging to the T-Ampoule, e.g., “strongest” plutonium metal hollow cylinder dimensions to resist buckling; most dense, compact, and sharp shape for the delta Pu and Be composite cylinders; delta Pu contents have higher density of alpha Pu; sharpest orientation for the strong Be cylinders, etc. Also, the material properties for these contents are conservatively assumed to have infinite plasticity, when in fact the alpha Pu is very brittle and the Be has rather limited ductility. The Be cylinders were conservatively assumed to have delta Pu density, thus maximizing their impact velocity (due to smaller size). These conservative assumptions maximize the loading and damage potential to the T-Ampoule (as well as TB-1), yet it retains structural integrity as a eutectic barrier.

Table 2-19. High Velocity (Aircraft) Impact Analyses Peak Tearing Parameter Values

Run No.	Component	Model Orientation	Maximum Tearing Parameter (T-Ampoule)
1	831 g Plutonium Metal Hollow Cylinder	Bottom position, top impact	0.0528
2	831 g Plutonium Metal Hollow Cylinder	Bottom position (angled), top impact	0.2115
3	831 g Plutonium Metal Hollow Cylinder	Bottom position (angled), CGOC impact	0.6177
4	831 g Plutonium Metal Hollow Cylinder	Far side position, side impact	0.2896
5	831 g Plutonium Metal Hollow Cylinder	Far side position (angled), side impact	0.2389
6	731 g Plutonium Metal Hollow Cylinder	Bottom position, top impact	0.1507
7	731 g Plutonium Metal Hollow Cylinder	Bottom position (angled), top impact	0.2831
8	731 g Plutonium Metal Hollow Cylinder	Bottom position (angled), CGOC impact	0.3967
9	731 g Plutonium Metal Hollow Cylinder	Far side position, side impact	0.4896
10	731 g Plutonium Metal Hollow Cylinder	Far side position (angled), side impact	0.2842
11	SC-1 – Pu	Bottom position, support structure 0°, top impact	0.0319
12	SC-1 – Pu	Far side position, support structure 0°, side impact	0.2417
13	SC-1 – Pu	Far side position, support structure 45°, side impact	0.1958
14	SC-1 – Pu	Bottom position, support structure 0°, CGOC impact	0.0935
15	SC-1 – Pu	Bottom position, support structure 45°, CGOC impact	0.3061

Run No.	Component	Model Orientation	Maximum Tearing Parameter (T-Ampoule)
16	SC-2 – Pu	Bottom position, support structure 0°, top impact	0.0132
17	SC-2 – Pu	Far side position, support structure 0°,side impact	0.4788
18	SC-2 – Pu	Far side position, support structure 45°, side impact	0.5137
19	SC-2 – Pu	Bottom position, support structure 0°, CGOC impact	0.0953
20	SC-2 – Pu	Bottom position, support structure 45°, CGOC impact	0.0540
21	SC-1 - Be	Bottom position, angled Be, support structure 0°, top impact	0.0155
22	SC-1 – Be	Far side position, angled Be, support structure 0°, side impact	0.2075
23	SC-1 – Be	Far side position, angled Be, support structure 45°, side impact	0.4970
24	SC-1 – Be	Bottom position, angled Be, support structure 0°, CGOC impact	0.0597
25	SC-1 – Be	Bottom position, angled Be, support structure 45°, CGOC impact	0.1197
26	SC-2 – Pu	Far side position, support structure 45°, side impact, friction 0.4	0.4888
27	SC-2 – Pu	Far side position, support structure 45°, side impact, friction 0.2	0.4673

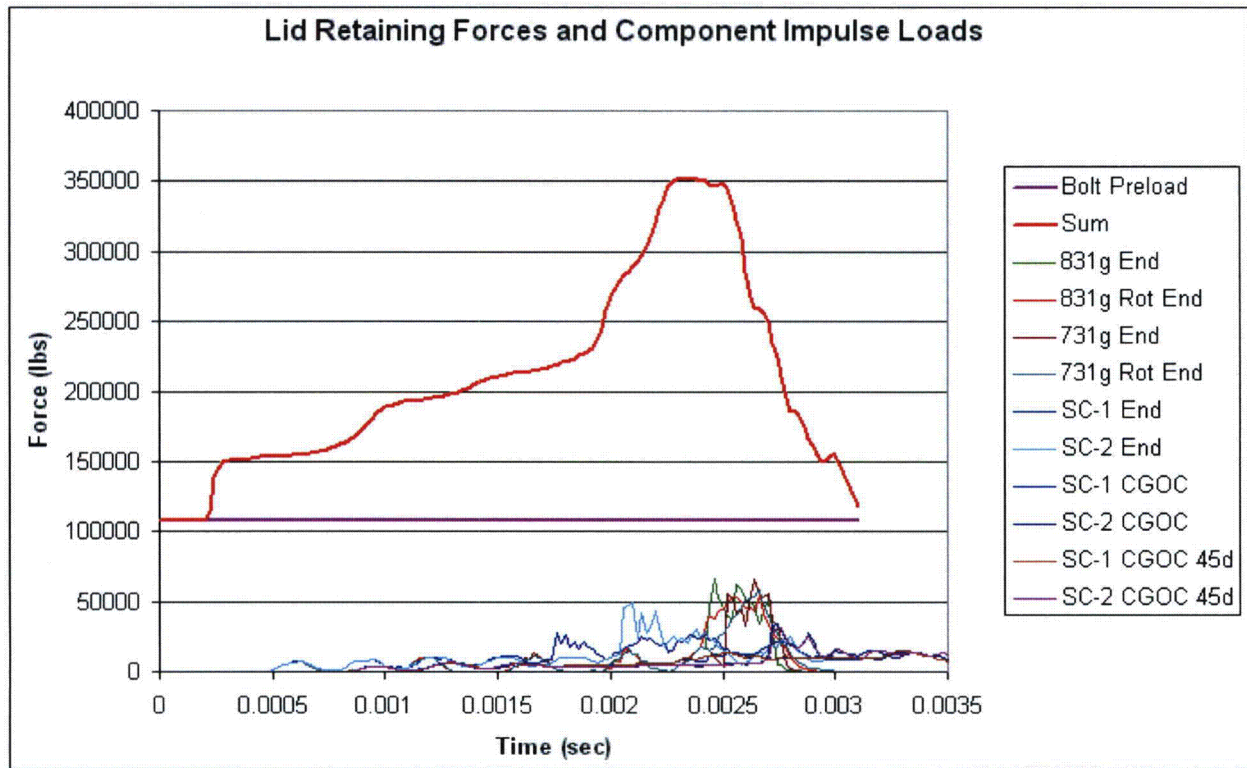


Figure 2-356. Summary Plot of Lid Retaining Forces and Component Impulse Loads

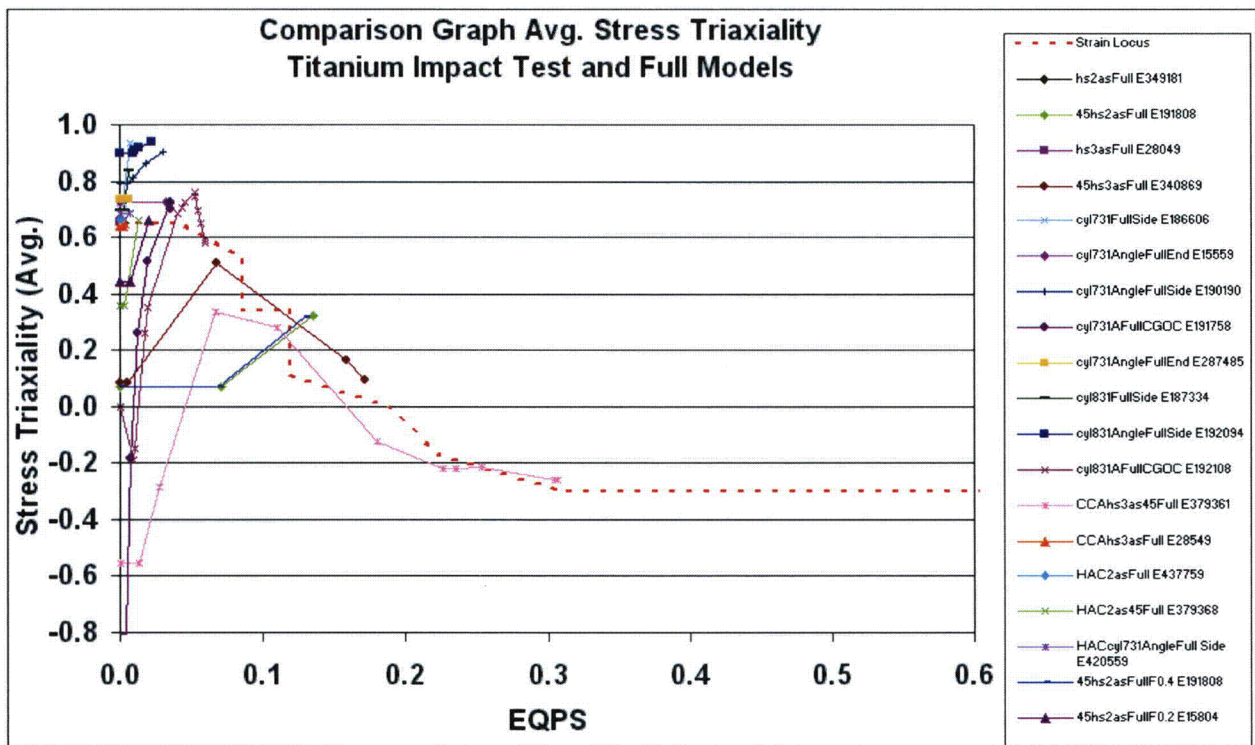


Figure 2-357. Summary Plot of Plastic Stress Triaxiality for Selected Runs

2.12.5.6 HAC – Dynamic Crush Analysis Results

In addition to the high-speed aircraft accident analyses, twenty analyses were performed to explore the HAC dynamic crush event described in 10 CFR 71.73. A description of these analyses is provided in Table 2-20. In all of these models, the 1100-lb plate was given an initial velocity of 528 in/s (which corresponds to a 30 ft drop), and was positioned within 0.12 in (3 mm) of the overpack. The overpack and contents had an initial velocity of 0, and gravity was included to ensure proper contact between the contents and the T-Ampoule. The material properties used for each analysis are the same as for the high-speed aircraft impacts and are provided in Section 2.12.4.

The performance of the T-Ampoule for each run was assessed using the same criteria as in the aircraft impact analyses. The maximum Tearing Parameter results for each run are listed in Table 2-20. None of the runs resulted in Tearing Parameters exceeding the maximum allowable Tearing Parameter, termed critical Tearing Parameter ($TP_{crit} = 1.012$ for Ti-6Al-4V, based on tensile tests to failure). The relatively large 0.44 and 0.22 Tearing Parameter values in run numbers 2 and 3 came from single elements in each analysis associated with a minor localized contact issue, and would otherwise be much smaller or zero (similar to the other analyses listed).

In addition, the stresses in the TB-1 were compared against HAC Reg. Guide 7.6 and ASME B&PV Code stress allowables. None of the runs resulted in through-thickness containment vessel stresses exceeding the ASME limit of 106.6 ksi, shown in Table 2-4. More conservatively, even using the NCT stress intensity limit of 50.8 ksi (see Table 2-4) or 50.0 from Section II, Part D of the ASME Boiler and Pressure Vessel Code for the S13800 material, none of the runs resulted in through-thickness TB-1 stresses exceeding these values in the dynamic crush environment.⁸ Nonmandatory Appendix F of the ASME BPVC⁹ lists stress intensity limits for inelastic analysis as the greater of $0.7S_u = 106.6$ ksi or $S_y + 0.33(S_u - S_y) = 144.8$ ksi for the general primary membrane stress intensity, not to exceed $0.9S_u = 137.1$ ksi at any location. Conservatively, this limits the peak stress in the dynamic crush events to 137.1 ksi, which is never even approached in any of the HAC analyses, except at the irrelevant regions (due to minor contact modeling artifacts) on some very localized outer surfaces of the TB-1. For example, in Run 3, Section 2.12.5.6.3 for the SC-2 side impact (45-degree rotated) dynamic crush analysis, the through-thickness stress intensity (Tresca stress) is less than 23.5 ksi (Figure 2-382), and the peak stress intensity (excepting the highly localized 226.2 ksi peak due to a contact modeling artifact) was 70.5 ksi where the TB-1 closure diameter necks down to the main body smaller diameter. This 70.5 ksi peak stress intensity is below the Nonmandatory Appendix F peak stress limit of 137.1 ksi.

Table 2-20. Summary of Hypothetical Accident Condition (HAC) Dynamic Crush Analyses (20), Components, and Orientations

Run No.	Component	Submodel Orientation	Maximum Tearing Parameter
1	2 SC-2 Sample Containers, delta Pu	Lid end impact	0
2	2 SC-2 Sample Containers, delta Pu	Side impact	0.4464
3	2 SC-2 Sample Containers, delta Pu	Side impact, 45-degree-rotated	0.2288
4	2 SC-2 Sample Containers, delta Pu	CGOC impact	2.78e-3
5	2 SC-2 Sample Containers, delta Pu	CGOC impact, 45-degree-rotated	0
6	3 SC-1 Sample Containers, delta Pu	Lid end impact	0
7	3 SC-1 Sample Containers, delta Pu	Side impact	3.03e-5
8	3 SC-1 Sample Containers, delta Pu	Side impact, 45-degree-rotated	1.6e-2
9	3 SC-1 Sample Containers, delta Pu	CGOC impact	0
10	3 SC-1 Sample Containers, delta Pu	CGOC impact, 45-degree-rotated	0
11	831 g Plutonium Metal Hollow Cylinder, alpha Pu	Lid end impact	0
12	831 g Plutonium Metal Hollow Cylinder, alpha Pu	Side impact	2.94e-6
13	831 g Plutonium Metal Hollow Cylinder, alpha Pu	Lid end impact, angled cylinder	0
14	831 g Plutonium Metal Hollow Cylinder, alpha Pu	Side impact, angled cylinder	2.01e-2
15	831 g Plutonium Metal Hollow Cylinder, alpha Pu	CGOC impact, angled cylinder	0
16	731 g Plutonium Metal Hollow Cylinder, alpha Pu	Lid end impact	0
17	731 g Plutonium Metal Hollow Cylinder, alpha Pu	Side impact	0
18	731 g Plutonium Metal Hollow Cylinder, alpha Pu	Lid end impact, angled cylinder	0
19	731 g Plutonium Metal Hollow Cylinder, alpha Pu	Side impact, angled cylinder	5.09e-2
20	731 g Plutonium Metal Hollow Cylinder, alpha Pu	CGOC impact, angled cylinder	0

2.12.5.6.1 HAC – Run 1, SC-2, End Impact

The dynamic crush end impact HAC analysis for the 2 SC-2 sample container run uses the same model as that used for the 4-ft-drop, but the flange is added to both ends so that it is available to deform where impacted by the plate and the rigid surface upon which it is resting. The finite element mesh and initial position of the model is shown in Figure 2-358. The Pu contents and support structure within the T-Ampoule are positioned at the bottom of the model because it was considered to be at rest.

The post-impact deformation is shown in Figure 2-359 and its kinetic energy history in Figure 2-360. The flanges on the overpack deform, and the contents bounce due to the impact of the plate, but there is no plastic deformation in the T-Ampoule or the TB-1.

Figures 2-361 and 2-362 are plots of the Tresca stresses within the TB-1. The maximum Tresca stress (stress intensity) in the TB-1 is 137.9 ksi due again to a contact modeling artifact, but there are no through thickness stresses exceeding the limit of 106.6 ksi, which can be seen clearly in Figure 2-362. Figure 2-363 is a plot of the Tresca stresses at the time when all of the kinetic energy of the plate has been transferred to the package, just as the plate begins to rebound. The maximum through thickness stress at this time is below 16.7 ksi, below the allowable through thickness stress of 106.6 ksi, as seen in the figure.

As in the high velocity impact analyses, there is a minor modeling artifact occurring due to slight contact over closure between the redwood and the ring of TB-1 top surface elements which is causing this very slight non-realistic localized plasticity.

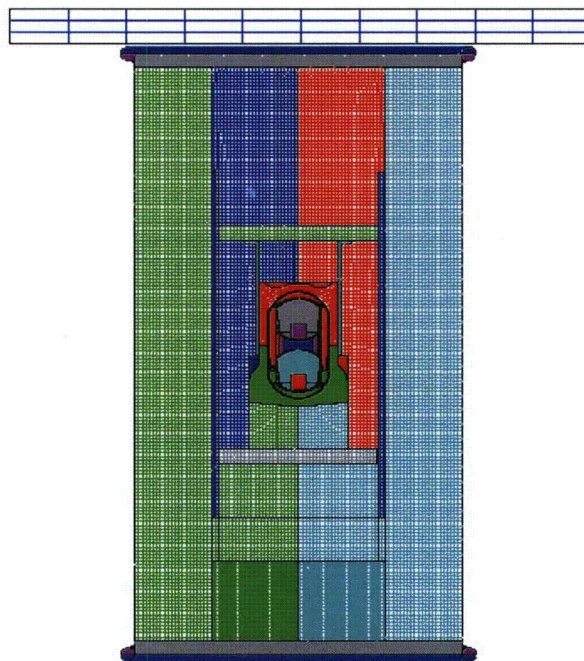


Figure 2-358. Finite Element Mesh for HAC Run 1, SC-2, End Impact

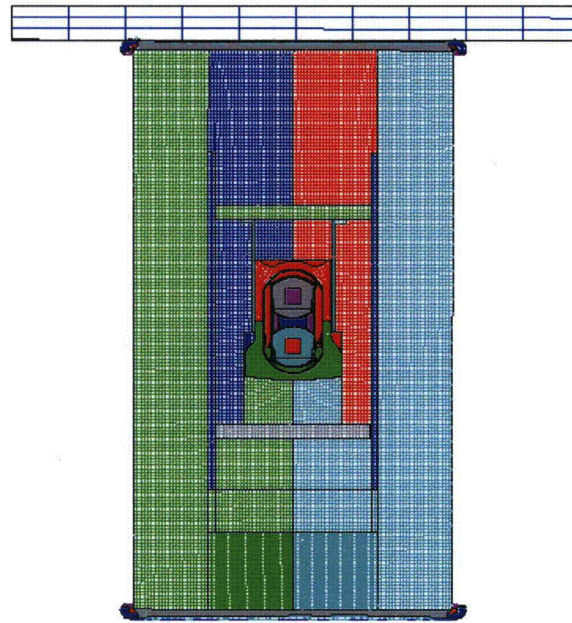


Figure 2-359. Finite Element Mesh for HAC Run 1, SC-2, End Impact – Final Displacement

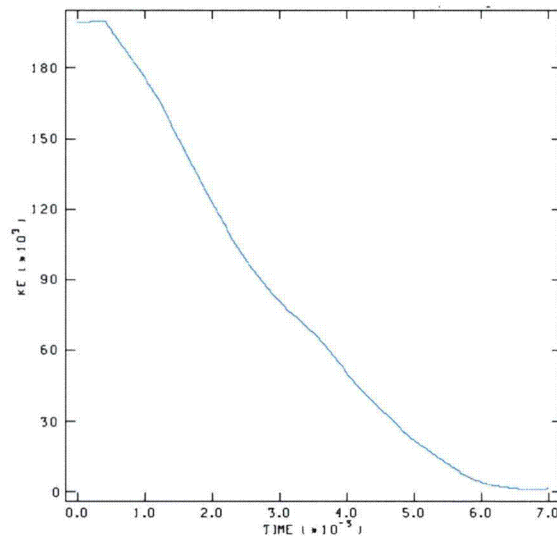


Figure 2-360. Kinetic Energy Time History for HAC Run 1, SC-2, End Impact

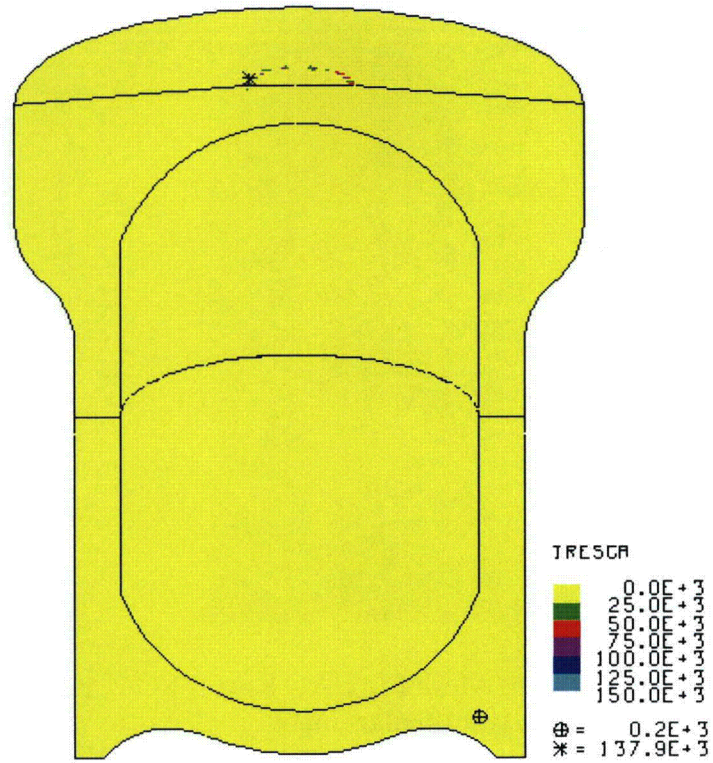


Figure 2-361. Tresca Stress in TB-1 for HAC Run 1, SC-2, End Impact

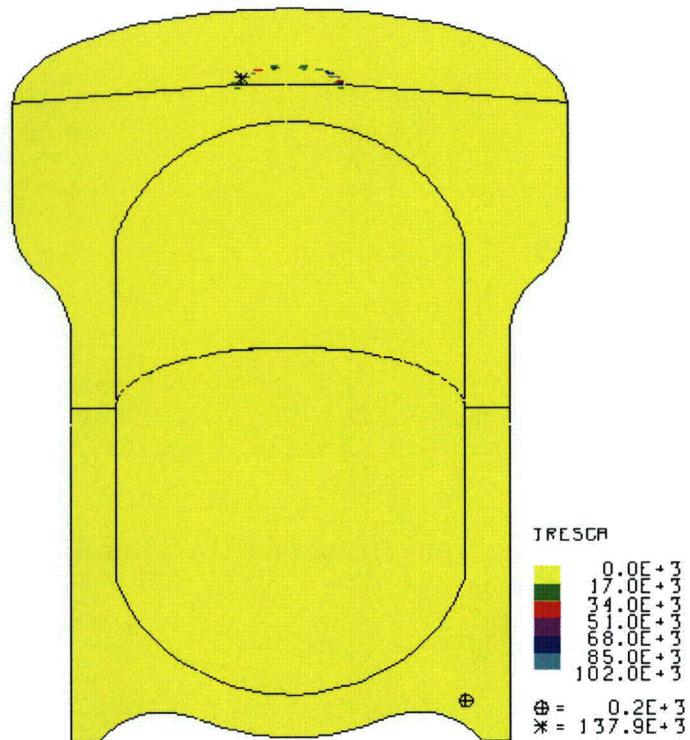


Figure 2-362. Tresca Stress of TB-1 for HAC Run 1, SC-2, End Impact

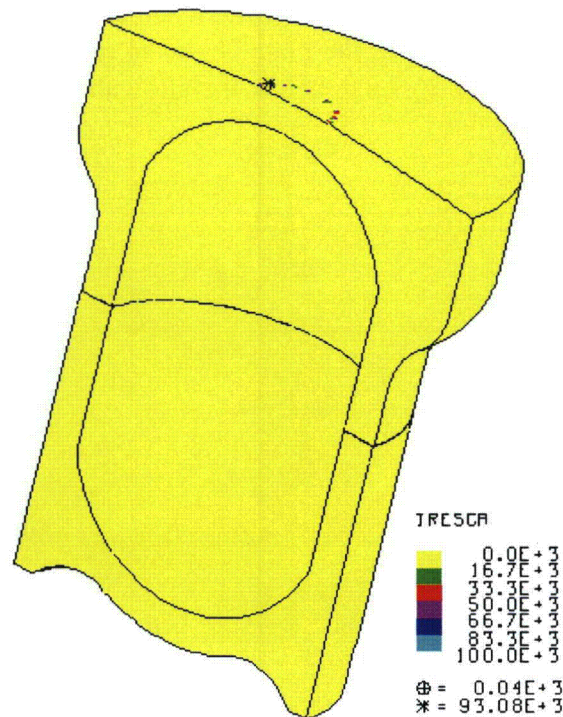


Figure 2-363. Tresca Stress of TB-1 for HAC Run 1, SC-2, End Impact when Plate Velocity Reaches Zero

2.12.5.6.2 HAC- Run 2, SC-2, Side Impact, Support Structure 0°

The dynamic crush end impact HAC analysis for the 2 SC-2 sample container runs uses the same model as that used for the 4-ft-drop, but the flange is added to both ends so that it is available to deform where impacted by the plate and the rigid surface upon which it is resting. The finite element mesh and initial position of the model are shown in Figure 2-364. The Pu contents and support structure within the T-Ampoule are positioned at the bottom of the model because it was considered to be at rest. The plate was positioned between the flanges to be most damaging to the TB-1 and contents by preventing the flanges from absorbing energy and slowing down the plate before it hits the overpack.

The post-impact deformation is shown in Figure 2-365 and its kinetic energy history in Figure 2-366. The flanges on the overpack deform, and the contents bounce due to the impact of the plate. Average stress-triaxiality versus EQPS is shown in Figures 2-367 and 2-368 for the one element extending beyond the tested Bao-Wierzbicki strain locus. This element is at high stress triaxiality and low EQPS. The Tearing Parameter values for this same element are shown in Figure 2-369, and are below the critical Tearing Parameter value of 1.012 for Ti-6Al-4V. This element is highlighted in red Figure 2-370, but note that this element is below the initiation of a ductile tear, thus T-Ampoule integrity is maintained.

Peak EQPS in the TB-1 vessel is shown in Figure 2-371 to be 28.31e-3, and is localized in the outer contact regions with the redwood overpack. Figure 2-372 is a plot of the Tresca stresses within the TB-1. The maximum Tresca stress in the TB-1 is 172.3 ksi, but there are no through thickness stresses exceeding the limit of 106.6 ksi, which can be seen clearly in the figure.

Figure 2-373 is a plot of the Tresca stresses at the time when all of the kinetic energy of the plate has been transferred to the package, just as the plate begins to rebound. The maximum through thickness stress at this time is below 26.7 ksi, below the allowable through thickness stress of 106.6 ksi, as seen in the figure.

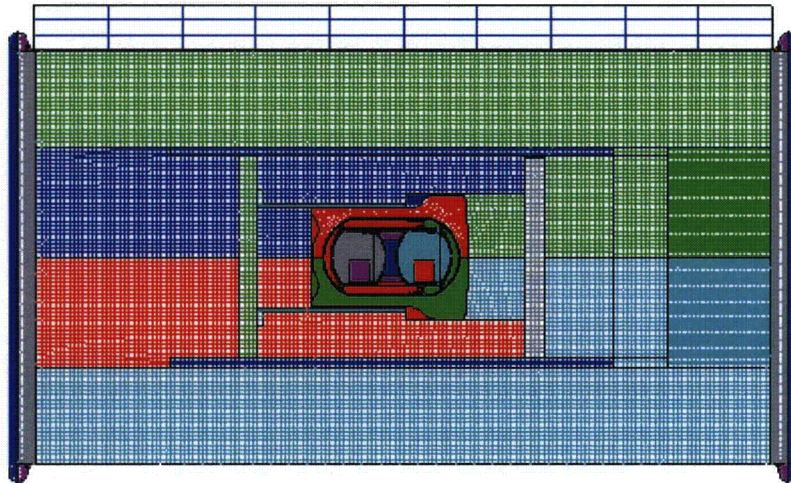


Figure 2-364. Finite Element Mesh for HAC Run 2, SC-2, Side Impact, Support Structure 0°

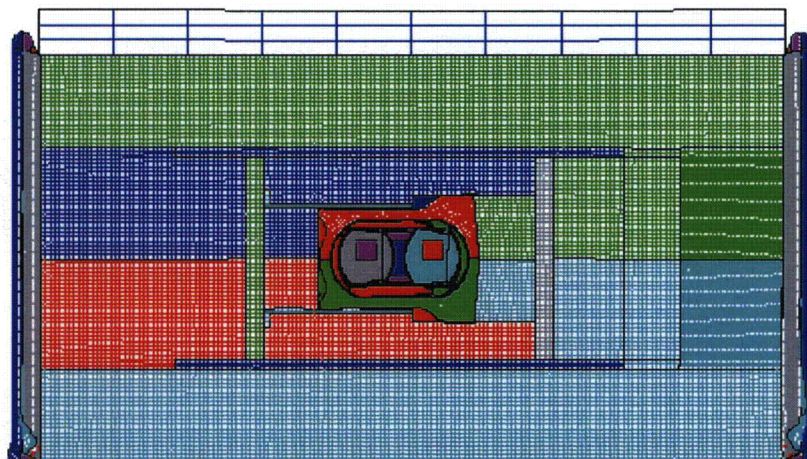


Figure 2-365. Finite Element Mesh for HAC Run 2, SC-2, Side Impact, Support Structure 0° - Final Displacement

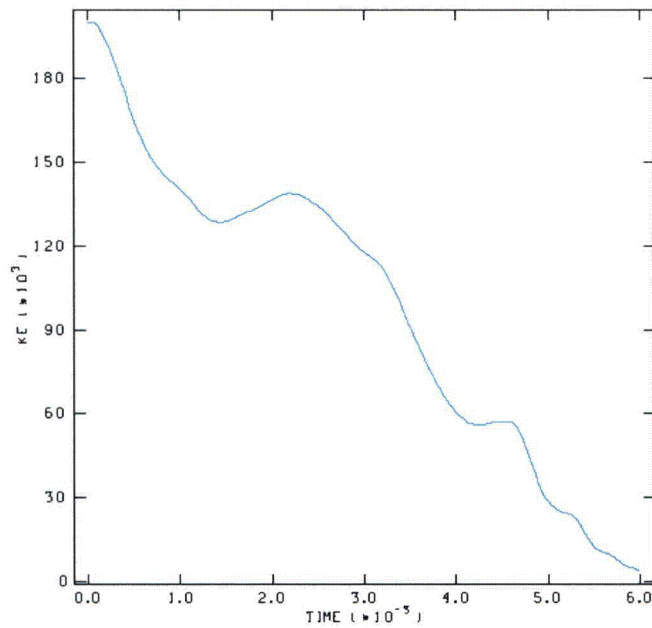


Figure 2-366. Kinetic Energy Time History for HAC Run 2, SC-2, Side Impact, Support Structure 0°

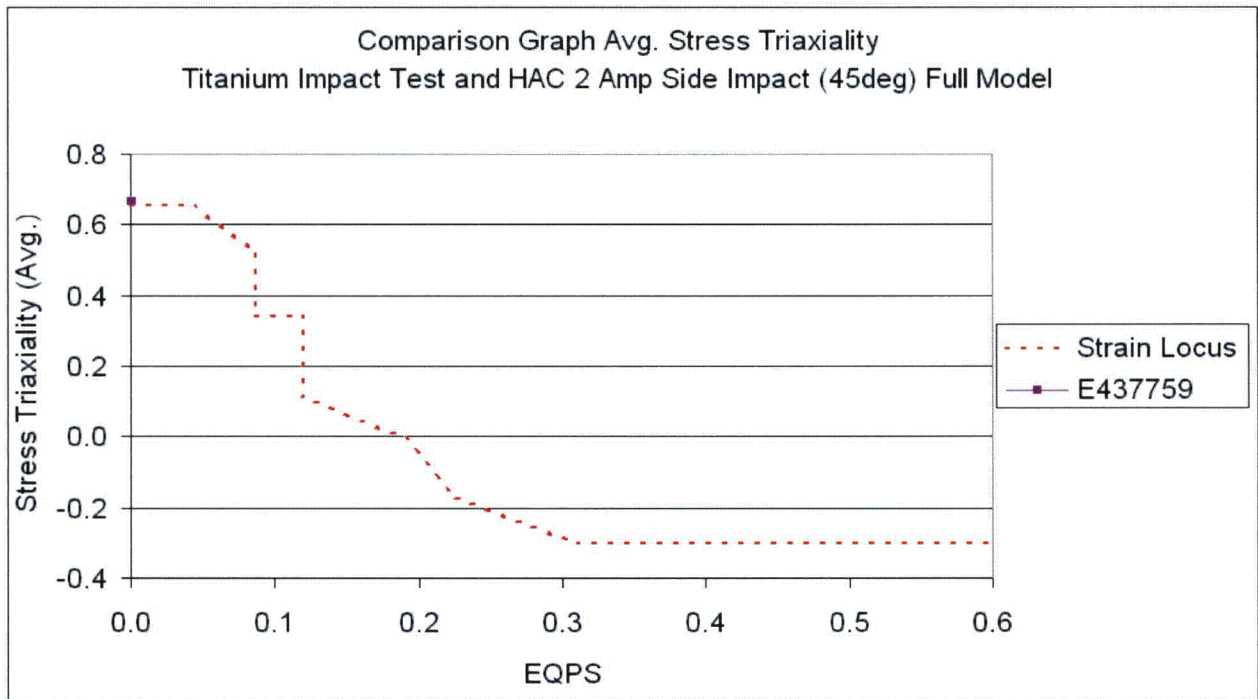


Figure 2-367. Graph of Average Stress Triaxiality versus EQPS for Element Exceeding Experimental Strain Locus for HAC Run 2, SC-2, Side Impact, Support Structure 0°

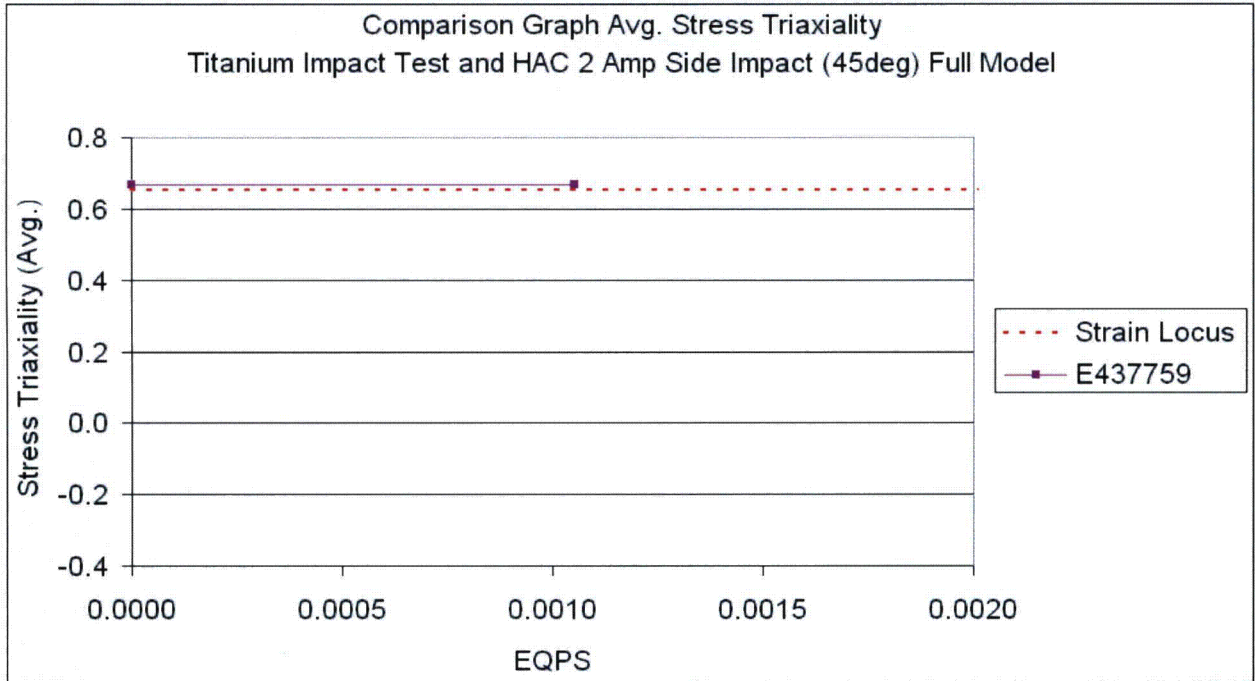


Figure 2-368. Graph of Average Stress Triaxiality versus EQPS for Element Exceeding Experimental Strain Locus (Zoomed In) for HAC Run 2, SC-2, Side Impact, Support Structure 0°

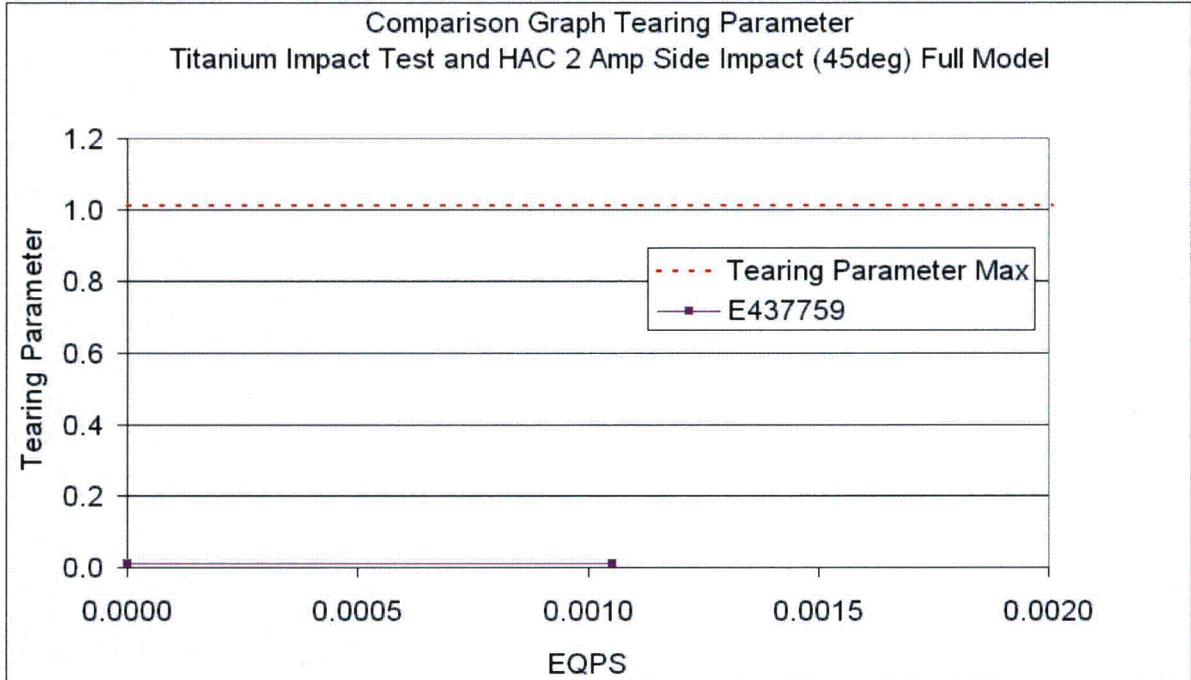


Figure 2-369. Graph of Tearing Parameter versus EQPS for Element Exceeding Experimental Strain Locus for HAC Run 2, SC-2, Side Impact, Support Structure 0°

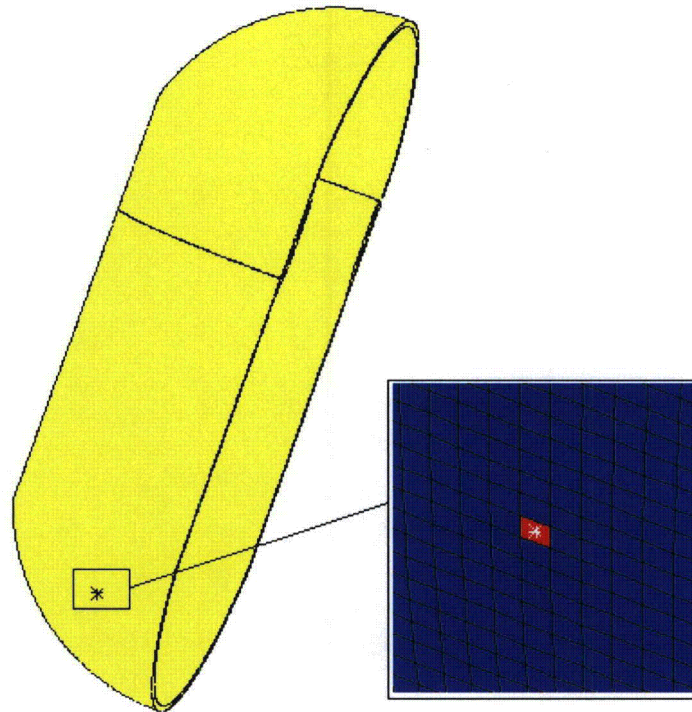


Figure 2-370. Plot of Element Exceeding Experimental Strain Locus for HAC Run 2, SC-2, Side Impact, Support Structure 0°

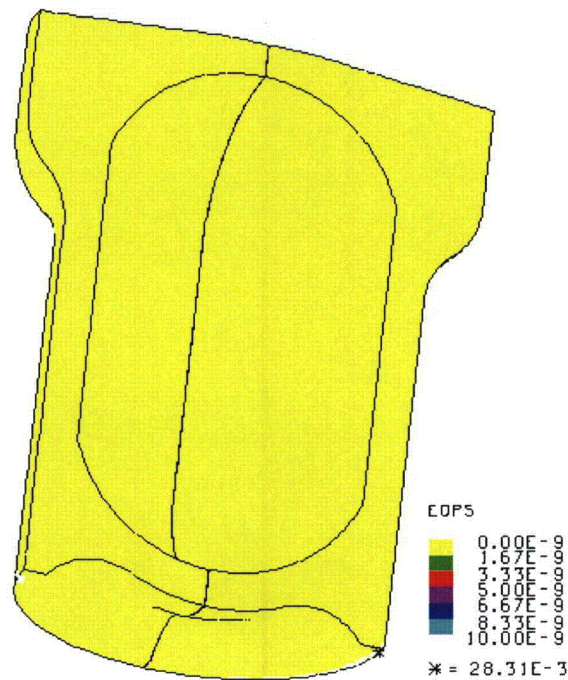


Figure 2-371. Graph of EQPS in the TB-1 for HAC Run 2, SC-2, Side Impact, Support Structure 0°

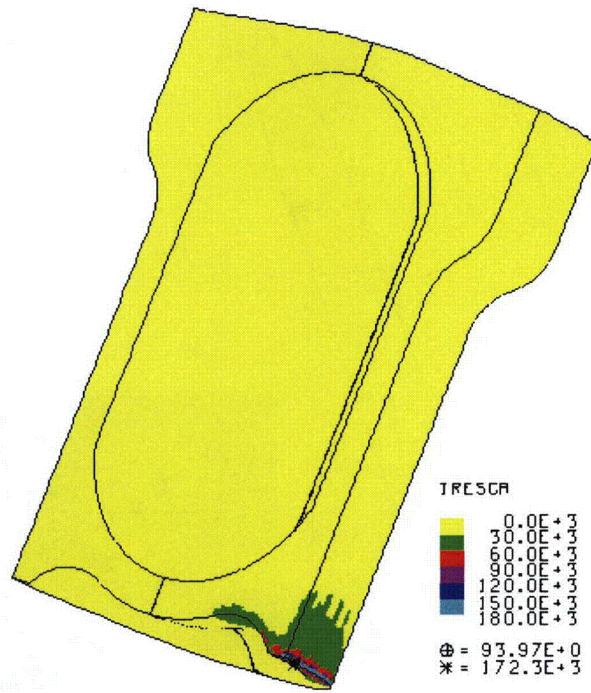


Figure 2-372. Plot of Tresca Stress in the TB-1 for HAC Run 2, SC-2, Side Impact, Support Structure 0°

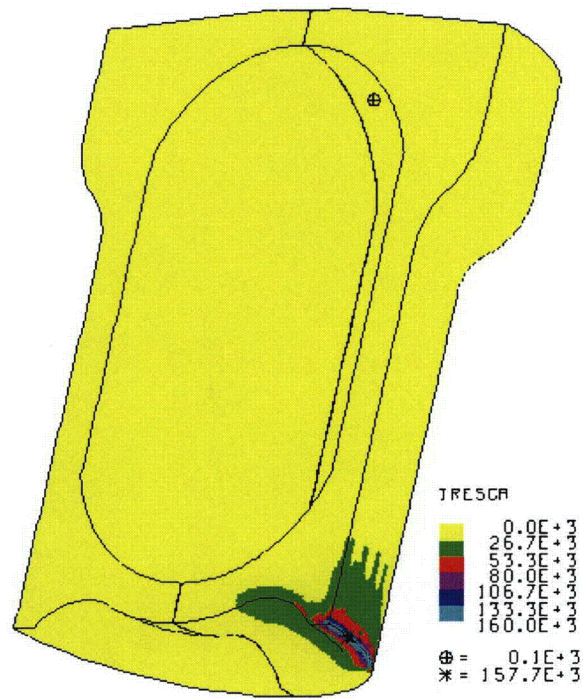


Figure 2-373. Plot of Tresca Stress in the TB-1 for HAC Run 2, SC-2, Side Impact, Support Structure 0° when Plate Velocity Reaches Zero

2.12.5.6.3 HAC- Run 3, SC-2, Side Impact, Support Structure 45°

The dynamic crush side impact HAC analysis run for the 2 SC-2 sample container with its support structure rotated 45° uses the same model as that used for the 4-ft-drop, but the flange is added to both ends so that it is available to deform where impacted by the plate and the rigid surface upon which it is resting. The finite element mesh and initial position of the model are shown in Figure 2-374. The Pu contents and support structure within the T-Ampoule are positioned at the bottom of the model because it was considered to be at rest at the time of impact. The plate was positioned between the flanges to be most damaging to the TB-1 and contents by preventing the flanges from absorbing energy and slowing down the plate before it hits the overpack.

The post-impact deformation is shown in Figure 2-375 and its kinetic energy history in Figure 2-376. The flanges on the overpack deform, and the contents bounce due to the impact of the plate. Average stress-triaxiality versus EQPS is shown in Figure 2-377 for the one element extending beyond the tested Bao-Wierzbicki strain locus. This element is at high stress triaxiality and low EQPS. The Tearing Parameter value for this same element is shown in Figure 2-378 and is below the critical Tearing Parameter value of 1.012 for Ti-6Al-4V. This element is highlighted in red Figure 2-379, but note that this element is below the initiation of a ductile tear, thus T-Ampoule integrity is maintained.

Peak EQPS in the TB-1 vessel is shown in Figure 2-380 to be 0.21, and is localized in the outer contact regions with the redwood overpack. Figures 2-381 and 2-382 are plots of the Tresca stresses within the TB-1. The maximum Tresca stress in the TB-1 is 226.7 ksi, but there are no through thickness stresses exceeding the limit of 106.6 ksi, which can be seen clearly in the figures. Figure 2-383 is a plot of the Tresca stresses at the time when all of the kinetic energy of the plate has been transferred to the package, just as the plate begins to rebound. The maximum through thickness stress at this time is below 16.7 ksi, below the allowable through thickness stress of 106.6 ksi, as seen in the figure.

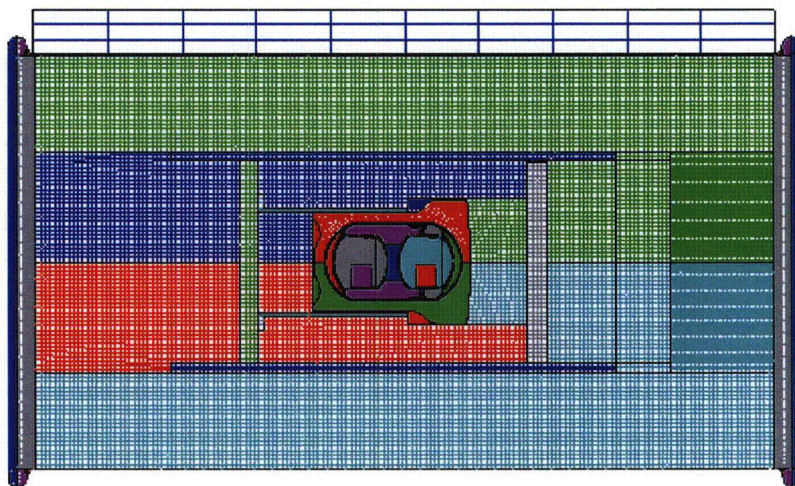


Figure 2-374. Finite Element Mesh for HAC Run 3, SC-2, Side Impact, Support Structure 45°

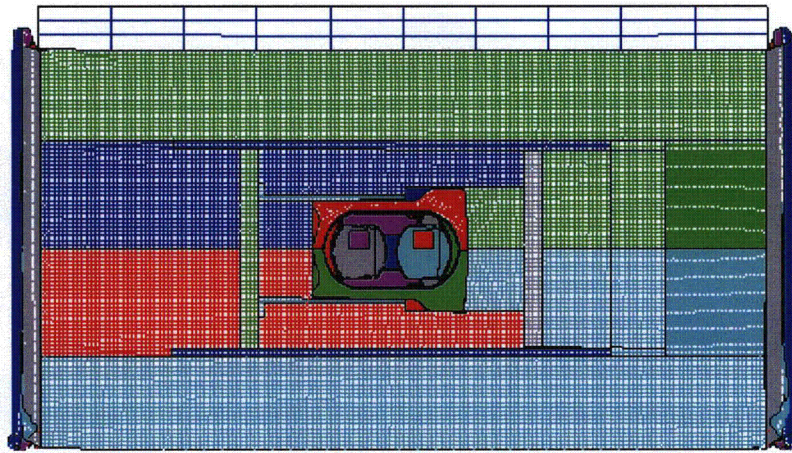


Figure 2-375. Finite Element Mesh for HAC Run 3, SC-2, Side Impact, Support Structure 45° - Final Displacement

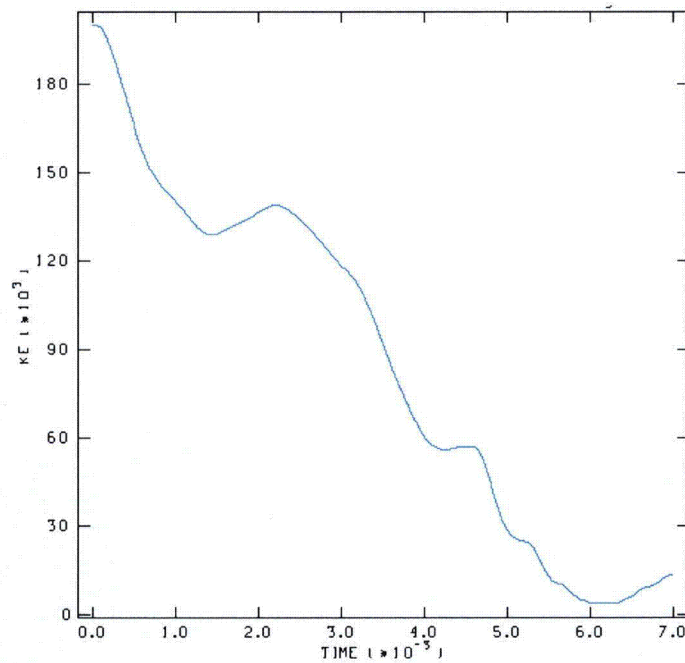


Figure 2-376. Kinetic Energy Time History for HAC Run 3, SC-2, Side Impact, Support Structure 45°

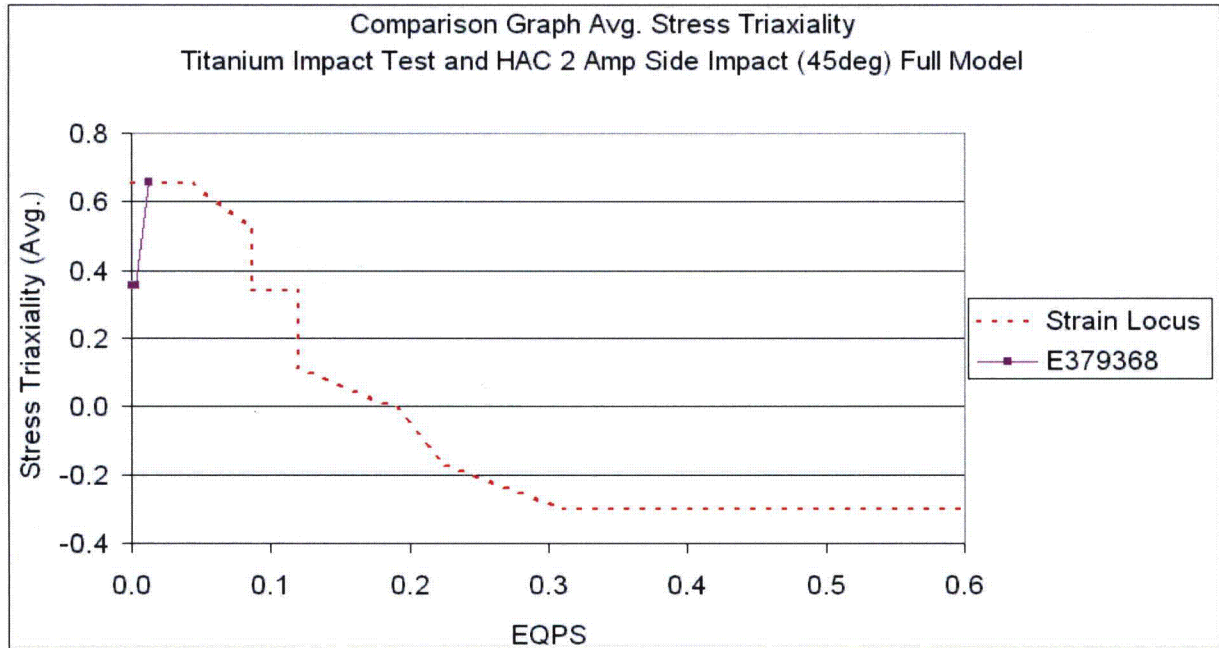


Figure 2-377. Graph of Average Stress Triaxiality versus EQPS of Element Exceeding Experimental Strain Locus for HAC Run 3, SC-2, Side Impact, Support Structure 45°

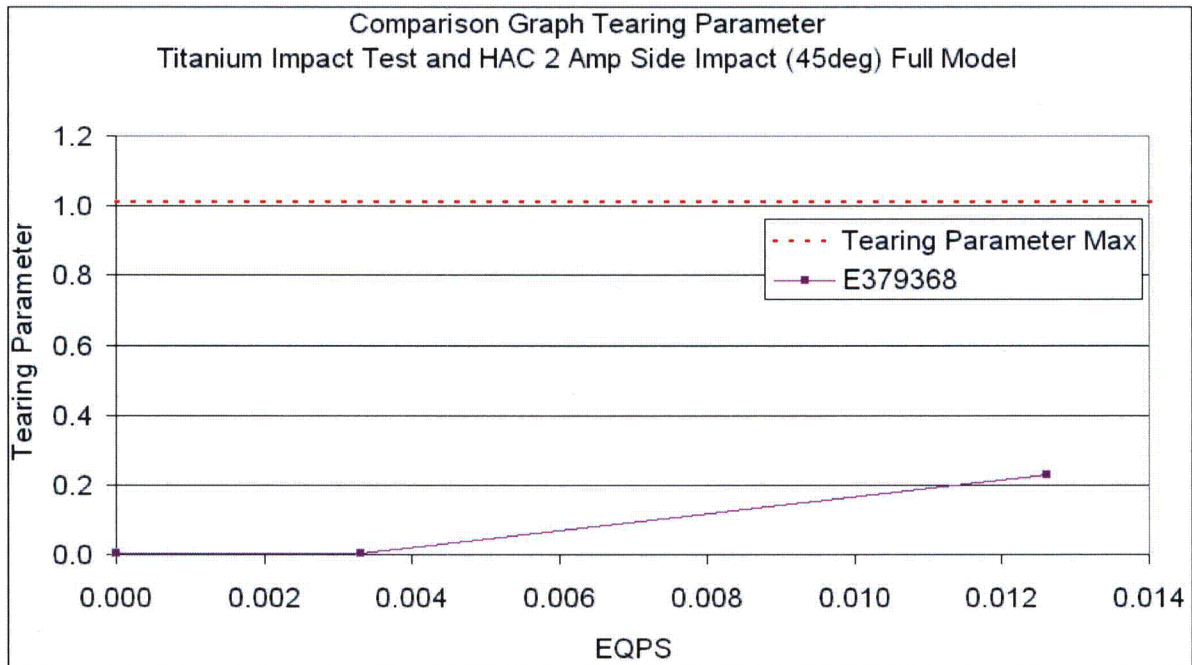


Figure 2-378. Graph of Tearing Parameter versus EQPS of Element Exceeding Experimental Strain Locus (Zoomed In) for HAC Run 3, SC-2, Side Impact, Support Structure 45°

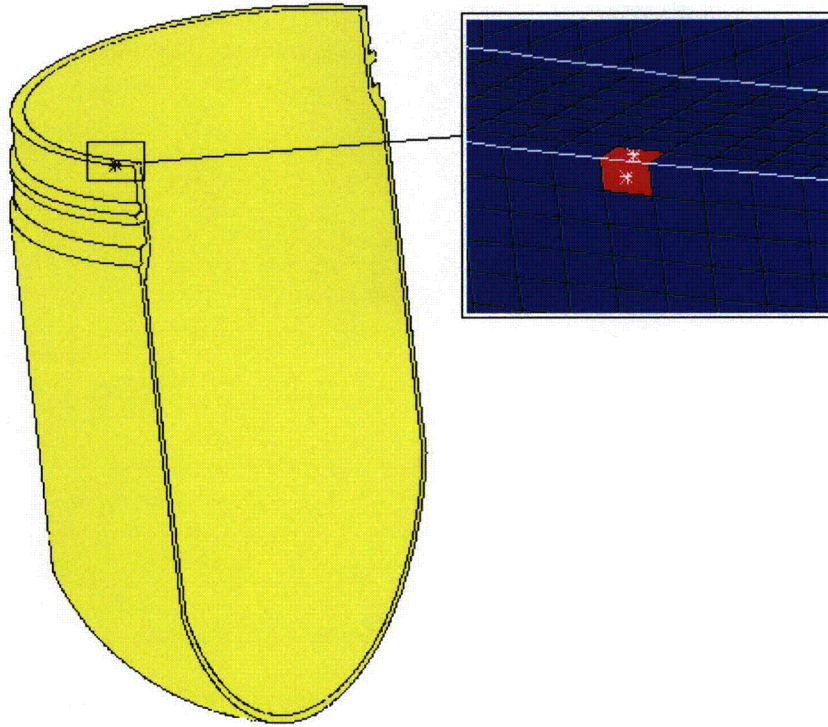


Figure 2-379. Plot of Element Exceeding Experimental Strain Locus for HAC Run 3, SC-2, Side Impact, Support Structure 45°

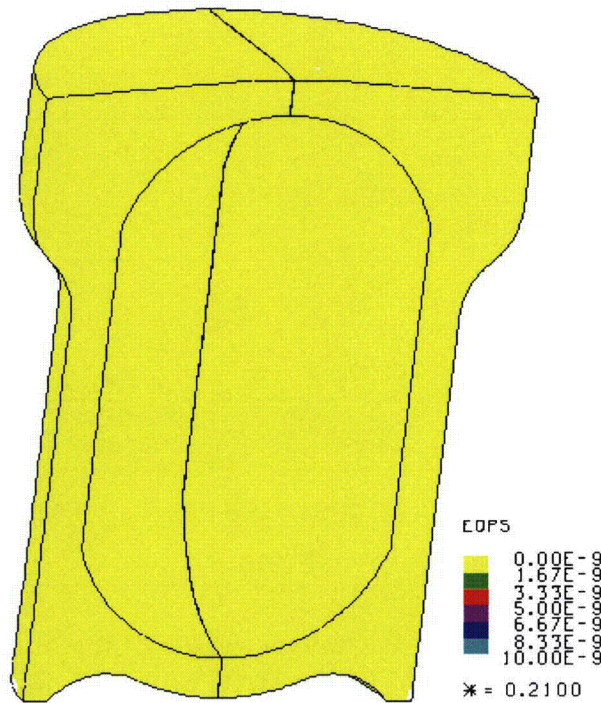


Figure 2-380. Plot of EQPS in the TB-1 for HAC Run 3, SC-2, Side Impact, Support Structure 45°

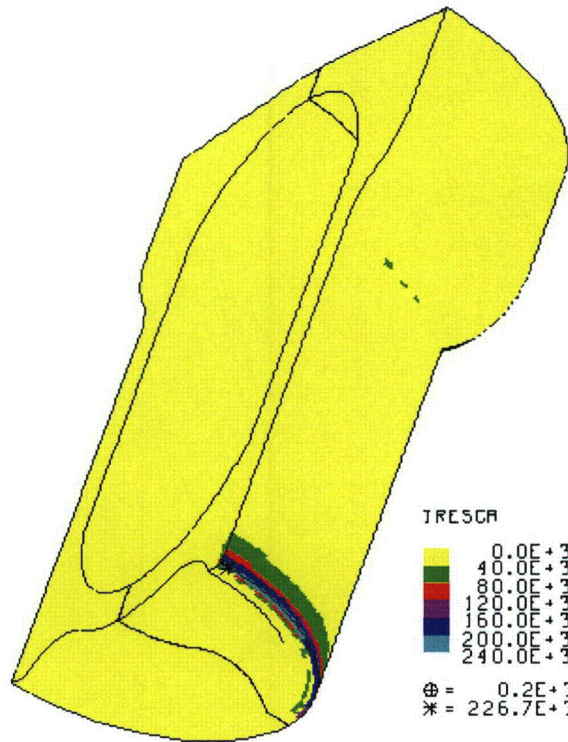


Figure 2-381. Plot of Tresca Stress in the TB-1 for HAC Run 3, SC-2, Side Impact, Support Structure 45°

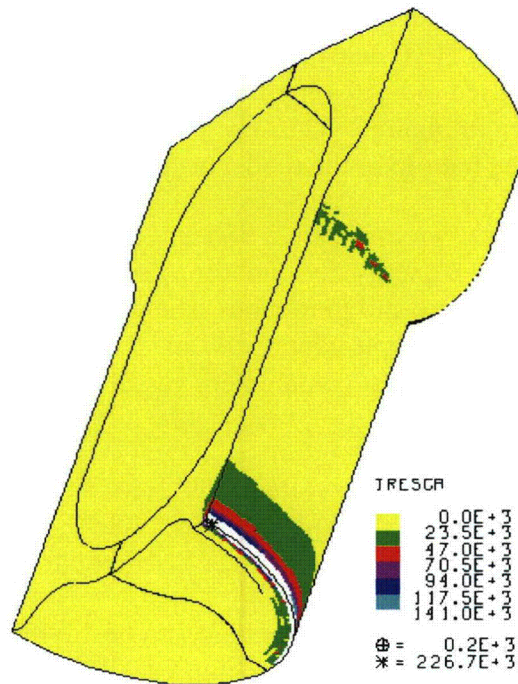


Figure 2-382. Plot of Tresca Stress in the TB-1 for HAC Run 3, SC-2, Side Impact, Support Structure 45°

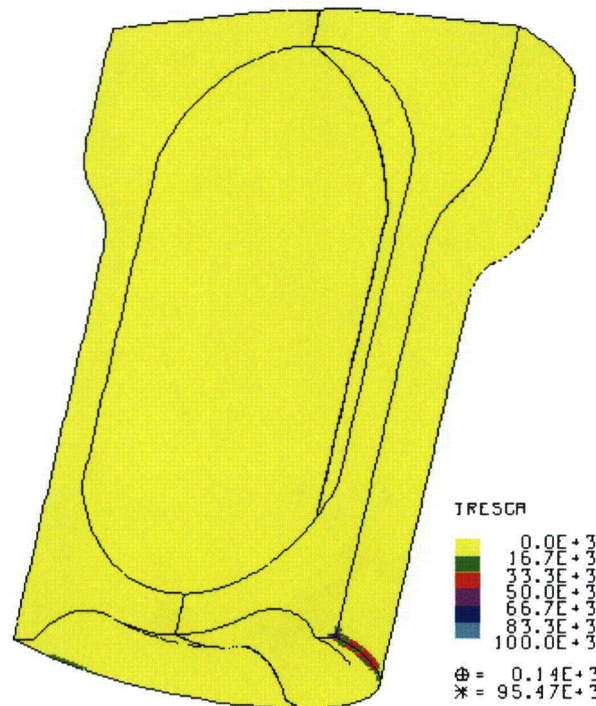


Figure 2-383. Plot of Tresca Stress in the TB-1 for HAC Run 3, SC-2, Side Impact, Support Structure 45° when Plate Velocity Reaches Zero

2.12.5.6.4 HAC- Run 4, SC-2, CGOC Impact, Support Structure 0°

The dynamic crush CGOC impact HAC analysis for the 2 SC-2 sample container run uses the same overpack model as those used in HAC runs 1 through 3. The finite element mesh and initial position of the model are shown in Figure 2-384. The Pu contents and support structure within the T-Ampoule are positioned at the bottom of the model because it was considered to be at rest.

The post-impact deformation is shown in Figure 2-385 and the resulting kinetic energy history is shown in Figure 2-386. The kinetic energy does not drop completely to zero because the plate is still vibrating and internal contents are still in motion. The plutonium cylinders have bounced off of the top and bottom surface of the sample containers, and the plate is now rebounding slowly with the package, ensuring that the highest containment vessel and contents loadings have occurred.

There were no elements that extended beyond the tested Bao-Wierzbicki strain locus. The maximum Tearing Parameter value for this analysis was 2.78e-3, which is below the critical Tearing Parameter value of 1.012 for Ti-6Al-4V, thus T-Ampoule integrity is maintained.

Peak EQPS in the TB-1 vessel is shown in Figure 2-387 to be 1.548e-3, and is localized in the outer contact regions with the redwood overpack. Figures 2-388 and 2-389 are plots of the Tresca stresses within the TB-1. The maximum Tresca stress in the TB-1 is 159.1 ksi, but there are no through thickness stresses exceeding the limit of 106.6 ksi, which can be seen clearly in the figures. Figure 2-389 is a plot of the Tresca stresses at the time when all of the kinetic energy of the plate has been transferred to the package, just as the plate begins to rebound. The

maximum through thickness stress at this time is below 8.33 ksi, below the allowable through thickness stress of 106.6 ksi, as seen in the figure.

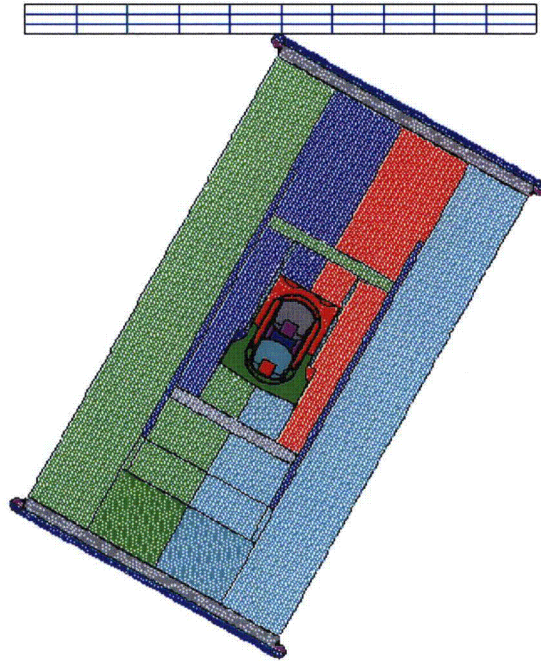


Figure 2-384. Finite Element Mesh for HAC Run 4, SC-2, CGOC Impact, Support Structure 0°

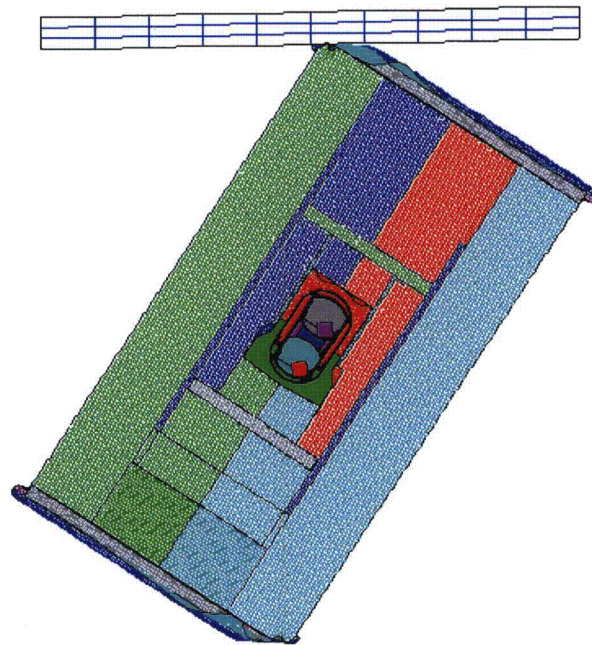


Figure 2-385. Finite Element Mesh for HAC Run 4, SC-2, CGOC Impact, Support Structure 0°, Final Displacement

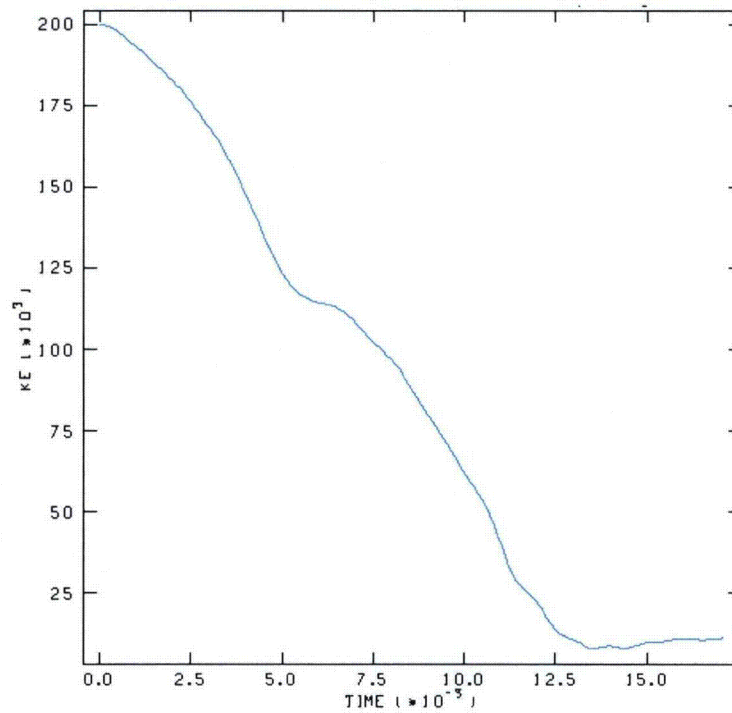


Figure 2-386. Kinetic Energy Time History for HAC Run 4, SC-2, CGOC Impact, Support Structure 0°

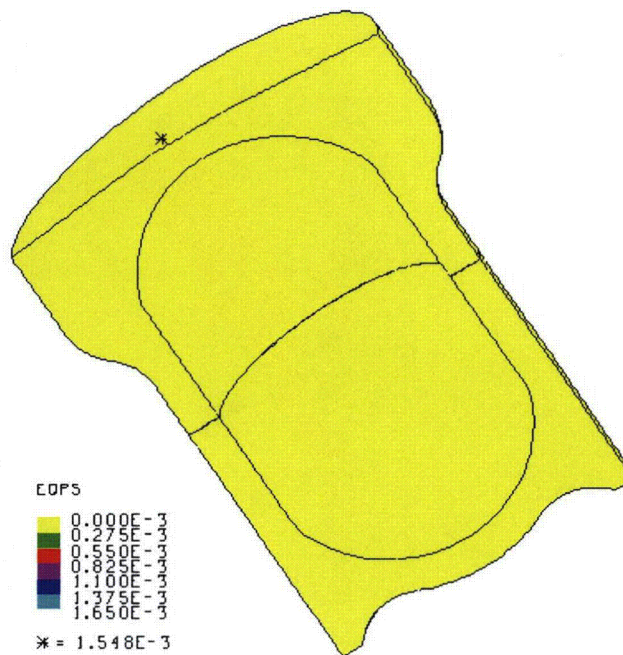


Figure 2-387. Plot of EQPS in TB-1 for HAC Run 4, SC-2, CGOC Impact, Support Structure 0°

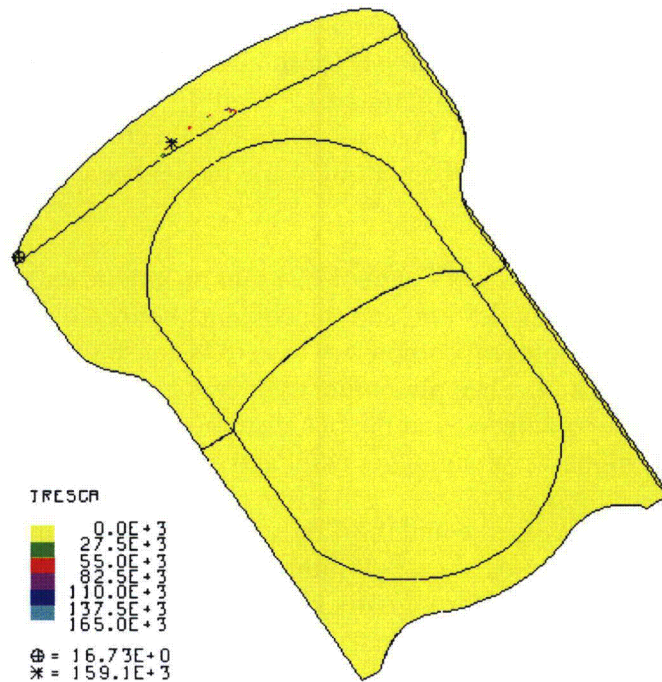


Figure 2-388. Plot of Tresca Stress in TB-1 for HAC Run 4, SC-2, CGOC Impact, Support Structure 0°

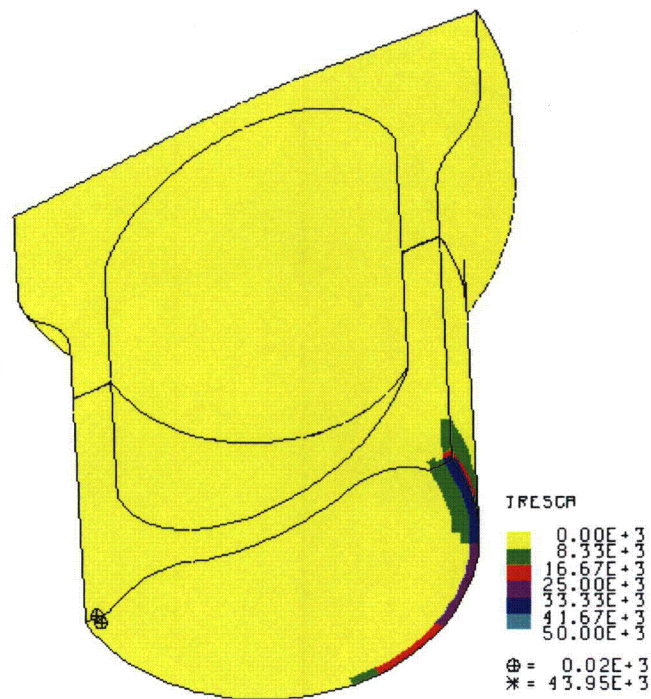


Figure 2-389. Plot of Tresca Stress in the TB-1 for HAC Run 4, SC-2, CGOC Impact, Support Structure 0° when Plate Velocity Reaches Zero

2.12.5.6.5 HAC- Run 5, SC-2, CGOC Impact, Support Structure 45°

The dynamic crush CGOC impact HAC analysis for the 2 SC-2 sample container run uses the same overpack model as those used in HAC runs 1 through 4. The finite element mesh and initial position of the model are shown in Figure 2-390. The Pu contents and support structure within the T-Ampoule are positioned at the bottom of the model because it was considered to be at rest.

The post-impact deformation is shown in Figure 2-391 and its kinetic energy history in Figure 2-392. The flanges on the overpack deform, and the contents bounce due to the impact of the plate. The kinetic energy does not drop completely to zero because the plate is still vibrating and internal contents are still in motion. The plutonium cylinders have bounced off of the top and bottom surface of the sample containers, and the plate is now rebounding slowly with the package, ensuring that the highest containment vessel and contents loadings have occurred.

There was zero EQPS in the T-Ampoule and the TB-1, and the maximum Tearing Parameter was 0. Figure 2-393 is a plot of the Tresca stresses within the TB-1. The maximum Tresca stress in the TB-1 is 157.0 ksi, but there are no through thickness stresses exceeding the limit of 106.6 ksi, which can be seen clearly in the figure. Figure 2-393 is a plot of the Tresca stresses at the time when all of the kinetic energy of the plate has been transferred to the package, just as the plate begins to rebound. The maximum through thickness stress at this time is below 16.7 ksi, below the allowable through thickness stress of 106.6 ksi, as seen in the figure.

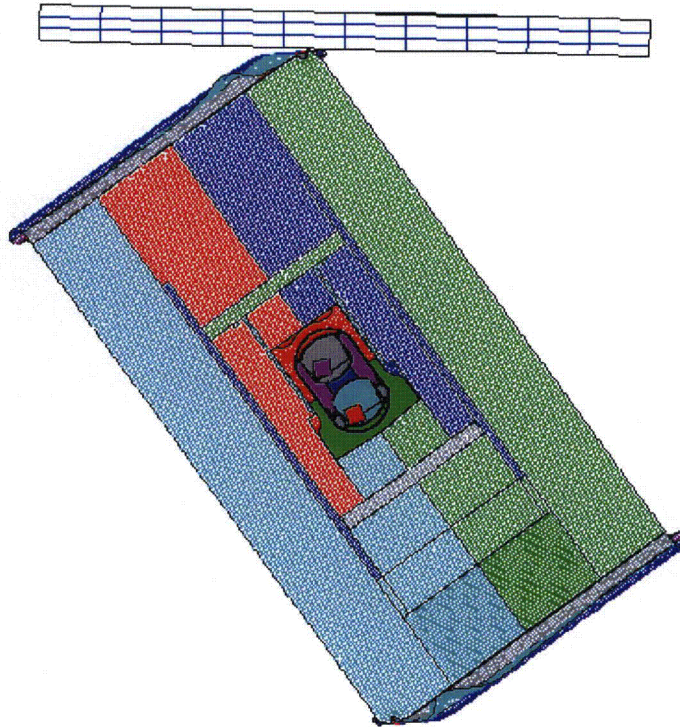


Figure 2-390. Finite Element Mesh for HAC Run 5, SC-2, CGOC Impact, Support Structure 45°